

University of Windsor

## Scholarship at UWindor

---

Electronic Theses and Dissertations

Theses, Dissertations, and Major Papers

---

2009

### Applications of gold nanoparticles to thiol and nitric oxide chemistry

Suzanne Durocher  
*University of Windsor*

Follow this and additional works at: <https://scholar.uwindsor.ca/etd>

---

#### Recommended Citation

Durocher, Suzanne, "Applications of gold nanoparticles to thiol and nitric oxide chemistry" (2009).  
*Electronic Theses and Dissertations*. 7974.  
<https://scholar.uwindsor.ca/etd/7974>

This online database contains the full-text of PhD dissertations and Masters' theses of University of Windsor students from 1954 forward. These documents are made available for personal study and research purposes only, in accordance with the Canadian Copyright Act and the Creative Commons license—CC BY-NC-ND (Attribution, Non-Commercial, No Derivative Works). Under this license, works must always be attributed to the copyright holder (original author), cannot be used for any commercial purposes, and may not be altered. Any other use would require the permission of the copyright holder. Students may inquire about withdrawing their dissertation and/or thesis from this database. For additional inquiries, please contact the repository administrator via email ([scholarship@uwindsor.ca](mailto:scholarship@uwindsor.ca)) or by telephone at 519-253-3000ext. 3208.

**APPLICATIONS OF GOLD NANOPARTICLES TO THIOL AND NITRIC  
OXIDE CHEMISTRY**

By

Suzanne Durocher

A Thesis  
Submitted to the Faculty of Graduate Studies  
Through the Department of Chemistry and Biochemistry  
In Partial Fulfillment of the Requirements for  
The Degree of Master of Science at the  
University of Windsor

Windsor, Ontario, Canada  
2009

© 2009 Suzanne Durocher



Library and Archives  
Canada

Published Heritage  
Branch

395 Wellington Street  
Ottawa ON K1A 0N4  
Canada

Bibliothèque et  
Archives Canada

Direction du  
Patrimoine de l'édition

395, rue Wellington  
Ottawa ON K1A 0N4  
Canada

*Your file* *Votre référence*  
ISBN: 978-0-494-57640-3  
*Our file* *Notre référence*  
ISBN: 978-0-494-57640-3

#### NOTICE:

The author has granted a non-exclusive license allowing Library and Archives Canada to reproduce, publish, archive, preserve, conserve, communicate to the public by telecommunication or on the Internet, loan, distribute and sell theses worldwide, for commercial or non-commercial purposes, in microform, paper, electronic and/or any other formats.

The author retains copyright ownership and moral rights in this thesis. Neither the thesis nor substantial extracts from it may be printed or otherwise reproduced without the author's permission.

#### AVIS:

L'auteur a accordé une licence non exclusive permettant à la Bibliothèque et Archives Canada de reproduire, publier, archiver, sauvegarder, conserver, transmettre au public par télécommunication ou par l'Internet, prêter, distribuer et vendre des thèses partout dans le monde, à des fins commerciales ou autres, sur support microforme, papier, électronique et/ou autres formats.

L'auteur conserve la propriété du droit d'auteur et des droits moraux qui protègent cette thèse. Ni la thèse ni des extraits substantiels de celle-ci ne doivent être imprimés ou autrement reproduits sans son autorisation.

---

In compliance with the Canadian Privacy Act some supporting forms may have been removed from this thesis.

While these forms may be included in the document page count, their removal does not represent any loss of content from the thesis.

Conformément à la loi canadienne sur la protection de la vie privée, quelques formulaires secondaires ont été enlevés de cette thèse.

Bien que ces formulaires aient inclus dans la pagination, il n'y aura aucun contenu manquant.

  
**Canada**

## DECLARATION OF CO-AUTHORSHIP/PREVIOUS PUBLICATION

### I. Declaration of Previous Publication

This thesis includes two original papers that have been previously published in peer reviewed journals, as follows:

Chapter 2	Mikula, I., Durocher, S., Martasek, P., Mutus, B. and Slama-Schwok, A. Isoform-specific differences in the nitrite reductase activity of nitric oxide synthases under hypoxia (2009). <i>Biochem J.</i> 418(3):673-82.	Published
Chapter 3	Durocher, S., Rezaee, A., Hamm, C., Rangan, C., Mittler, S. and Mutus, B. (2009). Disulfide-linked, gold nanoparticle-based reagent for detecting small molecular weight thiols. <i>J Am Chem Soc.</i> 131(7):2475-7.	Published

I certify that I have obtained a written permission from the copyright owners to include the above published materials in my thesis. I certify that the above material describes work completed during my registration as graduate student at the University of Windsor.

I declare that, to the best of my knowledge, my thesis does not infringe upon anyone's copyright nor violate any proprietary rights and that any ideas, techniques, quotations, or any other material from the work of other people included in my thesis, published or otherwise, are fully acknowledged in accordance with the standard referencing practices. Furthermore, to the extent that I have included copyrighted material that surpasses the bounds of fair dealing within the meaning of the Canada Copyright Act, I certify that I have obtained a written permission from the copyright owners to include such materials in my thesis.

I declare that this is a true copy of my thesis, including any final revisions, as approved by my thesis committee and the Graduate Studies office, and that this thesis has not been submitted for a higher degree to any other University or Institution.

### II. Co-Authorship Declaration

I hereby declare that this thesis incorporates material that is result of joint research, as follows. Chapter 2 incorporates joint research undertaken by the author under the supervision of Dr. Bulent Mutus, by Ivan Mikula and Dr. Anny Slama-Schwok of École Polytechnique in Paris, France, and by Dr. Pavel Martasek of Charles University in Prague, Czech Republic. Equal amounts of independent data presented in the publication were acquired by the author and Ivan Mikula. The other three co-authors contributed through research supervision, manuscript preparation, and funding. The data presented in this thesis reflect the author's contributions to the publication.

Chapter 3 was also the result of joint research. In all cases the experimental design, data and data interpretation were performed by the author under the supervision of Dr. Bulent Mutus. The collaborators, Dr. Chitra Rangan of the University of Windsor, Dr. Caroline Hamm of the Windsor Regional Cancer Centre in Windsor, Ontario, Asad Rezaee and Dr. Silvia Mittler of the University of Western Ontario in London, Ontario, contributed through funding and through discussion of experimental design and data interpretation.

I am aware of the University of Windsor Senate Policy on Authorship and I certify that I have properly acknowledged the contribution of other researchers to my thesis, and have obtained written permission from each of the co-authors to include the above materials in my thesis.

I certify that, with the above qualification, this thesis, and the research to which it refers, is the product of my own work.

## ABSTRACT

The first project studied the three nitric oxide synthases under different oxygen tensions. We found that eNOS can reduce  $\text{NO}_2^-$  to NO in hypoxia and anoxia, using endothelial cells and isolated enzymes. This suggests a new role for eNOS in times of restricted oxygen.

In the next project, gold nanoparticles were joined with a disulfide bond-bearing crosslinker to create a blue probe that turned red upon reduction with low molecular weight thiols. The rate depended on the size of the molecule. Since small thiols help control the redox of proteins their quantification helps identify oxidative stress.

In the third project, seven proteins isolated by gold nanoparticles were identified; these may have bound by their surface thiols. Additionally, gold nanoparticles were used to *S*-denitrosylate GSNO, and a flow device was designed that would automate this method. The prototype model is manually operated but shows potential to be developed for several applications.

## DEDICATION

*To Arvin*

## ACKNOWLEDGEMENTS

I am much indebted to Dr. Bulent Mutus for his mentorship during my time as a Master's student, both for his supervision over my research, and for his personal interest in the well-being of myself and his other students. He has been an invaluable person in my life.

My fellow graduate students, past and present, have greatly enhanced my experience as well. Dr. Arun Raturi, Dr. Inga Sliskovic, Rebecca Heeney, Adam Faccenda, Vasantha Kallakunta, Harmanpreet Kaur, and Ruchi Chaube have made the past 2 years very enjoyable, through sharing lunches, advice, and academic discussions. I wish everyone great success in their scientific careers.

I also wish to thank my friends and family for helping me grow as a person during this time. The support and pride of my mother, father, sister, and brother have been greatly motivating. Fun evenings out or in with my friends, especially Christine Koncan, Karl Leboeuf, and Erica Lee, have given me many wonderful memories. Thanks also to Christine for assistance in editing this thesis.

Finally, I would like to extend my gratitude to Arvin Singla. I could not have done this without his support, encouragement, and love.



## TABLE OF CONTENTS

DECLARATION OF CO-AUTHORSHIP/PREVIOUS PUBLICATION .....	iii
ABSTRACT .....	v
DEDICATION.....	vi
ACKNOWLEDGEMENTS.....	vii
LIST OF TABLES.....	xi
LIST OF FIGURES .....	xii
LIST OF SCHEMES .....	xiii
LIST OF ABBREVIATIONS.....	xiv
<b>CHAPTER 1 .....</b>	<b>1</b>
<b>1.1 Nitric Oxide .....</b>	<b>2</b>
1.1.1 Introduction.....	2
1.1.2 Biosynthesis .....	2
1.1.2.1 Nitric oxide synthase .....	2
1.1.2.2 <i>De novo</i> NO synthesis.....	4
1.1.3 Physical properties .....	6
1.1.4 Different forms .....	6
1.1.5 Reactions.....	8
1.1.6 Transport.....	12
1.1.7 Regulation .....	13
1.1.8 Detection methods .....	14
<b>1.2 Gold Nanoparticles .....</b>	<b>17</b>
1.2.1 History .....	17
1.2.2 Synthesis .....	17
1.2.3 PDMS and synthesis of surface gold nanoparticles.....	18
1.2.4 Localized surface plasmon resonance.....	20
1.2.5 Applications of AuNP.....	22
<b>CHAPTER 2.....</b>	<b>24</b>
<b>2.1 Introduction.....</b>	<b>25</b>
<b>2.2 Materials and Equipment .....</b>	<b>25</b>
2.2.1 Materials .....	25
2.2.2 Equipment .....	26
<b>2.3 Methods.....</b>	<b>27</b>
2.3.1 Cell culture.....	27
2.3.2 Treatment of cells .....	27
2.3.3 Inhibitor treatment of cells.....	28
2.3.4 Nitric oxide detection.....	28

2.3.5	Nitric oxide detection from <i>in vitro</i> NOS isoforms .....	28
<b>2.4</b>	<b>Results .....</b>	<b>30</b>
2.4.1	NO release by endothelial cells under normoxia, hypoxia or anoxia .....	30
2.4.2	Effect of inhibitors on NO release by endothelial cells under anoxia .....	32
2.4.3	NO formed by <i>in vitro</i> NOS or NOS reductase domain under anoxia .....	34
<b>2.5</b>	<b>Discussion .....</b>	<b>36</b>
<b>CHAPTER 3 .....</b>		<b>41</b>
<b>3.1</b>	<b>Introduction .....</b>	<b>42</b>
<b>3.2</b>	<b>Materials and Equipment .....</b>	<b>43</b>
3.2.1	Materials .....	43
3.2.2	Equipment .....	43
<b>3.3</b>	<b>Methods .....</b>	<b>44</b>
3.3.1	Synthesis of gold nanoparticles .....	44
3.3.2	Synthesis of the gold nanoparticle-based reagent .....	44
3.3.2.1	Coating with DSP .....	44
3.3.2.2	Crosslinking with GSSG .....	45
3.3.3	Transmission Electron Microscopy .....	45
3.3.4	Purification of recombinant human PDI .....	45
3.3.5	Reduction of the reagent with small thiols .....	46
3.3.6	Synthesis of disulfide-linked AuNP with a larger spacer ligand .....	46
3.3.6.1	Oxidation of peptides .....	46
3.3.6.2	Synthesis of the reagent .....	47
3.3.6.3	Reduction of the larger reagent .....	47
<b>3.4</b>	<b>Results .....</b>	<b>48</b>
3.4.1	Gold nanoparticle synthesis .....	48
3.4.2	Au-DSP-GSSG synthesis .....	48
3.4.2.1	Optimization of DSP concentration .....	48
3.4.2.2	Final product formation .....	51
3.4.3	TEM of Au-DSP-GSSG .....	51
3.4.4	Reaction with thiols .....	55
3.4.5	Effects of size and concentration on reduction rates .....	58
3.4.6	Synthesis of disulfide-linked AuNP with a larger spacer ligand .....	62
<b>3.5</b>	<b>Discussion .....</b>	<b>65</b>
<b>CHAPTER 4 .....</b>		<b>70</b>
<b>4.1</b>	<b>Introduction .....</b>	<b>71</b>

<b>4.2</b>	<b>Materials and Equipment .....</b>	<b>72</b>
4.2.1	Materials .....	72
4.2.2	Equipment.....	73
<b>4.3</b>	<b>Methods.....</b>	<b>74</b>
4.3.1	Synthesis of gold nanoparticles .....	74
4.3.2	Synthesis of PDMS-bound gold nanoparticles .....	74
4.3.3	Isolation of plasma from whole blood .....	74
4.3.4	Isolation of proteins from serum.....	74
	4.3.4.1 Using aqueous AuNP.....	74
	4.3.4.2 Using PDMS-AuNP.....	75
4.3.5	Identification of the isolated proteins .....	77
	4.3.5.1 SDS-PAGE and staining .....	77
	4.3.5.2 Analysis of gels.....	77
	4.3.5.3 Mass Spectrometry .....	77
	4.3.5.4 Western blot.....	78
4.3.6	Synthesis of GSNO .....	78
4.3.7	<i>S</i> -denitrosylation of GSNO by AuNP .....	79
	4.3.7.1 Aqueous AuNP .....	79
	4.3.7.2 PDMS-AuNP and PDMS.....	79
4.3.8	Flow device design .....	80
4.3.9	<i>S</i> -denitrosylation of GSNO using the flow device.....	80
<b>4.4</b>	<b>Results .....</b>	<b>81</b>
4.4.1	Synthesis of PDMS-AuNP.....	81
4.4.2	Identification of AuNP-bound plasma proteins .....	81
4.4.3	Properties of identified proteins.....	88
4.4.4	AuNP can <i>S</i> -denitrosylate GSNO .....	92
4.4.5	PDMS-AuNP can <i>S</i> -denitrosylate GSNO .....	94
4.4.6	<i>S</i> -denitrosylation of GSNO using the flow device.....	96
<b>4.5</b>	<b>Discussion .....</b>	<b>99</b>
<b>5.1</b>	<b>Conclusions.....</b>	<b>105</b>
	REFERENCES .....	107
	APPENDIX A.....	112
	VITA AUCTORIS.....	120

## **LIST OF TABLES**

Table 4.1	Locations and functions of the identified proteins.....	91
-----------	---	----

## LIST OF FIGURES

Figure 1.1	Structure of the active NOS .....	5
Figure 2.1	Detection of NO release from nitrite under normoxia, hypoxia and anoxia..	
	.....	31
Figure 2.2	Effect of inhibitors on nitrite reduction under anoxia.....	33
Figure 2.3	Detection of NO released by nNOS and eNOS under argon .....	35
Figure 3.1	Visualization of newly synthesized AuNP .....	49
Figure 3.2	DSP concentration optimization based on hydrolysis rates.....	50
Figure 3.3	Synthesis of Au-DSP-GSSG.....	53
Figure 3.4	Overnight stability of Au-DSP-GSSG after synthesis.....	54
Figure 3.5	Reduction of Au-DSP-GSSG by 1 $\mu$ M thiol .....	56
Figure 3.6	Effect of size on reduction rate .....	60
Figure 3.7	Effect of concentration on reduction .....	61
Figure 3.8	Oxidation of GGGGC.....	63
Figure 3.9	Synthesis of Au-DSP-G <sub>4</sub> CCG <sub>4</sub> .....	64
Figure 4.1	AuNP-bound proteins .....	83
Figure 4.2	Histograms of the protein banding of pre-mass spectrometry gels .....	85
Figure 4.3	Identification of PDI and HSP70 by Western blot .....	87
Figure 4.4	Structures of identified possible thiol proteome members .....	90
Figure 4.5	S-denitrosylation of GSNO by AuNP.....	93
Figure 4.6	S-denitrosylation of GSNO by PDMS and PDMS-AuNP .....	95
Figure 4.7	The flow device .....	97
Figure 4.8	S-denitrosylation of GSNO using a flow device.....	98

## LIST OF SCHEMES

Scheme 1	Synthesis process of Au-DSP-GSSG.....	52
Scheme 2	Experimental design for the isolation of serum proteins using PDMS-AuNP .....	76

## LIST OF ABBREVIATIONS

7-NI	3-bromo-7-nitroindazole
$\beta$ -ME	$\beta$ -mercaptoethanol
Au-DSP-GSSG	Disulfide-linked, gold nanoparticle-based reagent
AuNP	Gold nanoparticles
BH <sub>4</sub>	Tetrahydrobiopterin
cGMP	Cyclic guanosine monophosphate
Cys	L-cysteine
DMSO	Dimethyl sulfoxide
DSP	Dithiobis(succinimidyl propionate)
DTNB	5,5'-dithiobis(2-nitrobenzoic acid)
DTT	L-dithiothreitol
ECM	Endothelial cell medium
eNOS	Endothelial nitric oxide synthase
eNOSred	Endothelial nitric oxide synthase reductase domain
FAD	Flavin adenine dinucleotide
FMN	Flavin mononucleotide
GSH	Glutathione (reduced)
GSNO	S-nitroglutathione
GSSG	Glutathione (oxidized)
HDMEC	Human dermal microvascular endothelial cells
HMWT	High molecular weight thiol
HSP70	Heat-shock protein 70
iNOS	Inducible nitric oxide synthase
LMWT	Low molecular weight thiol
L-NMMA	N <sup>G</sup> -monomethyl-L-arginine
LSPR	Localized surface plasmon resonance
MALDI-TOF	Matrix-assisted laser desorption ionization – time of flight
NADPH	Nicotinamide adenine dinucleotide phosphate (reduced)
NaSH	Sodium hydrosulfide
nNOS	Neuronal nitric oxide synthase
nNOSred	Neuronal nitric oxide synthase reductase domain
NO	Nitric oxide
NO <sub>2</sub> -	Nitrite
NO <sub>3</sub> -	Nitrate
NOA	Nitric oxide analyzer
NOS	Nitric oxide synthase
NO <sub>x</sub>	Nitric oxide and its related species
PDI	Protein disulfide isomerase
PDMS	Poly(dimethylsiloxane)
PDMS-AuNP	Poly(dimethylsiloxane)-bound gold nanoparticles
PNGase F	Peptide N-glycosidase F
PRP	Platelet-rich plasma
RSNO	S-nitrosothiol
SDS-PAGE	Sodium dodecyl sulfate polyacrylamide gel electrophoresis
TEM	Transmission electron microscope

## **CHAPTER 1**

### **GENERAL INTRODUCTION**



## **1.1 Nitric Oxide**

### **1.1.1 Introduction**

Most people are aware of some effects of nitric oxide (NO) with no prior knowledge of the molecule itself. It is a component of air pollution, used to treat heart disease in the form of nitroglycerin, and the active ingredient of Viagra. Similarly, one of the main physiological roles of NO was known before the molecule itself was identified as the causative agent: that is the promotion of smooth muscle relaxation (1). The diversity of the effects of NO has resulted in interest from different groups of researchers such as athletes, doctors and academic scientists.

There was interest in the 1980s in a molecule dubbed endothelium-derived relaxing factor (EDRF). As more was learned about EDRF and NO, Ignarro (2), Palmer *et al* (3) and others independently discovered that they were the same molecule. This was only a few years after NO was found to activate the enzyme guanylate cyclase, which was already known to promote smooth muscle relaxation through its product cyclic guanosine monophosphate (cGMP) (1). Since then, NO research has held immense interest and scientists continue to learn more about its importance, underscored by the wide diversity of its roles and physiological effects such as platelet aggregation inhibition (4), angiogenesis (5), and immune response (6), among others.

This brief survey will attempt to impart an understanding of the fundamentals of NO. Beginning with synthesis and properties, it will then explain the reactions NO readily undergoes, touching on the influence this has in health and disease. Finally, current detection methods will be described as they are vital to NO research.

### **1.1.2 Biosynthesis**

#### **1.1.2.1 Nitric oxide synthase**

Nitric oxide synthase (NOS) is the enzyme responsible for the biosynthesis of NO. There are 3 isoforms, named for their role or location of first discovery: neuronal NOS (nNOS), also known as NOS I, which was first isolated in 1990 (7); inducible NOS (iNOS), originally discovered in murine macrophages and known as NOS II (8); and endothelial NOS (eNOS), also known as NOS III (9). nNOS is further divided into subtypes  $\mu$ ,  $\alpha$ ,  $\beta$ , or  $\gamma$  depending on the specific tissue in which it is expressed. eNOS and nNOS are constitutively expressed, producing low levels of NO upon receiving a signal. iNOS, however, is not expressed until it is activated (1). It can be activated in many tissue types, producing high amounts of NO until no longer needed.

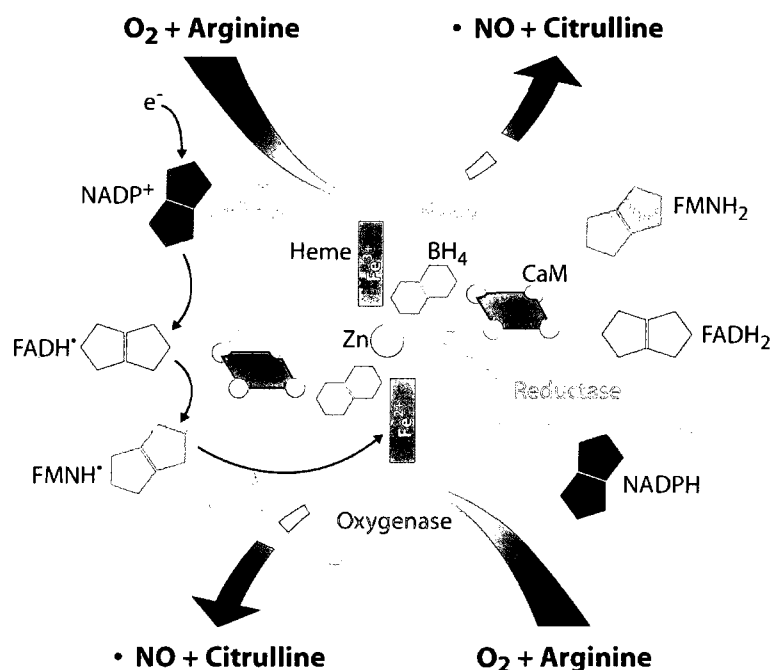
The 3 isozymes share basic structural similarities. NOS is a homodimer, each monomer containing an N-terminal oxygenase domain and a C-terminal reductase domain (10). The oxygenase domains bind to heme and tetrahydrobiopterin (BH<sub>4</sub>), while the reductase domains contain an electron transport system comprised of nicotinamide adenine dinucleotide phosphate (NADPH), flavin adenine dinucleotide (FAD), and flavin mononucleotide (FMN). The calmodulin and zinc cofactors are located at the interface between monomers, with two cysteine residues from each monomer coordinated to the zinc. While eNOS and nNOS bind calmodulin reversibly, its binding to iNOS is irreversible. The NOS active sites are highly conserved (9) as they all catalyze the same reaction to produce NO from arginine and oxygen (6). An image of NOS can be found in Figure 1.1.

Aside from these fundamental similarities, the NOS isozymes have important differences to accommodate their varied roles in the body. They only share 50-60% homology with one another and are somewhat different in size (11). eNOS and nNOS are mainly located at the cell membrane while iNOS is expressed internally (12). Their

regulation also varies and will be discussed later. These and other variations between the 3 isozymes allow them to maintain their separate roles based on the location of their expression.

#### **1.1.2.2 *De novo* NO synthesis**

NO is a product of the 5-electron oxidation reaction of arginine to citrulline (6). It is a multi-step mechanism involving the electron transport system of the reductase domain. Electron flow begins with NADPH, through FAD to FMN, which passes one electron at a time to the heme iron in the opposite monomer's oxygenase domain, as depicted in Figure 1.1. Once the iron is reduced, it is able to bind a molecule of oxygen and begin catalysis (13). The first main step is the formation of one mole of N<sup>G</sup>-hydroxy-L-arginine (NOHA) from one mole of arginine, NADPH and O<sub>2</sub>. Next, one electron (i.e., 0.5 moles of NADPH consumed) is transferred to heme where one more mole of O<sub>2</sub> is consumed to convert NOHA to citrulline, releasing NO. The overall stoichiometry of the reaction is 2 moles of O<sub>2</sub> and 1.5 moles of NADPH consumed per mole of arginine to produce one mole of NO and one of citrulline (14). Since the reaction occurs at the terminal amine of L-arginine, N<sup>G</sup>-monomethyl-L-arginine (L-NMMA) is a potent competitive inhibitor of NOS (15).



**Figure 1.1 Structure of the active NOS**

While maintaining differences in sequence and regulation, all 3 of the NOS isoforms follow the common, basic structure depicted above. In the catalytically active form, it is a homodimer with each monomer comprised of an oxygenase domain, shown in gray, and a reductase domain, depicted in pink. Electron flow is shown on the left-hand side, where an electron is transferred from  $\text{NADPH}$  to  $\text{FAD}$ , then to  $\text{FMN}$ , and from there to the heme of the opposite monomer. Oxygen can bind to the reduced heme and this begins the conversion of arginine to citrulline and  $\text{NO}$  via the  $\text{NOHA}$  intermediate. The image is from Cayman Chemical ([caymanchem.com](http://caymanchem.com)).

### 1.1.3 Physical properties

NO's small size and hydrophobic nature are responsible for its opportunities for reactivity inside the body (1). It is slightly more soluble in water than O<sub>2</sub> and it is 9 times more soluble in organic solvents than in water (16). This means it can freely diffuse across cell membranes as well as react inside them. Since the cell membrane occupies only 3% of a cell's volume, it serves to concentrate existing NO into a smaller area, enabling faster reactions (1).

More powerful, however, is the diffusibility of NO. It has a diffusion constant of 3300  $\mu\text{m}^2\text{s}^{-1}$  in water (17) and takes 2 ms to diffuse out of a 5- $\mu\text{m}$  cell; therefore, given a half-life of 5-10 s, NO is a very effective signaling molecule capable of reaching several hundred thousand cells surrounding that in which it was produced (18). To underscore this statement, it has been theoretically shown that since NO diffuses more rapidly than it reacts, in reactions occurring within NO-producing cells, the NO is more likely to have come from a different cell than itself (19). These two properties of solubility and diffusibility are thus responsible for the rapid reaction rates and the paracrine nature of NO signaling.

### 1.1.4 Different forms

NO has 11 valence electrons, making it an uncharged, paramagnetic, free radical and consequently highly reactive (20). Its reactivity is the reason it has a half-life of only a few seconds in the body. The nitrogen-oxygen bond itself is a double bond, N=O. While it is capable of forming a dimer, O=N—N=O, the N—N bond is weak and not energetically favourable (21), supporting the hypothesis that dimerization is transient at best at room temperature and pressure (1).

Although it does not readily dimerize, NO reacts with O<sub>2</sub> which can be considered a biradical given its two unpaired electrons. •NO<sub>2</sub>, another free radical, can be formed from NO and O<sub>2</sub> in a multi-step reaction (22). This is a strong oxidant which is able to abstract hydrogen atoms, add to unsaturated bonds, or react with anions (23). It is also able to react with other radicals, including itself and NO. It dimerizes much more readily than NO, producing N<sub>2</sub>O<sub>4</sub> which is a good NO donor to thiols. However, it is unstable and dissociates in water to nitrite (NO<sub>2</sub><sup>-</sup>) and nitrate (NO<sub>3</sub><sup>-</sup>). In addition, •NO<sub>2</sub> will react with NO to form the NO donor N<sub>2</sub>O<sub>3</sub>. In water this will remain in equilibrium with two equivalents of NO<sub>2</sub><sup>-</sup>, but in a hydrophobic environment it is more stable. This includes not only the cell membrane but interior hydrophobic pockets of proteins such as protein disulfide isomerase (PDI) (24). NO<sub>2</sub><sup>-</sup> can also be formed more directly through a reaction between NO, O<sub>2</sub>, and H<sub>2</sub>O (25).

Oxygen can gain one electron to become superoxide (O<sub>2</sub><sup>•-</sup>). It is negatively charged and still a free radical because one electron remains unpaired; therefore, it is very highly reactive. One common reaction occurs between O<sub>2</sub><sup>•-</sup> and NO, resulting in peroxynitrite (ONOO<sup>-</sup>) (26). In aqueous solution it is in equilibrium with its acid, ONOOH, and is a strong oxidizing agent and nucleophile. Its most common reaction occurs with CO<sub>2</sub> to ultimately yield NO<sub>3</sub><sup>-</sup> and bicarbonate (HCO<sub>3</sub><sup>-</sup>) (27). However, it also reacts with O<sub>2</sub><sup>•-</sup> to produce O<sub>2</sub>, •NO<sub>2</sub> and H<sub>2</sub>O, or with NO to form •NO<sub>2</sub> and NO<sub>2</sub><sup>-</sup> (28).

It had previously been thought that that NO<sub>2</sub><sup>-</sup> and NO<sub>3</sub><sup>-</sup> are inert end products of NO metabolism; however, recent evidence shows that they can exert the same influence on physiology as NO (29). For example, ingestion of NO<sub>2</sub><sup>-</sup> relaxes smooth muscle and leads to an increase in Hb-Fe-NO, similarly to when NO is synthesized (30). Furthermore, studies have shown that NO<sub>2</sub><sup>-</sup> is protective during ischemia. While it is known that NO<sub>2</sub><sup>-</sup>

can be chemically reduced to NO, the reaction is prohibitively slow except in acidic conditions such as the stomach (31). In recent years several mammalian enzymes have been identified as being capable of catalyzing this reduction in addition to their main functions. These include xanthine oxidase, cytochrome c oxidase, and deoxyhemoglobin (30). Interestingly, this nitrite reduction is observed only when there is a lack of oxygen: xanthine oxidase is up-regulated in hypoxia, and deoxyhemoglobin by definition has no bound O<sub>2</sub> molecules. While mammals have no such enzyme, commensal bacteria are able to reduce NO<sub>3</sub><sup>-</sup> to NO<sub>2</sub><sup>-</sup>, making ingested nitrate protective under hypoxia as well.

In addition to functional similarities, several NO derivatives described above are also potent oxidizing agents and generally highly reactive, especially N<sub>2</sub>O<sub>3</sub> and •NO<sub>2</sub>. It is this property that allows NO to affect the cell physiology as it does, through reactions with lipids, thiols, and other essential components as discussed in the next section.

#### **1.1.5 Reactions**

Unsaturated fatty acid side chains are subject to hydrogen abstraction, either by enzymes or by radicals, resulting in a lipid free radical denoted as L• (32). Oxygen binds to it to yield LOO•; this is known as lipid peroxidation. The formation of one LOO• begins a chain of reactions whereby affected fatty acids oxidize their neighbours, and so on. This regularly occurs in a controlled manner since LOO• serve as signaling molecules, and the peroxidation reactions cease upon low oxygen availability. However, in a situation of oxidative stress lipid peroxidation becomes uncontrolled, undergoing what is known as propagation reactions.

NO can either initiate or quench these propagation reactions depending on the circumstances in the cell. ONOO<sup>-</sup> is known to directly induce it by abstracting H atoms from lipids including low-density lipoprotein (LDL) (33); NO<sub>2</sub>• also has this ability to a

lesser extent (32). Therefore, in cells where  $O_2^{\bullet-}$  is available, the chance of lipid peroxidation by NO-derived species becomes greater.

Conversely, since NO is a free radical it is able to react with  $LOO^{\bullet}$  to form  $LOONO$ , thus quenching the propagation (34). This may stay as is or hydrolyze to form  $LOOH$  and  $NO_2^-$ . By eliminating the lipid free radical, NO can terminate the reaction from propagating further. This is common in conditions where  $H_2O_2$ , transition metals or other sources initiate the propagation reaction rather than  $NO_x$ . NO can also act as a quenching agent in the presence of  $O_2^{\bullet-}$  as long as it is in excess (32). In addition, NO can scavenge  $O_2^{\bullet-}$  and other reactive oxygen species directly, reducing the chance of  $ONOO^-$  initiating lipid peroxidation (35).

Low molecular weight thiols (LMWT) such as cysteine, N-acetylcysteine, glutathione, and others circulate through the blood where they perform a variety of functions. They may be reduced, bearing one or more free SH group, or oxidized, connected through disulfide (S—S) bonds (36). LMWT maintain the redox status of proteins and other high molecular weight thiols (HMWT) through the interchangeability of these two forms. For example, one function of PDI is to reduce disulfide bonds of other proteins; in the process, PDI becomes oxidized (37). It must return to its original reduced state to be able to perform the same reaction again, and LMWT allow this to occur. When there is a state of oxidative stress the LMWT reduce proteins to enable them to continue their functions, absorbing the oxidized state (36). Reduced LMWT can be replenished through *de novo* synthesis or via reduction by enzymes such as glutathione reductase.

NO is known to become bound to thiols which are then called S-nitrosothiols, denoted as RSNO (38). These can be LMWT and HMWT alike. This formation has several effects; one of them, importantly, is to extend the lifetime of NO. As with lipid



peroxidation, the ability of a thiol to become *S*-nitrosylated depends on its environment, specifically the local pH and the presence of oxygen and metals.

A mechanism was proposed in 1997 wherein NO directly reacts with a free thiol to produce an intermediate  $\text{RSN}^\bullet\text{-OH}$ , which donates an electron to an acceptor to yield RSNO (39). However, given NO's relative inability to react with non-radicals, and the fact that only specific RSNOs form *in vivo*, it is not likely that the reaction occurs spontaneously (1,40). Since then, copper ( $\text{Cu}^{2+}$ ) has been shown to act as a catalyst for the direct *S*-nitrosylation by NO (41).  $\text{Cu}^{2+}$  can oxidize NO to  $\text{NO}^+$ , as well as oxidize R-SH to thiolate,  $\text{RS}^-$ . When it performs one or both of the oxidations, the two species can directly bind to form RSNO.

*S*-nitrosothiols are mainly formed through the reaction between a thiol and an NO donor rather than directly (38). Transnitrosylation occurs when an RSNO donates its NO group to another thiol. LMWT in the blood such as glutathione (GSH) act as NO reservoirs, and upon a stimulus will donate the NO to proteins; this is an important signal transduction mechanism. As mentioned above,  $\text{N}_2\text{O}_3$  and  $\text{N}_2\text{O}_4$  are excellent NO donors as well (42). These will react with thiols directly to form RSNO and  $\text{NO}_2^-$  or  $\text{NO}_3^-$  respectively. In addition, ONOOH – the acid of peroxynitrite – will react with thiolates and release peroxide ( $\text{HOO}^-$ ) along with RSNO; however, this occurs less readily due to competition from  $\text{CO}_2$  (43).

Although *S*-nitrosothiols are important carriers of NO, which extend its lifetime and mediate signal transduction, they are susceptible to decomposition. While  $\text{Cu}^{2+}$  can oxidize NO to  $\text{NO}^+$ , allowing it to bind to thiolates,  $\text{Cu}^+$  is effective at reducing RSNO back to RSH (44). Other metals and reducing agents effect this decomposition as well,

and RSNO is light sensitive. Thus, the occurrence of *S*-nitrosothiols is highly regulated via its formation and decomposition pathways.

Finally, NO will react with metal centres, with the notable example of reaction with iron inside heme groups. The M—NO bond is usually linear but may be bent if NO acts as an electron acceptor from the metal (1). There are three main reactions that may undergo between NO and a hemoprotein such as hemoglobin (45). In one, NO reacts with deoxyhemoglobin (Hb-Fe(II)) to form Hb-Fe(II)-NO. Depending on the environment, this may then transfer an NO equivalent to a thiol, serving as an NO donor for *S*-nitrosothiol formation (46). NO may also react with oxyhemoglobin (Hb-Fe(II)-O<sub>2</sub>), reducing the heme to Hb-Fe(III) and itself becoming oxidized to NO<sub>3</sub><sup>-</sup> in the process by the released O<sub>2</sub> (45). Thirdly, NO may react with Hb-Fe(III) (methemoglobin), resulting in its oxidation while methemoglobin becomes Hb-Fe(III)-OH<sub>2</sub>.

Many proteins contain a heme group and therefore regulate, or are regulated by, NO. Hemoglobin, myoglobin, cytochrome P450, and xanthine oxidase are a handful of examples. Importantly, NO activates guanylate cyclase by binding to its heme group, culminating in smooth muscle relaxation (47). Binding leads to a conformational change in which the weak bond between Fe(II) and its axial ligand, histidine 105, is broken (48). The active site then becomes exposed, substantially improving the affinity for its substrate, guanosine triphosphate (GTP). The product, cyclic guanosine monophosphate (cGMP), activates cGMP-dependent protein kinases and phosphodiesterases (PDE); PDE3 stimulates the sarcoplasmic reticulum calcium pump (SERCA2) to sequester calcium, leading to the relaxation of smooth muscle (49). This example highlights the significance of NO's ability to bind to metal centres of proteins.

Overall, the reactivity of NO can be either positive or detrimental to the cell, depending in part on its concentration (50). Under normal circumstances the amount of NO is sufficient to reversibly activate certain enzymes, such as guanylate cyclase (47), or inhibit others through *S*-nitrosylation, such as PDI (24). In the event of high concentrations of NO, however, nitrosative stress can occur in which excessive levels of ONOO<sup>-</sup>, N<sub>2</sub>O<sub>3</sub> and other highly reactive species are produced. These can react with proteins unnecessarily, initiate lipid peroxidation, or damage DNA when unchecked (1). Therefore, it is critical that the body strictly regulates its NO supply to ensure that it can perform its functions without extraneous and damaging reactions occurring.

#### **1.1.6 Transport**

As stated above, NO is able to freely diffuse due to its small size and hydrophobicity. However, free NO has a short half-life and is more likely to react than to diffuse for very long (19). RSNOs therefore act as vehicles for the transport of NO from cells into serum, through the circulatory system, and to specific tissues.

PDI has been shown to *S*-denitrosylate RSNOs such as GSNO or PDI-SNO (24). This can produce free NO or PDI itself may become *S*-nitrosylated in the process. In addition, N<sub>2</sub>O<sub>3</sub> formed in a hydrophobic region inside PDI may directly *S*-nitrosylate PDI's active site thiols. Since PDI is known to be excreted to the cell surface in low amounts, and may cycle back in as well (51), it is likely that PDI carries NO across the cell membrane where it is then released by free PDI. This would serve as an important mechanism to bring NO from a location of high concentration – inside an NO-producing cell or platelet – to a site of low concentration, the cell exterior (24).

*S*-nitrosoalbumin (Alb-SNO) is one of the primary reservoirs of NO in human blood (52). Although it only has one free thiol able to be *S*-nitrosylated, the concentration

of Alb-SNO may be as high as 5  $\mu$ M due to the abundance of albumin circulating (1). Studies have shown that hydrophobic pockets in albumin facilitate the formation of  $N_2O_3$ , which can then *S*-nitrosylate the same albumin (53). Additionally, transnitrosylation reactions occur readily from low molecular weight RSNOs, especially GSNO and *S*-nitrosocysteine (CysNO), to albumin (52). Alb-SNO may thus be a transport vessel to circulate NO in the blood while it is released in places where it is needed. Hemoglobin binds NO both in its heme and by *S*-nitrosylation of cys93 of the  $\beta$  subunit, but its role in the possible transport of NO remains unclear (54).

### **1.1.7 Regulation**

The formation of RSNOs and metal-NO complexes regulates the levels of free NO, and facilitates its transport to tissues where its activity is needed. However, most of the regulation of the amount of NO or  $NO_x$  occur at the level of the enzyme NOS. eNOS and nNOS are the most similar to one another and consequently are regulated in similar manners (1). Before it is catalytically active, e/nNOS must form a dimer and bind all of its cofactors; the cofactor which has the most influence on this process is calmodulin (55). e/nNOS exists as a monomer before its activation by  $Ca^{2+}$ . When NO is required,  $Ca^{2+}$  is released to the cytosol where it binds to calmodulin. This induces a conformational change in calmodulin, allowing it to bind to specific consensus sites on certain proteins. On NOS the site is located such that two calmodulins bind to two oxygenase domains, bringing them together (Figure 1.1). Dimerization is further stabilized by the cofactor  $BH_4$ . Holoenzyme assembly is thus the main temporal regulation of the amount of NO produced by those two isozymes.

eNOS and nNOS are also regulated spatially. These isozymes are active when they are associated with the cell membrane. eNOS associates with caveolae when it is

myristoylated and palmitoylated, and while it is there it is constitutively phosphorylated at serine 1179, making it active (56). It is inactive in the cytosol when it lacks phosphorylation at that site. nNOS is also active at the plasma membrane where it localizes through protein-protein interactions (57). The last major sources of e/nNOS regulation are substrate availability, namely arginine and O<sub>2</sub> (58), and feedback inhibition by NO (59).

iNOS has its own forms of regulation. Calmodulin binding to iNOS is so tight that it is considered a subunit more so than a cofactor, and consequently Ca<sup>2+</sup> availability has no effect on induction of NO synthesis (55). Rather, the synthesis and inhibition of iNOS itself are the main sources of regulation (1). In most cell types, iNOS is not expressed until a stimulus induces it. Effective stimulants include lipopolysaccharide (LPS) (60), cytokines such as interleukin 1 or tumour necrosis factor (TNF) (61), and endotoxins. Once activated, iNOS synthesizes copious amounts of NO continuously until it is stopped. One method of down-regulation is feedback inhibition by NO itself through its ability to bind to the heme group, which is the site of catalysis (62). iNOS is also limited by arginine availability (58); arginase is co-induced along with iNOS, ensuring that arginine will deplete so that NO levels will no longer increase after a certain length of time (63). iNOS is eventually degraded by the usual cellular mechanism and once the induction signal is no longer present, it will stop being produced by the cell.

#### **1.1.8 Detection methods**

Several detection methods exist that are specific for one form of NO; others are more general and simply detect NO<sub>x</sub>. 4,5-diaminofluorescein diacetate (DAF-2-DA) is commonly used on cells for the purpose of detection (64). The acetate groups allow it to enter cells, wherein they are cleaved. NO<sub>x</sub> inside the cell – •NO<sub>2</sub>, N<sub>2</sub>O<sub>3</sub>, and other reactive

forms – reacts with DAF-2 in the presence of oxygen, resulting in the formation of a fluorescent product that can be quantified with a microscope. As a probe that only requires 30 minutes to finish reacting, this makes it a convenient detector for changes in NO concentrations in the cell after a stimulus such as lipopolysaccharide.

Nitric oxide analyzers (NOA) are available from Sievers (General Electric) and can be used to detect either NO or  $\text{NO}_2^-$  by chemiluminescence (65). The purge vessel can be filled with acetic acid and 50 mg of sodium iodide. The iodide ions reduce injected  $\text{NO}_2^-$  to NO, with the acid providing protons for the reaction, while the injected solution is carried to the NOA. Inside, the NO is mixed with ozone,  $\text{O}_3$ , and they react to form an excited  $\text{NO}_2^*$  which releases a photon to become  $\text{NO}_2^\bullet$ . The photon is detected in the photomultiplier tube and displayed in the software as a peak; the area under the peak is directly proportional to the number of photons detected, which in turn is directly proportional to the number of NO molecules produced. Therefore, by taking the integral of the peak area and interpolating it into an  $\text{NO}_2^-$  standard curve, one can calculate the concentration of  $\text{NO}_2^-$  originally injected. If NO is being measured directly instead of  $\text{NO}_2^-$  then acid and iodide are not needed; simply water or buffer can be used to fill the purge vessel so that only NO itself will be detected. This can be used for a variety of solutions including cell culture media, exhaled breath, or serum.

The biotin switch assay is a commonly used method to detect S-nitrosylated proteins, developed in 2001 by Jaffrey *et al* (66). In the first step, methyl methanethiosulfonate (MMTS) is added to a sample of S-nitrosoprotein(s) to block free thiols with a methyl group. Once excess MMTS is removed, ascorbate is added to reduce the S-NO bond, leaving newly formed free thiols. Finally, biotin is conjugated to the protein through a short thiol-reactive crosslinker. Disulfide bonds are not affected by this

process. In short, biotin is conjugated to proteins only at sites that were *S*-nitrosylated, making *S*-nitrosoproteins detectable by Western blot through anti-biotin primary antibodies. This method is useful for determining whether a particular protein is able to be *S*-nitrosylated, or for determining the proteome of *S*-nitrosoproteins in serum, among other applications.

These are the most commonly used methods for their respective applications. While they are for the most part effective, they still all have their drawbacks. DAF reacts with radicals inside the cell which are not necessarily  $\text{NO}_x$  (67), and the biotin switch assay is convoluted and has been known to produce false positives (68). Therefore, as NO research continues to develop, so will its detection techniques.

## **1.2 Gold Nanoparticles**

### **1.2.1 History**

Gold nanoparticles (AuNP), also referred to as colloidal gold, have been used for millennia, but it is only in the last ~150 years that they have been extensively characterized and studied (69). The first known cultures to make use of AuNP were ancient Egypt and China (400-500 years B.C.E.) which used the wine-red solution as a dye for glass and ceramic due to its brilliant colour; this is still in practice today. In addition, solutions of AuNP were thought to be medicinal and were drunk to cure a variety of ailments throughout the middle ages and up until the 19<sup>th</sup> century (70).

In 1857 Michael Faraday published the first scientific investigation into the properties of the gold nanoparticles (71). While he was not the first to speculate that the particles were too small to view with the naked eye (69), he was able to estimate them to be in the 10-nm range. He also realized that he could produce them by reducing the  $\text{AuCl}_4^-$  ion. Since then, a variety of methods have been established to synthesize AuNP which will be briefly outlined below.

### **1.2.2 Synthesis**

Many types of nonmetal and metal nanoparticles exist, including iron, copper, silver, cadmium, and platinum (72); however, for the purpose of brevity, only synthesis methods of AuNP will be discussed here. As mentioned above, Faraday was the first person to synthesize AuNP by reducing  $\text{AuCl}_4^-$  with phosphorus in  $\text{CS}_2$  (71). Currently used methods are able to produce nanoparticles of specific sizes and shapes. The Turkevich method (73), as modified by Frens (74), uses trisodium citrate to both reduce aqueous  $\text{AuCl}_4^-$  and stabilize the resultant spherical AuNP. While Turkevich's protocol produced nanoparticles with a 20-nm diameter, Frens was able to vary the ratio of  $\text{AuCl}_4^-$



and citrate to result in nanoparticles ranging from 16 to 147 nm. The method has been further modified by various groups including Grabar *et al* (75) to produce smaller spherical AuNP – in the case of Grabar’s group, 12 nm in diameter.

The seeded growth method is used to control the shape of the AuNP (76). In this protocol,  $\text{AuCl}_4^-$  is mixed with trisodium citrate and the resultant “seed” is mixed in specific proportions with cetyltrimethylammonium bromide (CTAB),  $\text{HAuCl}_4$ , and ascorbic acid. Simply by adjusting the concentrations of each reagent as well as the timing and sequence of each reagent’s addition, one can obtain nanoparticles shaped like triangles, rods of specific aspect ratios, hexagons, cubes, and others (77).

Gold nanoparticles can be produced using reducing agents other than trisodium citrate. The Brust-Schiffrin method utilizes tetraoctylammonium bromide to transfer  $\text{AuCl}_4^-$  to toluene where it is reduced by  $\text{NaBH}_4$  (78). The nanoparticles are commonly protected by the subsequent addition of a monolayer of thiol. Alternatively, top-down methods can be used for synthesis in which a larger material is effectively whittled down to the nanoparticles; these include photolithography and electron beam lithography (79-80).

While this description of AuNP synthesis is not exhaustive, these are some of the most commonly used methods which have been refined over the past 1-2 decades. It is clear that just by using the methods discussed above, one can obtain nanoparticles of any desired size and shape and consequently develop a variety of applications.

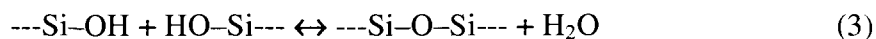
### **1.2.3 PDMS and synthesis of surface gold nanoparticles**

Poly(dimethylsiloxane) (PDMS) is a type of silicone used in many household and industrial products, such as contact lenses and microfluidic devices (81). Its notable features are that it conforms to the shape of its container (82), it is transparent,

inexpensive (81), and it is chemically inert, though it can be made reactive through oxidation if needed. PDMS is prepared by mixing the vinyl-containing, silicon-based monomer with a crosslinker that includes silyl (SiH) groups in the presence of a platinum catalyst and heat (82). It forms a three-dimensional network based on two reactions. The primary reaction occurs between the SiH of the crosslinker and the vinyl group of the monomer, shown in Reaction 1:



The secondary reaction is favoured in a high excess of crosslinker. The Si-H group is hydrolyzed to become Si-OH and this reacts with either another Si-OH or with Si-H to form Si-O-Si chains, as seen in Reactions 2 and 3:



Changing the ratio of monomer to curing agent changes the polymer's properties: for example, adding more crosslinker makes PDMS more rigid. Although it was omitted from Reactions 1-3 for simplicity, each silicon atom is bonded to methyl groups or hydrogen atoms wherever a bond is not shown, making PDMS very hydrophobic and thus inert.

In 2007, Zhang *et al* (83) published a new technique which allows AuNP to be formed on the surface of PDMS. Simply by incubating a 0.5% (w/v) solution of  $\text{AuCl}_4^-$  on the surface of the pre-formed polymer for 24-48 hours, they were able to obtain a pink layer of nanoparticles on the surface. Their explanation is that excess SiH groups acted as the reducing agent, and the nanoparticles embedded into the pores between crosslinker molecules. Adjusting the  $\eta$  – the ratio of curing agent to monomer – resulted in

morphology and size variation; for example, a ratio of 0.06 led to the formation of spherical nanoparticles with an average diameter of 7 nm, while a ratio of 0.1 resulted in variably-shaped nanoparticles averaging 13 nm in diameter.

The Mutus lab recently optimized this process to achieve a greater density of AuNP on the surface of the PDMS (unpublished observations). PDMS was polymerized using a ratio of either 0.02 or 0.04 and then  $\text{AuCl}_4^-$  and trisodium citrate were simultaneously added to the surface. With this method the citrate acts as the reducing agent and the large pores caused by the low  $\eta$  gives the nanoparticles a site to embed. The colour of the solution is a darker red compared to when there is a lack of citrate, indicating that a higher density of nanoparticles is present on the PDMS surface.

#### **1.2.4 Localized surface plasmon resonance**

The characteristic brilliant colour of gold nanoparticles is a property unique to materials in the 1-100 nm range (84). They behave neither as bulk objects nor as single molecules. At this point, their identities becomes negligible and the only factors affecting their colour are size, shape, and the dielectric constants of the nanoparticles and the surrounding media (85). Gold has d-orbital electrons that travel more freely than those of lower orbitals. Since the AuNP are smaller than the wavelength of light, passing light waves are able to influence the positions of all the d electrons of a nanoparticle, rather than individual atoms. The light causes them to cohesively oscillate between ends of the nanoparticles, creating a dipole (84). This is known as localized surface plasmon resonance (LSPR).

The frequency of the oscillation lies in the visible region of the light spectrum and absorbs strongly at characteristic wavelengths. In the case of unmodified 11-nm spherical AuNP in water, the LSPR absorption peaks at 520 nm. The exact size of the nanoparticles

does not greatly affect this peak. However, if the nanoparticles were rod-shaped then the resonance is more complicated, as there is one transverse and one longitudinal plasmon resonance, each with their own absorbance peak (86). Altering the aspect ratio greatly influences the overall oscillation frequency and therefore the colour. Thus, each shape of AuNP has its own characteristic LSPR absorption.

The presence of other molecules on the surface is the factor which has the greatest effect on the LSPR absorption for nanoparticles of given size and shape. Sulfur has a strong attraction to AuNP. It has been shown with x-ray crystallography that while the distance between gold atoms within a nanoparticle is 2.8-3.1 Å, the distance between gold and sulfur atoms is 2.2-2.6 Å (87). The bond is not covalent, but it is far stronger than electrostatic, so that thiol-containing molecules are stably attached to the surface. Each sulfur atom binds between two gold atoms of the nanoparticle. The presence of bonded molecules changes the electron density on the surface of the nanoparticles and consequently a small red-shift in absorbance peak is seen (84). Many of the applications of AuNP involve coating the surface with molecules via their thiols, so this phenomenon is frequently observed.

When molecules are added to AuNP such that they become linked together into 3-dimensional networks, the LSPR absorption undergoes a more extensive shift (88). The crosslinking molecules act as conductors for the electrons, with interparticle distance (determined by crosslinker length) controlling the conductivity (89). Consequently, the plasmon resonance becomes synced for all of the connected AuNP, leading to a new LSPR absorption. Specifically, the absorbance peak will broaden and red-shift, though the extent will depend on the nature and length of the connecting molecules. This colour change is commonly exploited in applications of AuNP.

### 1.2.5 Applications of AuNP

Gold nanoparticles are brightly coloured, are able to undergo colour change when crosslinked, and are visible in transmission electron microscopy (TEM). They can be synthesized in solution or on a surface, are dense enough to centrifuge, and enhance the fluorescence of nearby molecules (70,90). They are similar in size to some proteins and are non-cytotoxic (91). These properties make them useful in a large variety of applications. Here, only a selection will be discussed with the intention of portraying the versatility of AuNP.

AuNP are becoming important assets in bioimaging. In one example, angiogenesis was monitored in rabbits using AuNP specifically targeted to neovasculature (92). They were made paramagnetic and bonded to molecules reactive to  $\alpha_v\beta_3$  integrins. These targeted and paramagnetic nanoparticles were injected into rabbits fed high-cholesterol diets, and control rabbits on a normal diet. MRI was done using typical hospital protocol. The presence of nanoparticles greatly enhanced the visibility of the newly forming vasculature and the researchers could detect a 47% increase in angiogenesis in cholesterol-fed rabbits over controls. The MRI process took about 2 hours, allowing rapid detection of one of the warning signs before a stroke or heart attack; this experimental design may also be used to image angiogenesis in tumours.

Surface-enhanced Raman scattering is an advancement of Raman spectroscopy (93). The surface plasmons from nanoparticles become coupled to the molecule of interest, which enhances the Raman signal up to  $10^{14}$  times (94). Once again the shape of the nanoparticles plays a role; for example, rod-shaped nanoparticles cause higher signals than spherical ones (95). Regardless of the shape, the sensitivity is so highly improved that single molecules become detectable. This is not only important for the typical

chemistry done, but the heightened sensitivity makes it useful in biological settings, for example the detection of specific molecules in low concentrations. Thus, the use of AuNP increases the scope of experiments to which Raman scattering can be applied.

The colour change exhibited by clusters of AuNP has been exploited to various ends. The reaction between two complimentary DNA strands, each conjugated to AuNP, brings the nanoparticles close enough together to induce the LSPR absorption shift described above (96). When reflected light is measured from this reaction, using ~50-nm AuNP, the detection limit of this assay is 10 fmol of DNA. While this is sensitive, the disadvantage is that many nanoparticles must react before a detectable red-shift in absorbance occurs. More recently, another group has developed a similar assay in which scattered light was measured instead of reflected light by spotting the reaction on a waveguide (97). This modification in the detection method is 4 orders of magnitude more sensitive, reaching zeptomole quantities, which means the DNA in question does not need to be amplified in PCR before it can be detected. This assay can be useful to a variety of scientists, such as academic labs doing cloning, or clinical labs identifying certain bacteria for rapid diagnosis.

While this list is not comprehensive, it is clear that AuNP can be easily adapted for many uses because of the unique properties endowed on molecules of 1-100 nm size. Physics, chemistry, and biology labs all have their own applications for nanoparticles. In addition, AuNP are gaining more importance each year in clinical labs through their usefulness in imaging, diagnosis and treatment of infections and cancer. With this diversity in applications, it is clear that AuNP research is leading the way for new technology and will continue to do so for the foreseeable future.

## **CHAPTER 2<sup>1</sup>**

### **ISOFORM-SPECIFIC DIFFERENCES IN THE NITRITE REDUCTASE ACTIVITY OF NITRIC OXIDE SYNTHASES UNDER HYPOXIA**

---

<sup>1</sup> Reproduced with permission from Mikula *et al.* (2009). *Biochem J.* 418(3):673-82. ©2009 Portland Press Ltd.

## 2.1 Introduction

Nitrite has been observed to promote the same physiological effects as  $\text{NO}^2$ , and there is an increasing list of enzymes which catalyze the reduction of  $\text{NO}_2^-$  to NO to allow this to occur (31). In addition to that, eNOS has been shown to be protective in hypoxia (ischemia, stroke) while iNOS is cardioprotective and nNOS has no apparent role in hypoxia. This led Slama-Schwok and coworkers to examine whether eNOS is able to reduce  $\text{NO}_2^-$  in the absence of oxygen, and they gained evidence to support this hypothesis (98-99).

The goal of the present study was to characterize the roles of all three NOS isozyms in the reduction of  $\text{NO}_2^-$  to NO under hypoxia and anoxia. The full-length enzymes as well as the oxygenase domains alone (which contain the heme moiety) and the reductase domains alone were used in various studies performed by the Mutus lab or Slama-Schwok's group. In addition, endothelial cells were exposed to different levels of oxygen tension, with or without supplemental nitrite, and the NO released from the cells was detected after different lengths of time. It was found that eNOS was the only isozyne able to reduce the nitrite, and the reductase domain alone had no effect. Additionally, the endothelial cells released more NO under hypoxia compared to basal levels while anoxia caused the highest increase. These data provide a new role for eNOS as a source of NO in pathological conditions in the body, on top of its main role in a normal state.

## 2.2 Materials and Equipment

### 2.2.1 Materials

---

<sup>2</sup> Abbreviations used in this chapter: 7-NI, 3-bromo-7-nitroindazole;  $\text{BH}_4$ , tetrahydrobiopterin; ECM, endothelial cell media; eNOS, endothelial nitric oxide synthase; eNOSred, eNOS reductase domain; HDMEC, human dermal microvascular endothelial cells; iNOS, inducible nitric oxide synthase; L-NMMA,  $\text{N}^G$ -monomethyl-L-arginine; NADPH, nicotinamide adenine dinucleotide phosphate; nNOS, neuronal nitric oxide synthase; nNOSred, nNOS reductase domain; NO, nitric oxide;  $\text{NO}_2^-$ , nitrite;  $\text{NO}_3^-$ , nitrate; NOA, nitric oxide analyzer;  $\text{NO}_x$ , nitric oxide and related species.



3-bromo-7-nitroindazole: Cayman Chemical, Burlington, ON

Argon Grade 5 300 SZ: Praxair Distribution, Division of Praxair Canada Inc., Mississauga, ON

Calcium chloride ( $\text{CaCl}_2 \cdot 6\text{H}_2\text{O}$ ): Sigma-Aldrich Canada, Oakville, ON

Calmodulin: Sent from Dr. Rajendra Sharma, University of Saskatchewan, Saskatoon, SK

Endothelial cell medium (ECM): ScienCell, Carlsbad, CA

Endothelial nitric oxide synthase (eNOS), eNOS reductase domain (eNOSred), neuronal NOS (nNOS) and nNOSred: purified by and sent from Dr. Anny Slama-Schwok, École Polytechnique, Paris, France

Human dermal microvascular endothelial cells (HDMEC): ScienCell, Carlsbad, CA

L-arginine: Sigma-Aldrich Canada, Oakville, ON

Nicotinamide adenine dinucleotide phosphate (NADPH): Sigma-Aldrich Canada, Oakville, ON

$\text{N}^G$ -monomethyl-L-arginine (L-NMMA): Sigma-Aldrich Canada, Oakville, ON

Oxygen 2ppm balance argon, size 30, 0.8M3 certified: Praxair Distribution, Division of Praxair Canada Inc., Mississauga, ON

Oxypurinol: Sent from Dr. Anny Slama-Schwok, École Polytechnique, Paris, France

Sodium chloride ( $\text{NaCl}$ ): ACP Chemicals, Montreal, PQ

Sodium iodide ( $\text{NaI}$ ): Sigma-Aldrich Canada, Oakville, ON

Sodium nitrate: Sigma-Aldrich Canada, Oakville, ON

Sodium nitrite: Sigma-Aldrich Canada, Oakville, ON

T-75 tissue culture flasks: Sarstedt Inc., Montreal, PQ

Tetrahydrobiopterin ( $\text{BH}_4$ ): Sent from Dr. Guy Guillemette, University of Waterloo, Waterloo, ON

Tris hydroxyaminomethane and Tris-HCl: Sigma-Aldrich Canada, Oakville, ON

TrypLE™ trypsin: Invitrogen Canada Inc., Burlington, ON

### **2.2.2 Equipment**

2 ml glass vials with black polypropylene screw top and septa: Supelco, Bellefonte, PA

27.5G syringe needles: Becton-Dickenson, Franklin Lakes, NJ

Agilent 8453 UV-VIS Spectrophotometer: Agilent Technologies Canada Inc., Mississauga, ON

Bright-Line Hemacytometer: Hausser Scientific, Horsham, PA, USA

Hamilton<sup>®</sup> syringe, 1800 series gastight, model 1801RN: Sigma-Aldrich Canada, Oakville, ON

Jouan CR3i Centrifuge: Jouan Inc., Winchester, VA

Nikon TMS microscope: Nikon, Japan

NuAire Biological Safety Cabinet Class II Type A/B3: Thermo Electron Corp. Canada, Burlington, ON

NuAire Direct Heat AutoFlow CO<sub>2</sub> Automatic Air-Jacketed Incubator: Thermo Electron Corp. Canada, Burlington, ON

Sievers 280i Nitric Oxide Analyzer: General Electric Canada, Mississauga, ON

## **2.3 Methods**

### **2.3.1 Cell culture**

HDMEC were grown in ECM containing basal medium, 5% fetal bovine serum, 1% endothelial cell growth supplement, and 1% penicillin/streptomycin solution. Cells were maintained in T-75 culture flasks at 37°C in 5% CO<sub>2</sub> and grown to 80% confluence.

### **2.3.2 Treatment of cells**

Once at confluence, the cells' media were decanted and kept aside. Cells were trypsinized and concentrated by centrifugation at 1700 rpm for 5 minutes. They were then resuspended in either old media or fresh ECM with added 10  $\mu$ M NO<sub>2</sub><sup>-</sup> and each suspension was aliquotted into septa-topped screw cap glass vials, 0.5 ml per vial. The vials were incubated in a 37°C water bath for the duration of the experiment. In total there were 36 vials of cells used in each experiment. One-third had their caps loosely screwed

on to permit oxygen entry (normoxia). One-third had their caps tightly screwed and were blown with argon, via syringe needles inserted through the septa, for 10 minutes followed by incubation for 0, 4, 8, 12, 16, or 20 minutes (anoxia). Finally, one-third had their caps tightly screwed and were blown with 2 ppm oxygen in argon for 10 minutes and then incubated for 0, 6, 12, 16 or 20 minutes (hypoxia).

### **2.3.3 Inhibitor treatment of cells**

In another experiment, 80% confluent cells were trypsinized, centrifuged and resuspended in fresh media supplemented with 10  $\mu\text{M}$  nitrite. The cells were subdivided into suspensions treated with either L-NMMA (500  $\mu\text{M}$ ), 7-NI (10  $\mu\text{M}$ ), oxypurinol (100  $\mu\text{M}$ ) or left untreated as a control group. These suspensions were distributed into glass vials as described above and incubated in anoxia for 0 or 15 minutes after argon treatment. An additional group of vials contained media and 10  $\mu\text{M}$  nitrite but no cells; these were also exposed to anoxia for 0 or 15 minutes after argon exposure.

### **2.3.4 Nitric oxide detection**

Following the specified lengths of incubation under normoxia, hypoxia or anoxia, 10  $\mu\text{l}$  of media were injected via a Hamilton gas-tight syringe into a Sievers nitric oxide analyzer containing acetic acid and sodium iodide. The average of two repeat injections was taken and compared to a nitrite standard curve in order to determine the amount of NO detected.

### **2.3.5 Nitric oxide detection from *in vitro* NOS isoforms**

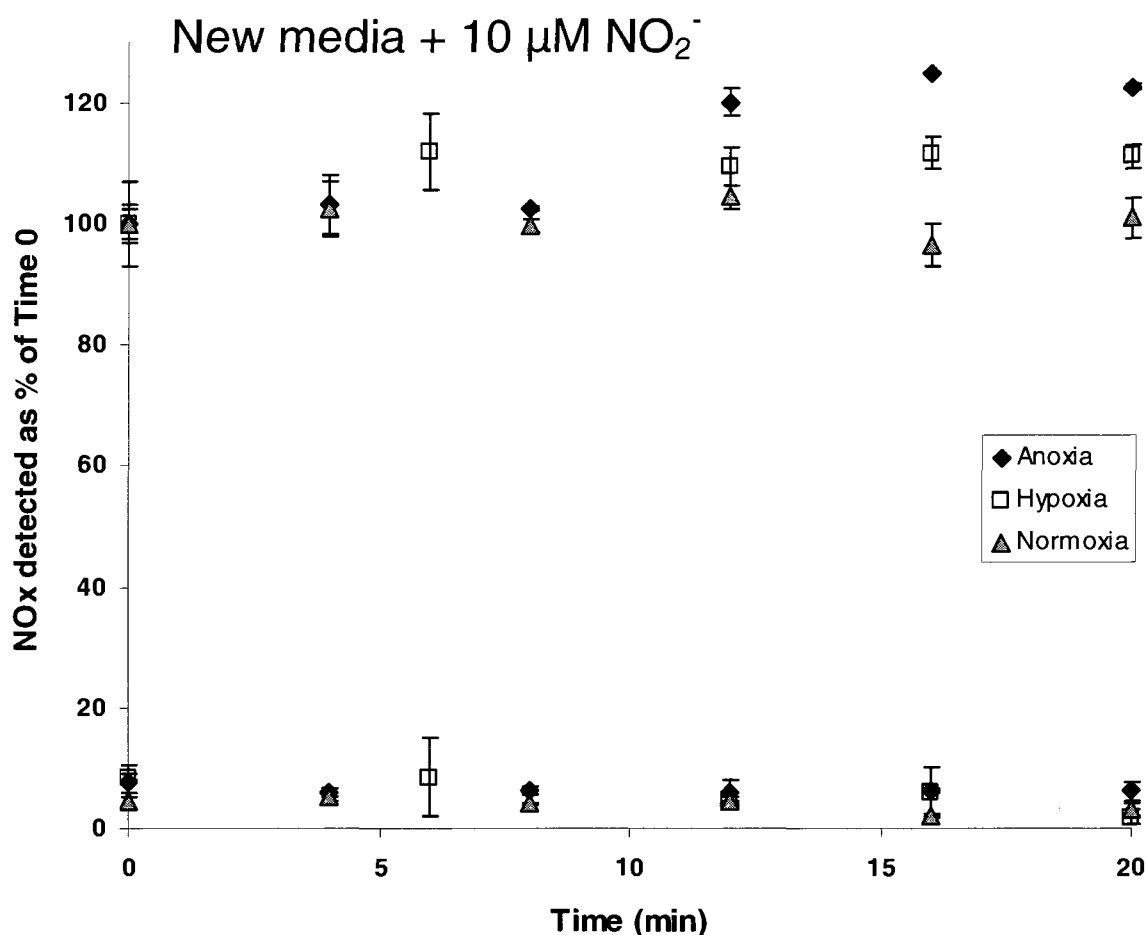
Samples of eNOS, eNOSred, nNOS, and nNOSred were suspended in 50 mM Tris buffer with 150 mM NaCl (pH 7.5). These were quantified in the UV-VIS spectrophotometer using the extinction coefficients 100 000  $\text{M}^{-1}\text{cm}^{-1}$  at 396 nm for eNOS and nNOS, and 23 300  $\text{M}^{-1}\text{cm}^{-1}$  at 455 nm for eNOSred and nNOSred. All concentrations

were adjusted to 10  $\mu\text{M}$  using the same buffer. These were aliquotted into the glass vials described above. Final concentrations of 10  $\mu\text{M}$  nitrite, 10  $\mu\text{M}$  calmodulin (quantified by the UV-VIS spectrophotometer with the extinction coefficient  $3006 \text{ M}^{-1}\text{cm}^{-1}$  at 257 nm), 1mM calcium, 40  $\mu\text{M}$   $\text{BH}_4$ , and 1 mM arginine were added such that each vial had a final volume of 500  $\mu\text{l}$ . Upon addition of 100  $\mu\text{M}$  NADPH the vial caps were screwed on tightly and blown with argon for 10 minutes; these were incubated for 0 or 15 minutes thereafter. Following incubation, 1 ml of the air above the samples was injected into the NOA in duplicate. NO production was calculated from a nitrite standard curve. Control vials had no NADPH added; in addition, other samples for each isozyme contained 10  $\mu\text{M}$  nitrate instead of nitrite.

## 2.4 Results

### 2.4.1 NO release by endothelial cells under normoxia, hypoxia or anoxia

*In vitro* experiments performed by Dr. Slama-Schwok and colleagues showed that eNOS is able to reduce nitrite to NO when oxygen is unavailable for its *de novo* synthesis from arginine. nNOS has a more limited capacity for this and iNOS is unable to do so. To further confirm these observations by using a cell system, we chose endothelial cells which express eNOS as its NO-producing enzyme (1). 80% confluent cells were trypsinized, concentrated and resuspended in media. Half of the cells were replaced into the old media decanted before trypsin application, and half of the cells were replaced into new media which had 10  $\mu$ M nitrite supplementation. Each group was subjected to treatment with argon (anoxia), 2ppm O<sub>2</sub> in argon (hypoxia) or room air (normoxia) for various lengths of time. As shown in Figure 2.1, when there was no nitrite added to the cells, there was no measurable change in NO<sub>x</sub> detected by the NOA over the 20-minute time course for any of the three conditions. There was also no significant change exhibited by the cells exposed to normoxia in the presence of nitrite. However, an 11% increase in NO<sub>x</sub> levels was detected under hypoxia and a 22% increase was observed from the cells exposed to anoxia, confirming that a component of the cells was reducing nitrite to NO in the absence of oxygen. Error bars on the data points were the calculated standard deviations from two repeat injections of media into the NOA.

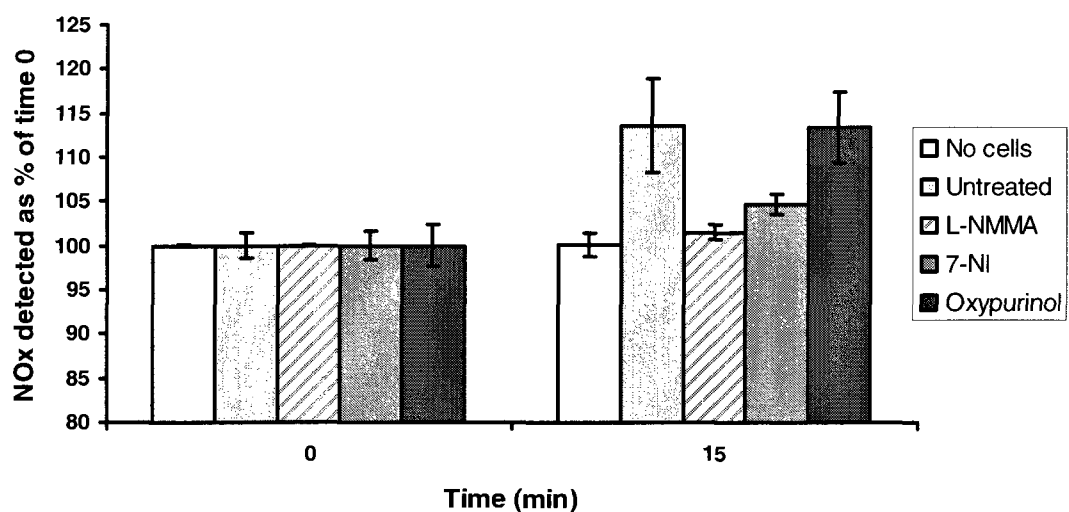


**Figure 2.1** Detection of NO release from nitrite under normoxia, hypoxia and anoxia

Endothelial cells were trypsinized, concentrated and resuspended in either the media in which they were grown or in fresh media supplemented with 10  $\mu\text{M}$  nitrite. These were subjected to treatment with argon (anoxia), 2ppm  $\text{O}_2$  in argon (hypoxia) or incubated in room air (normoxia) for various lengths of time. Results show that cells placed in the old media displayed no change in  $\text{NO}_x$  production over time regardless of oxygen levels. When exposed to 10  $\mu\text{M}$  nitrite, in normal oxygen conditions (gray triangles) there was little change in  $\text{NO}_x$  detected. However, after incubation in 2ppm  $\text{O}_2$  in argon (white squares), levels of  $\text{NO}_x$  increased by 11%. Anoxic cells (black diamonds) released the most  $\text{NO}_x$  with a 22% increase over normoxia.

#### **2.4.2 Effect of inhibitors on NO release by endothelial cells under anoxia**

Since the endothelial cells contain several enzymes which may be responsible for the reduction of nitrite to NO under anoxia, we treated cells with different inhibitors to determine the correct enzyme based on their effects. L-NMMA is a non-specific NOS inhibitor; 7-NI targets the specific isozyme nNOS and to a lesser extent iNOS; and oxypurinol inhibits xanthine oxidase. Glass vials were prepared as described above, with fresh media and 10  $\mu$ M nitrite. There were five categories: no cells, cells that were not treated with any inhibitor, and cells treated with one of the three inhibitors listed. After 10-minute argon exposure, 10  $\mu$ l of media was injected into the NOA in duplicate either immediately or following 15 additional minutes of anoxia. Results after the 15 minutes are shown in Figure 2.2 as a percentage of time 0, which was set to 100% for each group of vials. There was no change in NO<sub>x</sub> detected by the NOA in the absence of cells. Untreated cells had a similar NO<sub>x</sub> increase as that seen in Figure 2.1. Oxypurinol had no effect on the cells' nitrite reduction; as an inhibitor specific to xanthine oxidase, it shows that this enzyme is not involved in the process. The non-specific NOS inhibitor L-NMMA nearly eliminated the increase in NO<sub>x</sub> while the nNOS- and iNOS-specific 7-NI reduced it. This verifies the identification of NOS as the responsible enzyme for nitrite reduction but does not conclusively point to eNOS alone. Data are represented as the average of two repeat injections and their calculated standard deviations.



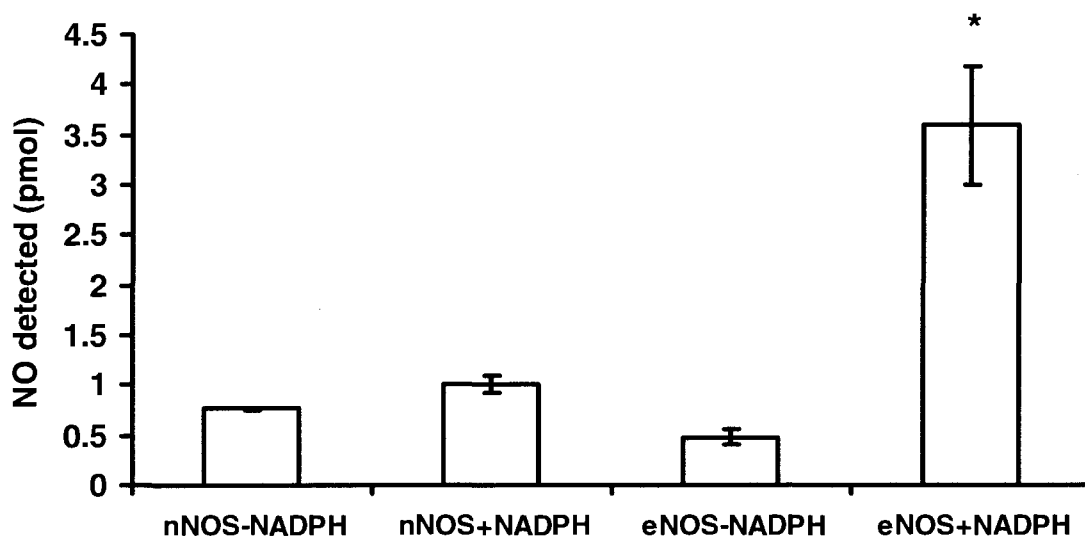
**Figure 2.2 Effect of inhibitors on nitrite reduction under anoxia**

Endothelial cells were trypsinized and distributed into glass vials as described above. Media was supplemented with 10  $\mu$ M nitrite and either L-NMMA, 7-NI, oxypurinol or no treatment. In addition, vials containing cell-free media and nitrite were included. These were exposed to anoxia and incubated for 0 or 15 minutes and media was injected into the NOA. As shown in the figure, in the absence of cells (white), there was no difference in NO<sub>x</sub> detected before or after anoxia treatment. Oxypurinol-treated cells (black) exhibited the same trend as untreated cells (light gray) indicating a lack of involvement by xanthine oxidase. Nitrite reduction was somewhat inhibited by 7-NI (dark gray) and almost completely inhibited by L-NMMA (gray hatched) which shows that NOS is the responsible enzyme.



### **2.4.3 NO formed by *in vitro* NOS or NOS reductase domain under anoxia**

As stated in 2.4.1 above, Dr. Slama-Schwok's group showed that eNOS is efficient at reducing nitrite to NO, and that nNOS has a limited ability. We then sought to determine whether the entire enzyme or simply the reductase domain was necessary to perform this reduction. Vials were prepared which contained 10  $\mu$ M eNOS, eNOSred, nNOS or nNOSred; 10  $\mu$ M nitrite or nitrate; and all of the required cofactors except NADPH. Half of the vials did not have NADPH added at all as a negative control; these were blown in argon and then incubated for 15 minutes. The other half had NADPH added immediately before the argon treatment. These were then incubated for 15 minutes as well. After the incubation period, 1 ml of air above the solution was injected into the NOA. There were no detectable peaks generated from either eNOSred or nNOSred, and therefore they did not produce NO under anoxia in the presence of all cofactors. Wild-type nNOS and eNOS released a low basal level of 0.76 and 0.48 pmol of NO, respectively, in the absence of NADPH (Figure 2.3). However, in the presence of all cofactors including NADPH, NO levels were  $1.0 \pm 0.08$  pmol for nNOS, a ~1.3-fold increase, and  $3.6 \pm 0.59$  pmol for eNOS which corresponds to a ~7.5-fold increase. NO was not detected in any condition in which nitrate was present rather than nitrite. Data is presented as the average of two repeat injections and their associated standard deviations.



**Figure 2.3** Detection of NO released by nNOS and eNOS under argon

Vials were made containing nitrite, calmodulin, calcium,  $\text{BH}_4$ , arginine and either nNOS or eNOS in 50 mM Tris buffer. These were blown with argon either immediately or after the addition of 100  $\mu\text{M}$  NADPH and the released NO was detected in duplicate using the NOA. nNOS in the presence of NADPH exhibited a ~1.3-fold increase in NO production compared to its control, while eNOS in the presence of NADPH showed a ~7.5-fold increase (\* $P < 0.05$ ). No NO was released in the presence of nitrate.

## 2.5 Discussion

Dr. Slama-Schwok's group had shown in two prior publications that eNOS is able to reduce nitrite to NO in the absence of oxygen, using both purified enzymes and endothelial cells (98-99). Here, they further characterized this ability for each isozyme as well as studied the oxygenase domain alone. They found that eNOS was the only isoform that efficiently released NO, while nNOS only released trace amounts (31). In addition they showed that while the oxygenase domain alone released 1.5  $\mu\text{M}$  NO in the presence of cofactors and high  $\text{NO}_2^-$ , this was not as high as the wild-type enzyme at 2.2  $\mu\text{M}$ . They had previously studied the role of arginine in the reduction and determined that it was necessary for the reaction but not a substrate of NOS in the absence of oxygen. The dependence on both arginine and the full enzyme with cofactors show that the structure of the enzyme is critical for maximum release of NO from  $\text{NO}_2^-$ , and infer that structural differences between the isozymes are the reason that only eNOS is capable of performing this reduction.

With these data, we sought to confirm the role of eNOS using endothelial cells. First, we performed experiments to test the release of NO in the absence of oxygen using cells in three conditions: normoxia, hypoxia, or anoxia. Cells were also further divided into treatment with 10  $\mu\text{M}$  nitrite or no nitrite added. Figure 2.1 shows that nitrite was required for an increase in NO release, and furthermore that the complete lack of oxygen resulted in the highest change. The 10-minute incubation in argon was sufficient to drive out oxygen, and the septa were sealed with tape afterwards. In addition, each vial of cells was only used once, with a different vial in place for each time point. These precautions were done to ensure that there would be no holes in the septa to allow the entry of oxygen, ruling out *de novo* synthesis as an explanation for the increase in nitrite.

Therefore, this experiment enabled the conclusion that nitrite was being utilized by endothelial cells to release NO in the absence of oxygen. Since 10  $\mu$ M nitrite is a physiologically relevant level, these results are significant to the body in conditions such as ischemia (30).

The next step was to verify that eNOS was responsible for the reduction by the cells, rather than xanthine oxidase, cytochrome c oxidase, or another NOS isoform. Sets of cells were treated with inhibitors to this end. If the NO release could be attenuated by an eNOS-specific inhibitor, but not by the others, then it points to eNOS as the reducing enzyme. The inhibitors used were L-NMMA, which is a non-specific inhibitor of all three NOS; 3-bromo-7-nitroindazole, which is potent against nNOS and less potent against iNOS; and oxypurinol, specific against xanthine oxidase. As seen in Figure 2.2, NOS was clearly the responsible enzyme since almost all NO<sub>x</sub> release was attenuated by L-NMMA, and 7-NI was a strong inhibitor as well. If eNOS were the sole isozyme performing the reduction, then 7-NI should not have had any effect. However, the IC<sub>50</sub> for nNOS, iNOS and eNOS are 0.17, 0.29, and 0.86  $\mu$ M, respectively (100). This means that while it is the most powerful against nNOS, it is not ineffective against eNOS. More in-depth studies are thus needed to conclusively state that eNOS is the one isozyme that can reduce nitrite to NO in HDMEC.

The data presented in Figures 2.1 and 2.2 are the results of single experiments. While each experiment was done multiple times, the exact amounts of NO<sub>x</sub> detected varied each time. Therefore, the graphs represent the typical results obtained and show the trend, namely that in the presence of nitrite, hypoxia resulted in increased NO<sub>x</sub> detected and anoxia led to the highest increase. The control in the inhibitor experiment

further verifies that the amount of NO released is substantially higher (15-22% increase) than original levels 15 minutes after argon treatment.

The final experiment that we contributed to this publication was a comparison between wild-type and reductase domains of eNOS and nNOS for NO release in the same circumstances as the endothelial cells. eNOS, eNOSred, nNOS or nNOSred were placed into vials containing calcium, calmodulin, arginine, BH<sub>4</sub> and 10 μM nitrite. As described in the previous papers by Slama-Schwok *et al*, it is necessary to add arginine because it induces a conformational change in eNOS necessary for it to carry out the reduction (98). Control vials had no NADPH added, and test vials had 100 μM NADPH added immediately before the 10-minute argon treatment and subsequent 15-minute incubation. In addition, 10 μM NO<sub>3</sub><sup>-</sup> was added to half the vials rather than NO<sub>2</sub><sup>-</sup> to determine whether NOS can reduce it to NO as xanthine oxidase does.

There was no signal from any of the vials containing nitrate which indicates clearly that NOS is not able to reduce it despite other heme-containing enzymes' ability to do so. Those vials can also be considered negative controls for nitrite. The complete lack of NO detected from vials without 10 μM NO<sub>2</sub><sup>-</sup> confirms that nitrite is the sole substrate for NO generation under anoxia.

Figure 2.3 shows the results of wild-type nNOS and eNOS. When no NADPH is added there is a basal amount of NO released by both isozymes. This may correspond to one turnover of the reaction, which cannot be repeated unless NADPH reduces the Fe(III) that forms during the nitrite reduction (31). Consequently, the addition of NADPH results in a very small increase in NO released by nNOS, and a statistically significant 7.5-fold increase by eNOS. This supports the data by Slama-Schwok's group that eNOS is the only isozyme that can efficiently reduce the nitrite. In addition, neither reductase domain

was able to catalyze the reaction alone; there was no signal in the NOA when they were treated with nitrite or nitrate. Given that the reductase domain alone cannot reduce nitrite, and the oxygenase domain alone has only a limited ability to do so, the hypothesis that the overall structure of eNOS is critical to the reduction of nitrite to NO has been supported by these experiments.

One key difference between the experiments with the cells and the purified enzymes was the method of NO detection. When simply eNOS or nNOS were used, the headspace above the solution was injected into the NOA, which contained the same Tris buffer as the solution. Therefore, only NO itself was being measured in that experiment since it is a gas. On the other hand, in both experiments using the endothelial cells, 10  $\mu$ l of media were injected into the NOA filled with acetic acid and iodide. This means that both nitrite and NO were able to be detected. During the minutes of treatment with argon or 2 ppm O<sub>2</sub> some of the nitrite added to the media would have had time to enter the cells. The peaks displayed by the NOA at time 0 in all cases represent the nitrite that was not internalized. During the later time points of hypoxia and especially anoxia some of the internalized nitrite was likely reduced to NO, which then diffused back out of the cells. Therefore, in these cases, the NOA had detected non-internalized nitrite plus NO that diffused out of the cells but did not yet go into the gas phase in the headspace. This would explain the increase in NO<sub>x</sub> over time in hypoxia/anoxia as well as the fact that only picomole amounts of NO were detected. Although this method of measuring NO is less direct than injecting headspace into the NOA, it nevertheless supports the other data that eNOS can reduce nitrite to NO in the absence of oxygen.

In summary, we have shown along with our collaborators, using purified enzymes as well as endothelial cells, that wild-type eNOS is the only NOS isozyme capable of

reducing nitrite to NO in anoxia. The reductase domain alone does not achieve this, and the oxygenase domain only does so in a limited capacity, with the whole enzyme and all its cofactors required for maximal reduction. Taken with the necessity for non-substrate arginine it can be inferred that the three-dimensional structure of eNOS allows it to be the specific isoform involved in hypoxic response. It is logical because oxygen is transported by hemoglobin in the blood stream and since endothelial cells line the blood vessels they would be among the first cells to detect a decrease in oxygen. Therefore, they would be appropriate agents to elicit an emergency response via the effects of NO, such as increasing blood flow, in conditions of acute hypoxia such as ischemia. The data support this hypothesis although further examination is needed.

Hypoxia is a dangerous phenomenon that many people experience at some point in their lives. This may be from a stroke, atherosclerosis or other form of ischemia, or even a sharp change to a high altitude. Consequently, ongoing research is necessary to understand the body's responses so that doctors can ameliorate the process in more severe cases. The identification of eNOS as an enzyme involved in response thus may have important implications in medicine.

## CHAPTER 3<sup>3</sup>

### DISULFIDE-LINKED, GOLD NANOPARTICLE-BASED REAGENT FOR DETECTING SMALL MOLECULAR WEIGHT THIOLS

---

<sup>3</sup> Reproduced with permission from Durocher *et al.* (2009). *J Am Chem Soc.* 131(7):2475-7. ©2009 American Chemical Society.



### 3.1 Introduction

As described in Chapter 1, LMWT<sup>4</sup> circulate in the blood and regulate the redox of proteins – the ratio of reduced to oxidized thiols (36). LMWT are also critical reservoirs for NO by *S*-nitrosylation (38). By carrying an NO equivalent the RSNO extends its lifetime and is able to transport it to where it is needed, transferring it to proteins by transnitrosylation (52). For example, RSNOs ameliorate NO-based platelet aggregation inhibition but when the NO is transferred to albumin and the thiols are free, platelet aggregation occurs more readily (101). In addition, the LMWT have other important functions when the thiols are free, including the promotion of T cell proliferation via regulation of interleukin-2 (36).

Both the concentrations and the redox status of thiols (LMWT and HMWT) are crucial for the maintenance of homeostasis in the blood. However, there is a distinct lack of fast, high-throughput methods to quantify these. Current methods of LMWT quantification require the use of high-performance liquid chromatography or capillary electrophoresis, followed by photometric or fluorescent detection (102-106). While this protocol has high sensitivity, it is a time-consuming, multi-step process. Here, we have developed a new reagent that specifically reacts only with free thiols of LMWT ~310 Da or smaller. The reagent is prepared in minutes and the reaction with thiols can be complete within a few minutes. The rate of the reaction depends on the size as well as the concentration of thiol. This makes it the most rapid detection system to date with ideal

---

<sup>4</sup> Abbreviations used in this chapter:  $\beta$ -ME,  $\beta$ -mercaptoethanol; AuNP, gold nanoparticles; BSA, bovine serum albumin; DMSO, dimethyl sulfoxide; DSP, dithiobis(succinimidyl propionate); DTNB, 5,5'-dithiobis(2-nitrobenzoic acid); DTT, dithiothreitol; GSH, reduced glutathione; GSSG, oxidized glutathione; HAuCl<sub>4</sub>, gold (III) chloride; HMWT, high molecular weight thiols; LMWT, low molecular weight thiols; NaSH, sodium hydrosulfide; PDI, protein disulfide isomerase; RSNO, *S*-nitrosothiols.

specificity. In addition, the synthesis of a similar reagent to detect LMWT + HMWT was attempted.

## **3.2 Materials and Equipment**

### **3.2.1 Materials**

5,5'-dithiobis(2-nitrobenzoic acid) (DTNB): Sigma-Aldrich Canada, Oakville, ON

$\beta$ -mercaptoethanol: Fluka/Sigma-Aldrich Canada, Oakville, ON

Bovine serum albumin, lyophilized powder (BSA): Sigma-Aldrich Canada, Oakville, ON

Cysteinyl-tyrosine: Genscript Corp., Piscataway, NJ

Dimethyl sulfoxide (DMSO): ACP Chemicals, Montreal, PQ

Dithiobis(succinimidyl propionate) (DSP): Fisher Canada, Nepean, ON

Dithiothreitol (DTT): MP Biomedicals, Solon, OH

GGGC, GGGGC, GGGGGC and GGGGGGC peptides: Genscript Corp., Piscataway, NJ

Glutathione, oxidized, lyophilized powder (GSSG): Sigma-Aldrich Canada, Oakville, ON

Glutathione, reduced, lyophilized powder (GSH): Sigma-Aldrich Canada, Oakville, ON

Gold (III) chloride ( $\text{HAuCl}_4$ ): Sigma-Aldrich Canada, Oakville, ON

Insulin  $\alpha$ -chain, recombinant human: Sigma-Aldrich Canada, Oakville, ON

L-cysteine: Fluka/Sigma-Aldrich Canada, Oakville, ON

Potassium phosphate monobasic: ACP Chemicals, Montreal, PQ

Potassium phosphate dibasic: ACP Chemicals, Montreal, PQ

Sodium hydrosulfide ( $\text{NaSH}$ ): Sigma-Aldrich Canada, Oakville, ON

Trisodium citrate: Sigma-Aldrich Canada, Oakville, ON

### **3.2.2 Equipment**

Acrylic square cuvettes: Sarstedt, Montreal, PQ

Agilent 8453 UV-VIS Spectrophotometer: Agilent Technologies Canada Inc., Mississauga, ON

Hettich EBA12 desktop centrifuge: Fisher Scientific, Mississauga, ON

Freeze dry system/Freezone® 4.5 lyophilizer: Labconco, Kansas City, MO and Maxima® C Plus vacuum pump: Fisher Scientific, Mississauga, ON

Millipore Milli-Q synthesis Q-Gard 2 purification pack: Millipore, Etobicoke, ON

Philips CM-10 Transmission electron microscope TEM: Electron Microscope Sciences, Hatfield, PA

### **3.3 Methods**

#### **3.3.1 Synthesis of gold nanoparticles**

Gold nanoparticles (AuNP) were synthesized based on the method of Grabar *et al* (75). 500 ml of a 1 mM solution of  $\text{HAuCl}_4$  in Milli-Q water was heated and vigorously stirred in a round-bottom flask under reflux for one hour. Upon boiling, 50 ml of a 38.8 mM solution of trisodium citrate was rapidly added. Stirring continued for 10 minutes, after which the apparatus was disassembled. The resultant red solution of gold nanoparticles were stored at 4°C in the dark. The success of the reaction was verified using the UV-VIS spectrophotometer, standard mode, where a peak absorbance at 520 nm indicates that ~11 nm AuNP are present.

#### **3.3.2 Synthesis of the gold nanoparticle-based reagent**

##### **3.3.2.1 Coating with DSP**

2.0 mg of DSP was dissolved in 500  $\mu\text{l}$  of DMSO and then 9.5 ml of 95% ethanol was added, resulting in a 500  $\mu\text{M}$  solution. This was added to gold nanoparticles such that the entire surface was coated with a monolayer of DSP. A titration was performed to ascertain saturation with no free DSP in solution. DSP was added to a cuvette containing 10 mM phosphate buffer, pH 9.4, in amounts ranging from 0.5 to 2 nmol (0.25 nmol

increments) with a final volume of 500  $\mu$ l. The spontaneous hydrolysis of the maleimide functional group was monitored for one minute at 260 nm using the UV-VIS spectrophotometer in kinetics mode. Hydrolysis rates were calculated as the change in absorbance at 260 nm per minute. The experiment was repeated in the presence of 50  $\mu$ l AuNP in 450  $\mu$ l of the same buffer. AuNP-bound DSP is protected from spontaneous hydrolysis; the saturation point was determined to be the last point before an increase in the rate of hydrolysis caused by free DSP, i.e. 1.25 nmol.

### **3.3.2.2 Crosslinking with GSSG**

GSSG was dissolved in 10 mM phosphate buffer, pH 7.0, to make a 100 mM solution. It was added to AuNP and DSP in 10 mM phosphate buffer, pH 9.4, to a final concentration of 7 mM. The reaction was monitored with the UV-VIS spectrophotometer in kinetics mode, at 520 nm and 610 nm. The reaction was complete when A<sub>610</sub> ceased to increase. At this point the now blue solution was centrifuged at 14 000 rpm for 15 minutes. The supernatant containing excess GSSG in pH 9.4 buffer was removed and the pellet was resuspended in 10 mM phosphate pH 7.0, as the final Au-DSP-GSSG reagent.

### **3.3.3 Transmission Electron Microscopy**

Samples of AuNP alone and Au-DSP-GSSG reagent were brought to the University of Western Ontario. For each sample, 20  $\mu$ l were placed onto a formvar-coated, carbon-reinforced 400 mesh grid and allowed to air-dry. The slides were viewed in a Philips CM-10 transmission electron microscope (TEM) and pictures were taken with an AMT digital camera.

### **3.3.4 Purification of recombinant human PDI**

PDI was previously cloned into a pET-28a vector containing the coding for an N-terminal histidine tag. This vector was expressed in the E. coli strain BL21 (DE3) and the

protein harvested according to the published protocol (24). The expressed PDI was reduced through incubation with 10 mM DTT for 30 minutes and purified from DTT by passing it through a G-25 column. Quantification was performed in the UV-VIS spectrophotometer using the extinction coefficient  $47\,000\text{ M}^{-1}\text{cm}^{-1}$  at 280 nm. PDI was stored at  $-80^{\circ}\text{C}$  until used.

### **3.3.5 Reduction of the reagent with small thiols**

The reduction of Au-DSP-GSSG with small thiols was monitored in the kinetics mode of the UV-VIS spectrophotometer. Measurements of the wavelengths 520 and 610 nm were taken every 15 seconds until the reaction was complete, or a maximum of 10 minutes. The reagent was diluted in the same pH 7.0 buffer to a total volume of 500  $\mu\text{l}$  in the cuvette. After starting the kinetics run, a small thiol was added to the solution with a final concentration of 1  $\mu\text{M}$ . The following thiols were used:  $\beta$ -ME, DTT, NaSH, L-cysteine, GSH, insulin  $\alpha$ -chain, and PDI. In addition, trials were run in which no thiol was added, to obtain a baseline rate of decomposition. NaSH was used to reduce Au-DSP-GSSG at a variety of concentrations ranging from 0.125 to 1.5 nmol to determine the reagent's detection limit.

### **3.3.6 Synthesis of disulfide-linked AuNP with a larger spacer ligand**

#### **3.3.6.1 Oxidation of peptides**

Four peptides were purchased from GenScript: GGGC, GGGGC, GGGGGC, and GGGGGGC. They were designed to be like GSSG, but greater in length to leave a larger space between AuNP. First, they had to be oxidized to have a disulfide bond meant to be cleavable by thiols; this was only done immediately before use. When one of the peptides was to be used, it was dissolved in 10 mM phosphate buffer, pH 9.4, to a concentration of 1 mg/ml. This solution was placed in a small round-bottom flask with a magnetic stir bar

and vigorously stirred until the reaction was complete. 5,5'-dithiobis(2-nitrobenzoic acid) (DTNB) was used to monitor the reaction. The UV-VIS spectrophotometer was blanked with 450  $\mu$ l of the phosphate buffer and 50  $\mu$ l of 10 mM DTNB. Then 5  $\mu$ l of the peptide solution was mixed in the cuvette for 15 seconds and the absorbance at 412 nm was taken. This was done for the initial solution and every so often until the absorbance was 0, a total lack of free thiol, indicating that the peptide was fully oxidized. At this point the solution was lyophilized to concentrate the sample.

### **3.3.6.2 Synthesis of the reagent**

The synthesis reaction was performed in a similar manner as for the GSSG reagent. 50  $\mu$ l of AuNP was mixed with 3  $\mu$ M DSP in 10 mM phosphate buffer, pH 9.4, followed 15 s later by 4 mM peptide which had been resuspended in water. The reaction was monitored in the UV-VIS spectrophotometer at wavelengths of 520 and 610 nm. Following completion of the reaction, the solution was centrifuged once at 14000 rpm for 10 minutes.

### **3.3.6.3 Reduction of the larger reagent**

The goal of synthesizing the larger reagent was to make it cleavable by PDI; however, before PDI was used we decided to test with the more inexpensive DTT. Therefore, reduction of the newly synthesized reagent was first attempted with 100  $\mu$ M DTT. If reduction was successful then lower concentrations of DTT would be used, followed by the same low concentration of PDI. Unfortunately, reduction never occurred.

## **3.4 Results**

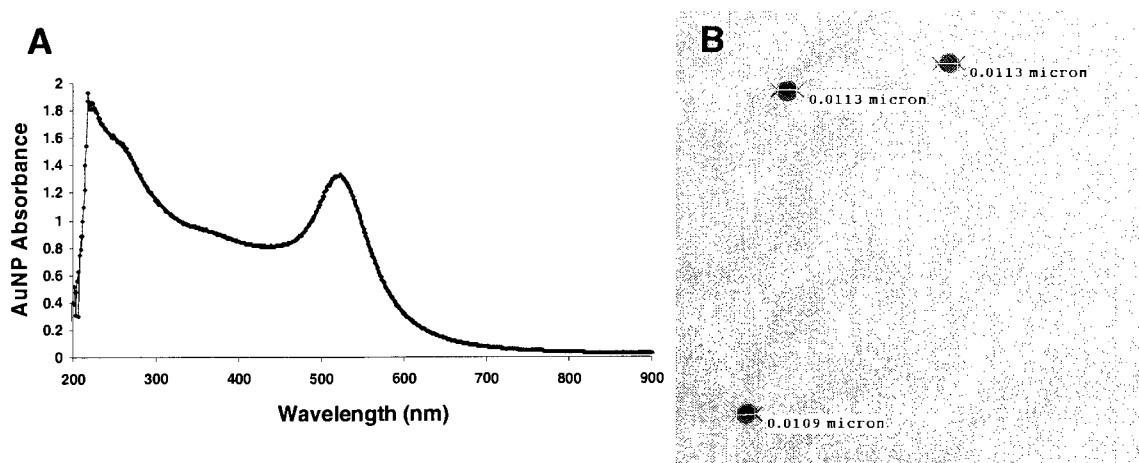
### **3.4.1 Gold nanoparticle synthesis**

Gold nanoparticles were successfully synthesized by the Grabar method. Figure 3.1 shows UV-VIS spectrophotometer visualization of the localized surface plasmon resonance of the AuNP diluted 1/10 in water (**A**). In addition it shows TEM visualization which enables confirmation that the size is  $11 \pm 1$  nm for most nanoparticles (**B**).

### **3.4.2 Au-DSP-GSSG synthesis**

#### **3.4.2.1 Optimization of DSP concentration**

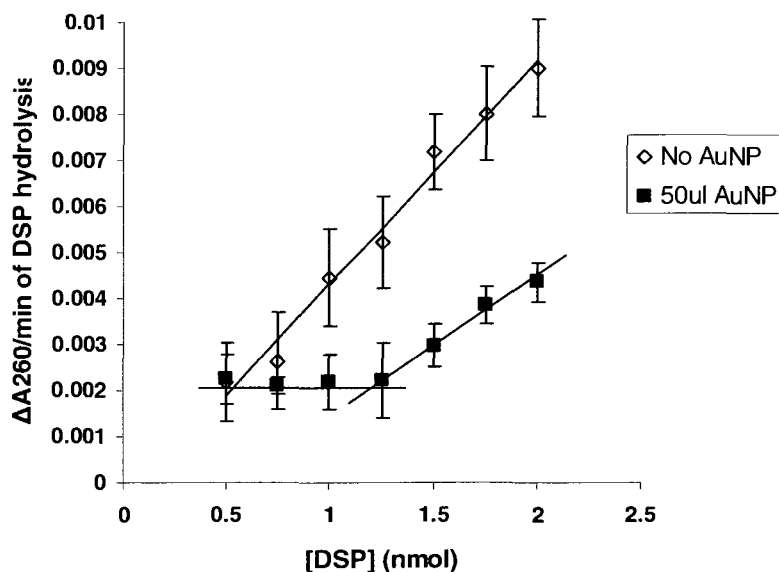
The first step in synthesizing the reagent was to optimize the concentration of DSP. It was chosen because it has a disulfide bond, allowing it to bond stably to the AuNP, as well as a homobifunctional amine-reactive succinimide group. The succinimide hydrolyzes readily in basic pH but is stabilized when bound to AuNP. Its absorbance at 260 nm in phosphate buffer pH 9.4 was observed over time in the UV/VIS spectrophotometer, kinetics mode, with or without AuNP present in the solution. The increase in absorbance at 260 nm over the course of one minute determined the rate of hydrolysis over various concentrations from 0.5 to 2 nmol. As seen in Figure 3.2, DSP has saturated the surface of 50  $\mu$ l AuNP at 1.25 nmol, corresponding to a final concentration of 2.5  $\mu$ M. This is based on the rapid increase in hydrolysis rate above that amount which indicates that there is now free DSP in solution. This DSP concentration was used throughout the rest of the experiments. Data presented in Figure 3.2 are the averages of three independent trials and their calculated standard deviations.



**Figure 3.1 Visualization of newly synthesized AuNP**

Gold nanoparticles were synthesized according to the method of Grabar *et al.* with modifications as described in the Methods. 1 mM  $\text{HAuCl}_4$  was heated and stirred under reflux until boiling after which 38.8 mM trisodium citrate was added. The citrate reduced the gold to  $\text{Au}^0$  and stabilized the spherical shape of the AuNP. The localized surface plasmon resonance peaked at 520 nm, making the solution appear red (A). In addition, the nanoparticles were seen by TEM to be  $11 \pm 1$  nm in diameter as expected from the protocol (B).





**Figure 3.2 DSP concentration optimization based on hydrolysis rates**

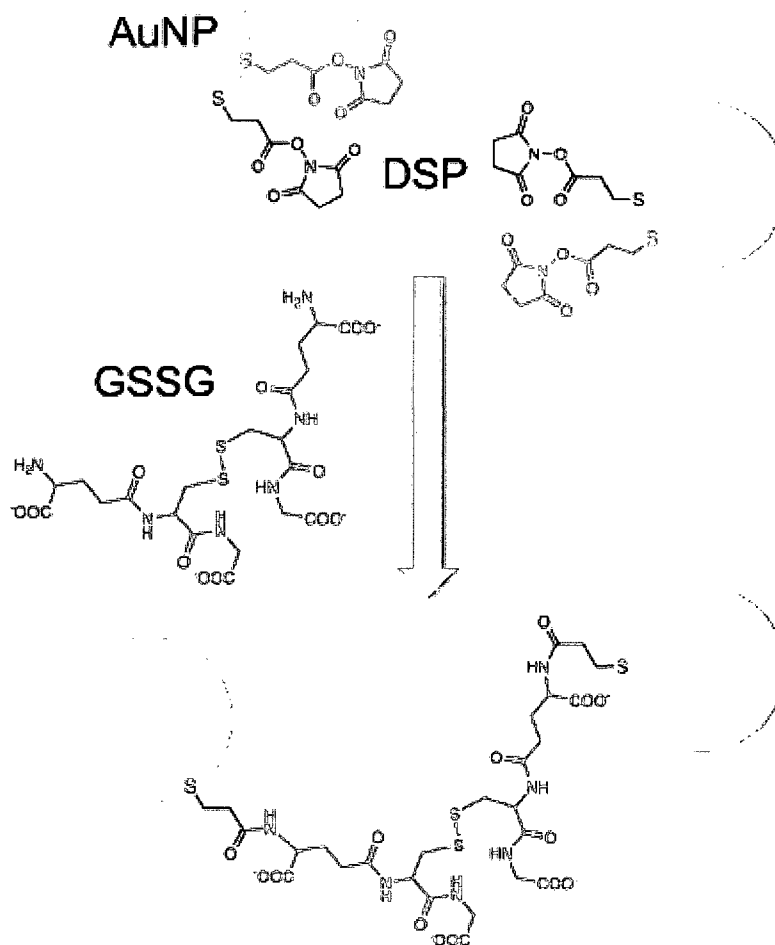
Various amounts of DSP from 0.5 to 2 nmol were added to cuvettes containing 10 mM phosphate buffer, pH 9.4, with (black squares) or without (white diamonds) 50  $\mu$ l AuNP. The final volume in the cuvettes was 500  $\mu$ l in all cases. The rate of DSP hydrolysis was measured as the change in absorbance at 260 nm per minute in the UV/VIS spectrophotometer kinetics mode. Saturation of 50  $\mu$ l of AuNP was determined to have occurred at 1.25 nmol, or 2.5  $\mu$ M, as the last point before an increase in hydrolysis rate. This amount of DSP was added to AuNP in all syntheses thereafter.

### 3.4.2.2 Final product formation

Once the DSP was optimized, a crosslinker was needed to connect the nanoparticles. GSSG was chosen because it has one free amine on either side of a disulfide bond, making it reactive with the DSP functional group and cleavable by thiols. Scheme 1 depicts the strategy utilized to synthesize the reagent. The optimization process for GSSG resulted in a final concentration of 7 mM being used. When this amount was added to AuNP alone there was no colour change, but when it was added to AuNP coated with DSP the solution turned from red to blue, or more specifically the LSPR broadened and its maximum shifted from 520 nm to 610 nm (Figure 3.3A). Figure 3.3B shows that the reaction between DSP's maleimide and GSSG's free amines was complete after 75 seconds. Afterwards the solution was centrifuged for 14 000 rpm for 15 minutes in a benchtop centrifuge and resuspended in 10 mM phosphate buffer, pH 7.0. At this lower pH the reagent was still susceptible to cleavage by thiols but stable at room temperature overnight as seen by the constant A<sub>610</sub>/A<sub>520</sub> ratio of hourly spectra taken in the UV/VIS spectrophotometer (Figure 3.4).

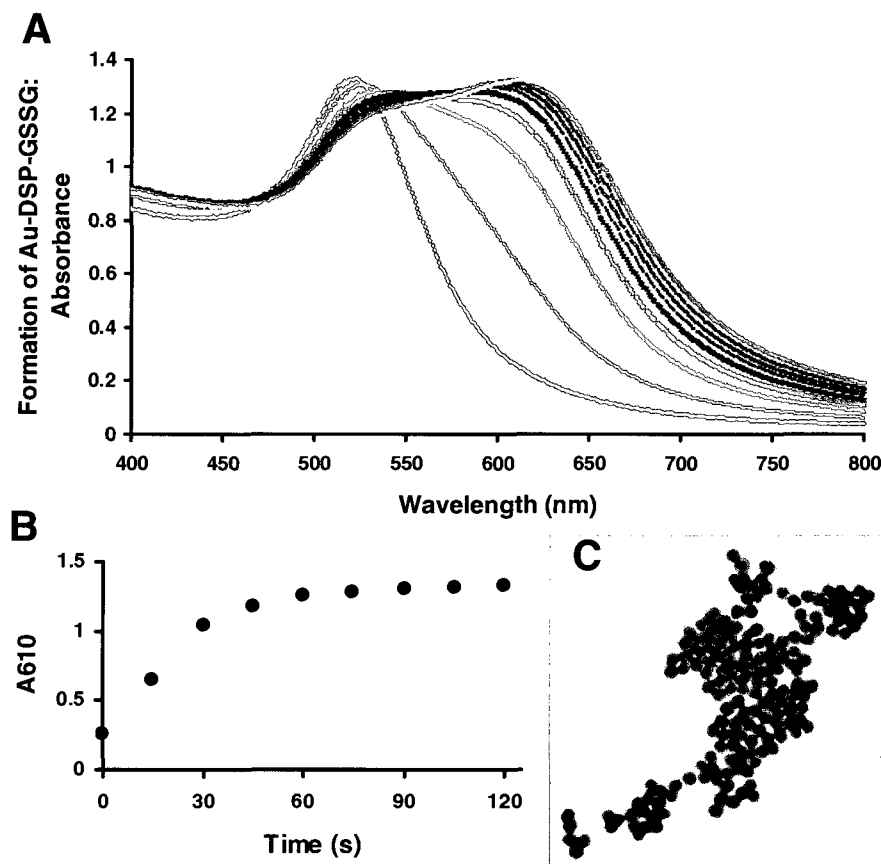
### 3.4.3 TEM of Au-DSP-GSSG

A sample of the synthesized Au-DSP-GSSG was brought to the University of Western Ontario. After drying 20 µl of the solution on the mesh grid as per the description in Methods, it was viewed in the TEM. Figure 3.3C shows that the reagent is a cluster of many AuNP crosslinked to one another. This is in comparison to the monodisperse AuNP seen in Figure 3.1B. The close proximity of many nanoparticles is responsible for the change in LSPR absorption yielding the blue colour seen and the absorbance maximum of 610 nm in the UV-VIS spectrophotometer.



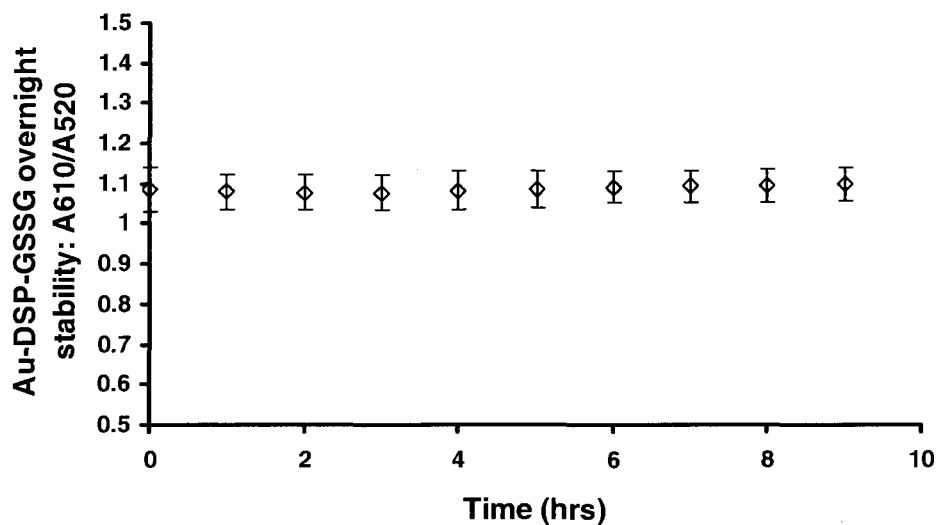
### Scheme 1      Synthesis process of Au-DSP-GSSG

The strategy for forming the reagent to detect low molecular weight thiols was to first coat AuNP with a saturating amount of DSP. It binds to the AuNP *via* its disulfide bond, leaving the amine-reacting maleimide group exposed. Then GSSG was added: its two amines react with DSP on different AuNP, bridging them close together to form the clusters. The disulfide bond in the middle of the crosslinker enables the breakdown of Au-DSP-GSSG by small thiols.



**Figure 3.3 Synthesis of Au-DSP-GSSG**

2.5  $\mu$ M DSP and 7 mM GSSG were added sequentially to 50  $\mu$ l AuNP in 450  $\mu$ l of 10 mM phosphate buffer, pH 9.4. The reaction was monitored in the UV-VIS spectrophotometer in kinetics mode. In addition, the final product was brought to the University of Western Ontario where it was viewed in the TEM. Figure 3.3A represents the course of the reaction from wavelengths 400 to 800 nm. It shows that the original AuNP solution had a maximum absorbance at 520 nm, as in Figure 3.1, but as the reaction took place the LSPR broadened and red-shifted to a new maximum absorbance of 610 nm which visually appears blue. **B** follows the course of the absorbance at 610 nm over time. It shows that the reaction is complete after 75 seconds. Following the reaction, the sample was centrifuged and resuspended in a 10 mM phosphate buffer, pH 7.0. One TEM image of the Au-DSP-GSSG is depicted in **C**, showing that it is composed of large clusters of many crosslinked nanoparticles each.

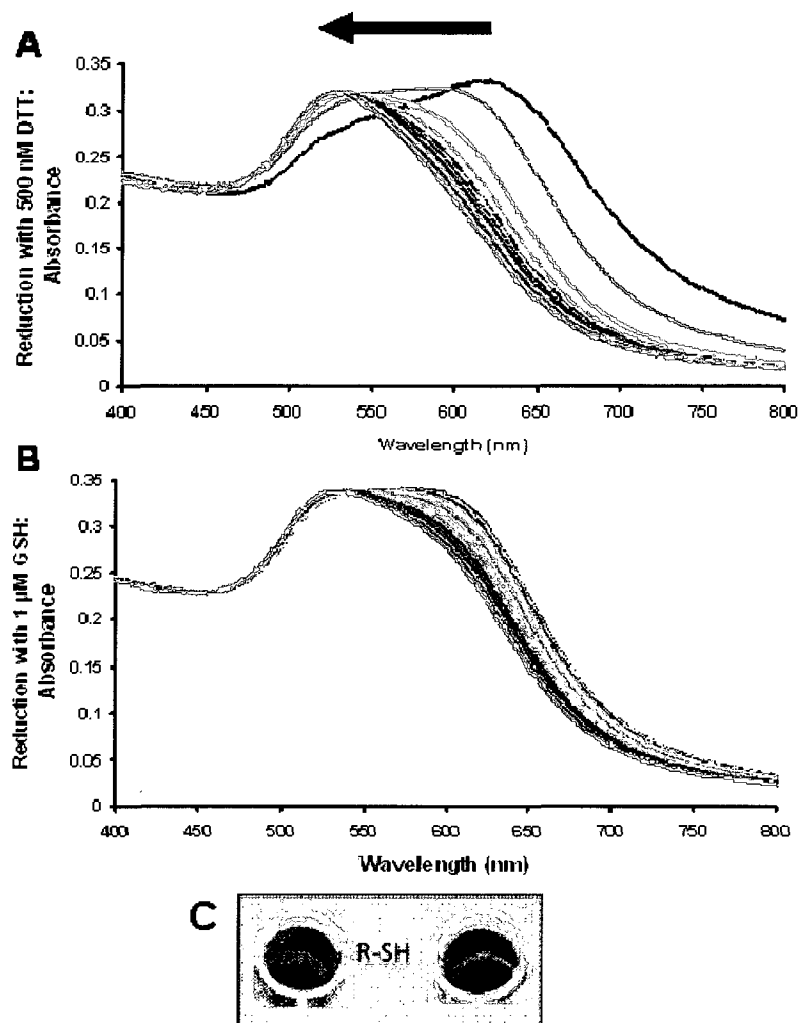


**Figure 3.4** Overnight stability of Au-DSP-GSSG after synthesis

Au-DSP-GSSG was synthesized as described above. To test its stability, the reagent was monitored overnight in the UV/VIS spectrophotometer in kinetics mode, with readings at 610 and 520 nm taken every hour. The ratio of A610/A520 was calculated for each time point (white diamonds) in two independent trials after synthesis. Data presented are the average result and error bars represent the calculated standard deviation for each average.

#### 3.4.4 Reaction with thiols

Au-DSP-GSSG was synthesized so that it could be used as a reagent to detect low molecular weight thiols. Consequently, after the synthesis method was optimized, it was tested with a variety of molecules containing free thiols. After centrifugation and resuspension in 100  $\mu$ l of 10 mM phosphate buffer, pH 7.0, 20  $\mu$ l was taken and diluted to 500  $\mu$ l in the same buffer inside a cuvette. It was placed into the UV/VIS spectrophotometer, kinetics mode, set to scan every 15 seconds. After the first scan, a thiol-containing molecule was mixed into the solution to a final concentration of 1  $\mu$ M. The reaction was allowed to progress to completion, or a maximum of 10 minutes. The thiols used were  $\beta$ -ME, DTT, NaSH, L-cysteine, GSH, insulin  $\alpha$ -chain, and reduced PDI. Only 500 nM of DTT was added because it has 2 free thiols, resulting in a concentration of 1  $\mu$ M thiol added. The results in Figure 3.5 represent two of all the 1  $\mu$ M thiol reactions: DTT (**A**) and GSH (**B**). These spectra are effectively the reverse of that of Figure 3.3A above. **C** is a photo of the same reaction carried out in a 96-well plate. Together these images show that in the beginning the nanoparticles are clustered and blue, with the absorbance maximum at 610 nm. As the thiol reduces the GSSG crosslinker, the nanoparticles become monodisperse once again and the LSPR shifts back to a maximum of 520 nm, resulting in a red solution like that of the original AuNP. The other notable result observed in Figure 3.5A and **B** is that the rate of the reaction is affected by the size of the thiol used: DTT was much faster at completing the reduction than the larger GSH. This observation led to more studies of the kinetics of the reaction.



**Figure 3.5 Reduction of Au-DSP-GSSG by 1  $\mu$ M thiol**

After the synthesis of Au-DSP-GSSG described above, it was diluted in pH 7.0 phosphate buffer to a final volume of 500  $\mu$ l in a cuvette and placed in the UV-VIS spectrophotometer in kinetics mode. The sample was scanned every 15 seconds. After the first scan, 1  $\mu$ M thiol was mixed and the reduction was allowed to progress for 10 minutes or until completion. These representative spectra show that the reductions are essentially the reverse of the synthesis, with the LSPR blue-shifting and becoming more narrow as the reaction progresses. It is also seen that larger reducing agents result in slower reductions. **A** shows the reaction with 500 nM DTT, which has two thiols resulting in a concentration of 1  $\mu$ M thiol. With its molecular weight of 154.2 Da, it reduces Au-

DSP-GSSG at a much faster rate than GSH (**B**) which has a molecular weight of 307.3 Da. **C** is the visual representation of the reaction done in a 96-well plate. There is a clear change from blue back to the original red colour, characteristic of 11 nm AuNP, upon the addition of 1  $\mu$ M thiol.

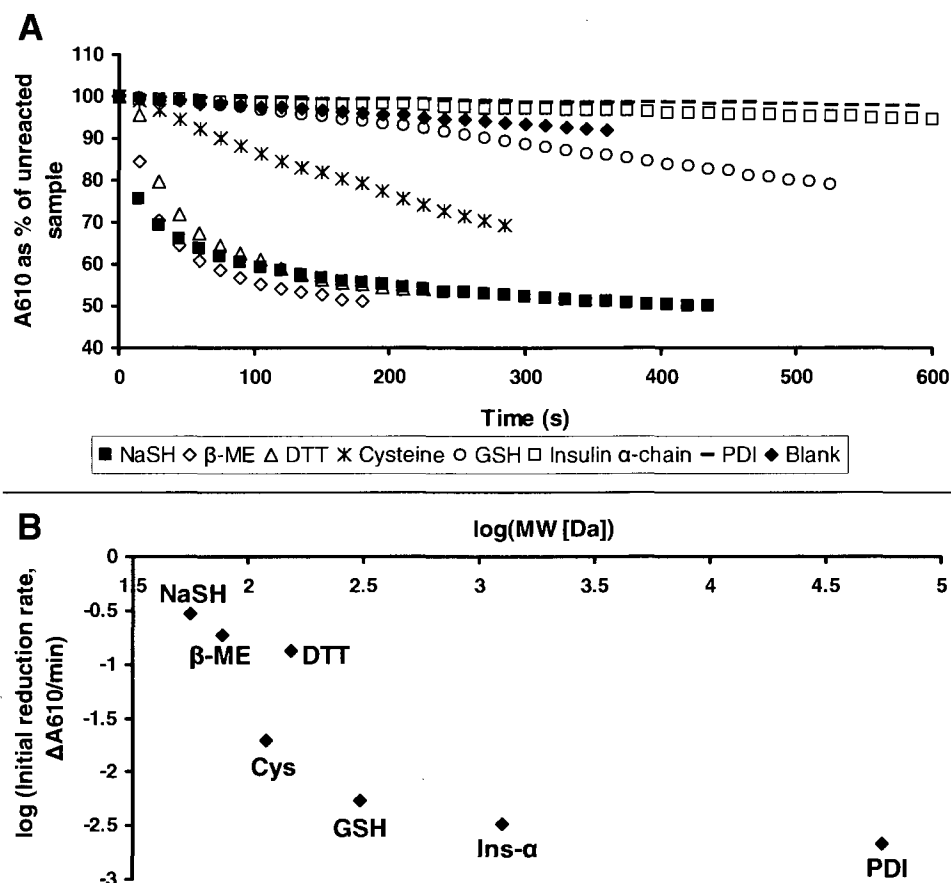


### 3.4.5 Effects of size and concentration on reduction rates

The results above show that thiols are able to reduce the blue clusters of Au-DSP-GSSG back to red nanoparticles coated with DSP-GSH. We used a variety of thiols all at the same concentration of 1  $\mu\text{M}$  to determine the effect that size has on the reaction rate. As shown in Figure 3.6A, each small molecule had its own rate as seen by the decrease in absorbance at 610 nm over time in the UV/VIS spectrophotometer. It can be seen that GSH is the slowest at reducing Au-DSP-GSSG and any thiol-containing molecule larger than that, i.e. insulin  $\alpha$ -chain and PDI, is unable to react at all. The blank, which was done simply by monitoring the reagent in the same conditions but with no thiol added, showed a basal rate of reduction caused by the bright light of the spectrophotometer. Interestingly, insulin  $\alpha$ -chain and PDI exhibited rates slower than that of the blank, which indicates that the additional coating of large molecules around the Au-DSP-GSSG clusters has a protective effect against the photo-reduction. Figure 3.6B is a graph of the log of each initial reduction rate (the change in absorbance at 610 nm per minute, taken from the first 30 seconds of the reaction) plotted against the log of the corresponding molecules' MW. Aside from the outlier DTT, which has a fast rate for its size, there is a clear correlation where larger molecules become increasingly slower reducing agents. An asymptote forms toward the larger molecules such that at MW larger than that of GSH, approximately 310 Da, there ceases to be a substantial change in the reaction rate.

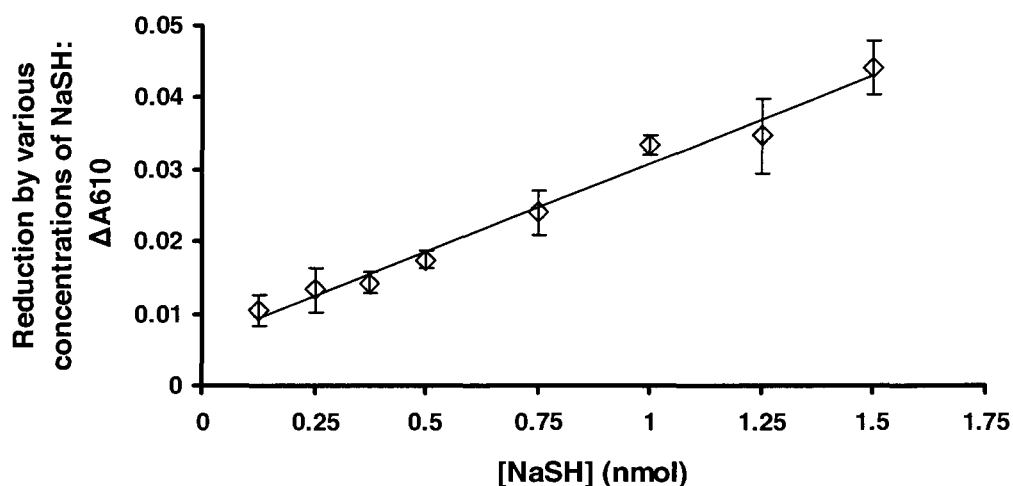
Aside from the effect of size on the small molecules' reduction rates, there is also a dependence on concentration. Different concentrations of NaSH, ranging from 0.125 nmol to 1.5 nmol, were added to Au-DSP-GSSG in the same conditions described above. After 10 minutes, which is more than sufficient time for the reaction to complete, the difference in absorbance at 610 nm was calculated for each concentration of NaSH and

plotted in Figure 3.7. There is a direct correlation seen between the amount added and the extent to which it can reduce Au-DSP-GSSG, with an  $R^2$  value of 0.983. In a solution with a final volume of 500  $\mu$ l, this translates to a detection limit below 250 nM. Data are the average of three independent trials for each concentration, and the error bars represent the calculated standard deviation for each average.



**Figure 3.6 Effect of size on reduction rate**

1  $\mu$ M NaSH,  $\beta$ -ME, DTT, cysteine, GSH, insulin  $\alpha$ -chain, or PDI was added to a solution of Au-DSP-GSSG diluted to 500  $\mu$ l in 10 mM phosphate buffer, pH 7.0 and scanned in the UV/VIS spectrophotometer every 15 seconds. A blank was done with no thiol present as well. Figure 3.6A exhibits the progress of the reaction as a decrease in absorbance at 610 nm for each thiol. The results show that each thiol has a characteristic reduction rate, which is connected to its molecular weight. **B** depicts a plot of the log of the initial reaction rate, calculated from the change in absorbance at 610 nm per minute, versus the log of the molecular weight. It reveals that beyond  $\sim 310$  Da, or the size of GSH, any change in reaction rate becomes negligible.



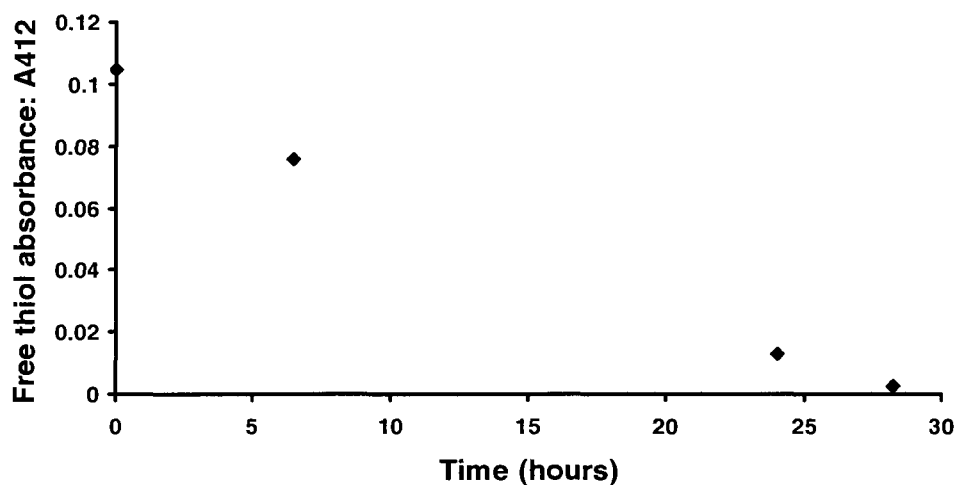
**Figure 3.7 Effect of concentration on reduction**

The concentration of the thiol added plays a role in the reduction of Au-DSP-GSSG. Amounts of NaSH ranging from 0.125 to 1.5 nmol were added to a 500  $\mu$ l solution in which the absorbance maximum was 0.2 at 610 nm. After adding the NaSH and allowing 10 minutes for the reduction to complete, the difference in absorbance at 610 nm was calculated for the reaction. Three trials for each concentration were done and the averages plotted. It can be seen that the amount of NaSH added is in direct proportion to the extent of reduction over a consistent time period. The equation of the line is  $y = 0.245x + 0.0063$  with  $R^2 = 0.983$ . The data show that the detection limit of this amount of Au-DSP-GSSG is less than 0.125 nmol, corresponding to 250 nM thiol. Error bars represent the standard deviation for each averaged sample.

### 3.4.6 Synthesis of disulfide-linked AuNP with a larger spacer ligand

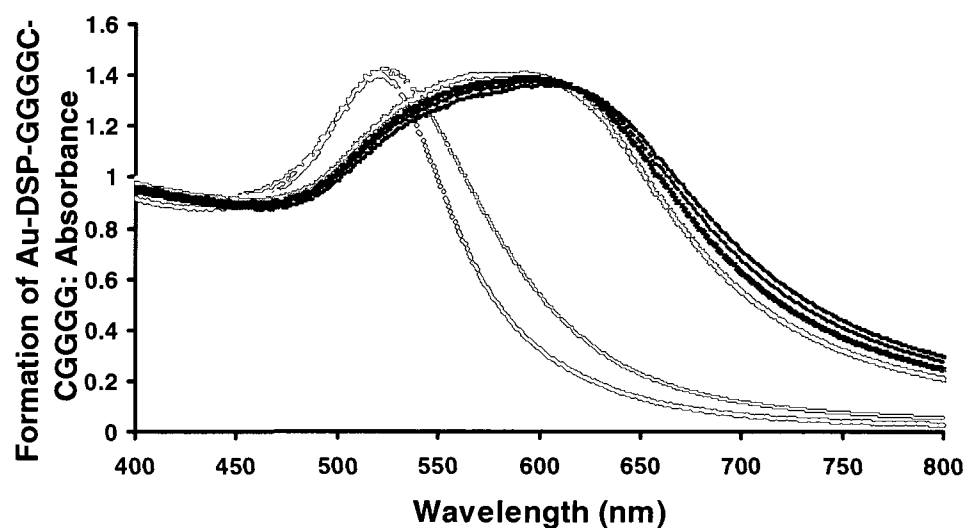
1 mg/ml of peptide was stirred vigorously in a high pH buffer to achieve thiol oxidation, and the reaction was monitored with DTNB until it was complete. Figure 3.8 is a representative graph of any time a peptide was oxidized, in this case 5 mg of GGGGC. It can be seen that at the given pH of 9.4 and concentration of 1 mg/ml, the reaction took approximately 28 hours to complete. The rate, however, depended on the concentration of the solution, as more dilute samples oxidize faster. As it progressed the reaction rate decreased slightly but overall was nearly linear and thus only time-dependent.

Once the oxidation was complete, the solution was lyophilized and resuspended in water. In a cuvette with 450  $\mu$ l of 10 mM phosphate buffer, pH 9.4, 50  $\mu$ l of AuNP were mixed with 3  $\mu$ M DSP, and then various concentrations of peptide. GGGC-CGGG and GGGGC-CGGGG were able to form blue products at 4 mM levels while the two larger peptides did not turn the solution blue at all, indicating that they did not react with DSP to crosslink the AuNP. Figure 3.9 shows a representative synthesis reaction using 4 mM GGGGC-CGGGG with the typical AuNP and DSP levels. While Au-DSP-G<sub>4</sub>CCG<sub>4</sub> appears similar to the synthesis using GSSG, shown in Figure 3.3, this product was unable to be reduced by 100  $\mu$ M DTT under any condition attempted: pH 9.4, pH 7.4, centrifuged to remove excess peptide, or uncentrifuged. Therefore, either the reagent did not form the way it was expected, or it did and its particular shape was simply inaccessible to thiols.



**Figure 3.8     Oxidation of GGGGC**

GGGC was dissolved to a concentration of 1 mg/ml in 10 mM potassium phosphate, pH 9.4. It was stirred in a round-bottom flask with free thiol content monitored using DTNB. Free thiols react with DTNB to form a mixed disulfide and  $\text{TNB}^-$  which absorbs at 412 nm; therefore, absorbance at 412 nm is directly proportional to free thiol added to the solution. Results show that this typical oxidation took about 28 hours to complete, based on the time required for the absorbance at 412 nm to reach 0. When the reaction was complete the solution was lyophilized and kept frozen until use.



**Figure 3.9**     **Synthesis of Au-DSP-G<sub>4</sub>CCG<sub>4</sub>**

50  $\mu$ l of AuNP, 3  $\mu$ M DSP and 4 mM G<sub>4</sub>CCG<sub>4</sub> were mixed in 450  $\mu$ l of phosphate buffer, pH 9.4, similarly to the synthesis process of the original reagent using GSSG. While the figure resembles Figure 3.3A above, based on the broadening and red-shift of the LSPR absorption spectrum, this reagent was unable to be reduced by 100  $\mu$ M DTT.

### 3.5 Discussion

The synthesis of probes has been an interest in the Mutus lab for several years. Raturi *et al* created, and subsequently improved, a sensitive fluorescent probe for monitoring PDI reductase activity (107-108). Other group members attempted to synthesize a fluorescent probe that reacts specifically with vicinal thiols; this would be used to characterize the redox status of PDI and other proteins that have cysteines in close proximity with one another. Gold nanoparticles are an ideal basis for a probe due to their optical properties. As described in the General Introduction, 11 nm AuNP are red when they are free in solution, but a change in LSPR frequency induced by connecting many nanoparticles close together results in a change in colour to blue (87-88).

With this in mind, we set out to exploit the colour change and design a probe that binds to two AuNP at once and contains a disulfide bond in the middle. This would cause the AuNP solution to turn blue on its synthesis but revert back to red upon reduction of the disulfide bond by a free thiol. The initial target planned for the probe was PDI. The fluorescent probe that had been already created used GSSG as the linker between two eosin molecules, which fluoresce when separated in space from one another. Here, the intention was to replace eosin molecules with AuNP and link GSSG to them, producing a visible-light probe that performs the same function as the fluorescent one. An AuNP-based reagent for monitoring PDI reductase activity did not come to fruition, but what did result is interesting nonetheless.

Gold as well as gold nanoparticles are known to form covalent-like bonds with thiols (87). Therefore, DSP was chosen as the linker between AuNP and GSSG. Its disulfide bond is able to bind to the AuNP, leaving two amine-reactive succinimidyl groups exposed. Two DSP molecules on separate AuNP could react with the two free



amines of GSSG, resulting in the AuNP being drawn close together and exhibiting the LSPR absorption shift that makes them appear blue.

This reaction does not simply form AuNP dimers. The entire surface area of the AuNP is available for reaction with thiols or disulfide bonds; therefore, it was important to ensure that DSP saturated the surface, so that no space was left available for GSSG to bind to the AuNP directly via its disulfide bond. In addition, having an excess of DSP in solution was undesirable since it would compete with AuNP-bound DSP for GSSG. This was accomplished as seen in Figure 3.2. We observed that AuNP protected the spontaneous hydrolysis of the functional groups of DSP, resulting in little to no increase in hydrolysis in the lower concentrations used (0.5-1.25 nmol), as monitored at 260 nm in the spectrophotometer. Once the surface was saturated, additional DSP was free in solution and consequently not protected from spontaneous hydrolysis. This was seen above 1.25 nmol; therefore, that was the amount of DSP used per 50  $\mu$ l AuNP. It is important to note that increasing the amount of AuNP requires a concomitant increase in DSP required to saturate the surface.

Following that experiment, increasing amounts of GSSG were added to the solution until a blue product formed. The 7 mM final concentration of GSSG was a large excess over the requirement to saturate the DSP functional groups. It is probable that the same protection the AuNP afforded DSP to attenuate spontaneous hydrolysis also made it relatively inaccessible to the GSSG, so that a high concentration was required for GSSG to “find” the functional groups and react with them. The excess GSSG was simply removed by centrifugation and washing of the disulfide-linked product.

Once the reagent was synthesized it was found that it could not react with thiols larger than GSH; in other words, ~310 Da was the detection limit of the reagent. Figure

3.6A shows the change in absorbance at 610 nm – the maximum absorbance of the blue reagent – over time after the addition of each thiol. The first observation made was that the smaller thiols led to faster decreases in absorbance at 610 nm, meaning they had higher reaction rates. This led to further investigation into the effect of size on reaction rate, depicted in Figure 3.6B. With the exception of DTT, the plot of log(reaction rate) vs log(MW) made a curve in which higher MW thiols had slower reaction rates until it reached an asymptote beginning at GSH. This indicates that any increase in size has negligible effect on the probe beyond ~310 Da.

DTT was the exception to the trend in that it was able to reduce the probe much faster than expected for its size. The fact that it has two thiols was taken into account in the experiment: whereas the other LMWT were added to the reagent at 1  $\mu$ M, only 500 nM DTT was used. The difference in rate between them may be mechanism-based. In a typical reduction reaction (108):



two thiols are consumed per reduction reaction. For DTT the two thiols involved are intramolecular, i.e. on the same molecule, and thus execute this reaction more efficiently. For the others, the concentration of 1  $\mu$ M may be too low for effective numbers of intermolecular collisions between the two thiols in comparison with DTT.

The ~310 D<sub>a</sub> detection limit of the reagent is due to the size and closeness of the AuNP. Since many molecules of DSP bind to each nanoparticle, the result of crosslinking them is a 3-dimensional network composed of many AuNP, as seen in the TEM micrograph in Figure 3.3C. Given that each AuNP is 11  $\pm$  1 nm in diameter, and the crosslinking DSP-GSSG is less than that, the complex would be too bulky for a large molecule to traverse to the interior and reduce the disulfide bonds. In addition, the

dihedral angle of the disulfide bond may play a role in the reagent's ability to be reduced. If the Au-DSP-GSSG is oriented such that the disulfide bond is less accessible to outside molecules, then smaller ones would be more likely to access the bond and reduce it.

Although the reagent was designed with the intention of use on PDI, the finding that it quantifies solely LMWT was welcome. There are several applications that this reagent can have in academic and/or industrial settings. LMWT are important molecules in the plasma of blood, both for their redox control of proteins and as reservoirs for NO in the form of *S*-nitrosothiols (37-38). Since glutathione is known to be at least 90% reduced in a healthy individual (109), the reagent may thus be used as a tool to rapidly diagnose oxidative stress in plasma samples. When a protein is purified in which the redox status is important, such as PDI, small thiols are frequently used to reduce the protein after which they are separated by column chromatography or other techniques. Au-DSP-GSSG can be used to rapidly detect contaminating LMWT in the protein sample after the separation process to ensure its success. A third application of this reagent could be for an environment in which small volatile thiols like H<sub>2</sub>S are routinely used. By employing the reagent as a sensor in the workspace, hazardous levels in the air would be detected in the event of leaks or other containment mishaps.

With the hypothesis that the size of the crosslinker controls the size of the thiols able to reduce the disulfide bond, the next step in the project was to systematically vary the crosslinking agent until the probe became cleavable by PDI. Four peptides were purchased to this end: GGGC, GGGGC, GGGGGC and GGGGGGC. It was thought that after oxidizing the peptides they could react with DSP via the terminal amines similarly to GSSG. However, a complete and functional reagent was not formed with any of these peptides. The smaller two appeared to be able to form the reagent (see Figure 3.9);

however, the fact that it was not reduced after treatment with 200 times the amount of DTT that was effective on Au-DSP-GSSG means that it may not have been formed as initially believed. The presence of high amounts of salt will cause AuNP to flocculate regardless of other molecules in the solution. The salt concentration in the G<sub>4</sub>C-CG<sub>4</sub> solution may have been high due to salt mixed with the peptide in the vial it came in, as well as from the phosphate buffer salt after the newly oxidized solution was concentrated by lyophilization and resuspension. Therefore, the solution may have turned blue when the peptides were added because of flocculation induced by salt, and not by the reaction between DSP and the peptides as with GSSG.

Another reason the reagent may not have reduced could be due to the final shape of the crosslinker. Glycine is a hydrophobic amino acid, and hydrophobic groups tend to aggregate together as protection from the environment. If the reagent did form through the reaction between the oxidized peptide and DSP, then the glycines may have clustered such that the disulfide bond became inaccessible to incoming thiols.

Regardless of the reason, these peptides are not effective as crosslinkers in a reagent for detecting thiols and alternatives must be explored. Future continuation of this work is to find a molecule that is as successful and inexpensive as GSSG, while being large enough to accommodate PDI and other HMWT. This may be insulin, which is a physiological substrate of PDI (110), or another peptide designed to be large with an accessible disulfide bond.

## **CHAPTER 4**

### **THE THIOL PROTEOME, AND RAPID DENITROSYLATION OF S- NITROSTHIOLS USING A FLOW DEVICE**

## 4.1 Introduction

As described in Chapter 1, thiols are responsible for the redox state of proteins and thus their activity. In addition, RSNO<sup>5</sup> – including both low and high molecular weight molecules – are important reservoirs of NO. *S*-nitrosothiols transport NO through the bloodstream and release it where appropriate, allowing NO to perform its functions when denitrosated. Thiols can only do this when in their reduced, sulfhydryl state. Therefore, the redox state is important for both proteins and NO to function properly. The characterization of thiol-bearing proteins – referred to here as the thiol proteome – is useful because thiol proteins have such an important impact on signaling, enzyme regulation, and other aspects of physiology (111-112). Additionally, the subset of the thiol proteome involved in NO transport is important to study, given NO's tremendous impact on health and disease.

This project had two overall goals. The first one was to characterize the thiol proteome, and identify specific proteins bearing surface thiols. This was prompted by experiments in which AuNP were mixed with samples of plasma or platelet-rich plasma (PRP), washed, and subjected to gel electrophoresis. Each time the same proteins seemed to be present in the samples. Under the hypothesis that proteins rich in surface thiols would be the ones to bind to the AuNP, a systematic protein identification process was begun. Mass spectrometry and Western blotting were performed and a total of 7 proteins

---

<sup>5</sup> Abbreviations used in this chapter: AuNP, gold nanoparticles; DTT, dithiothreitol; GSNO, *S*-nitrosogluthathione; HMWT, high molecular weight thiols; LMWT, low molecular weight thiols; MALDI-TOF, matrix-assisted laser desorption ionization – time of flight; NaSH, sodium hydrosulfide; NO, nitric oxide; NOA, nitric oxide analyzer; PDI, protein disulfide isomerase; PDMS, polydimethyl siloxane; PDMS-AuNP, PDMS-bound gold nanoparticles; PNGase F, peptide N-glycosidase F; PRP, platelet-rich plasma; RSNO, *S*-nitrosothiol; SDS-PAGE, sodium dodecyl sulphate polyacrylamide gel electrophoresis; TEM, transmission electron microscope.

have been identified so far from plasma and platelet surfaces, hypothesized to be members of the thiol proteome, including PDI which has 2 sets of surface vicinal thiols.

The *S*-nitrosoproteome is a subset of the thiol proteome. It is the set of proteins that are nitrosylated in a given tissue and condition. The second goal was to use AuNP to rapidly identify *S*-nitrosoproteins using a flow device of our design. Using GSNO as a model RSNO, it was first shown that AuNP is able to *S*-denitrosylate the GSNO either while free in solution or when bound to PDMS. Next, a flow device was designed to enable higher throughput of this reaction. The first model was built, and at the present time the process is manual. However, the ultimate intention is to optimize the flow device for plasma samples so that it can automatically quantify the total plasma RSNO content and identify the *S*-nitrosoproteome. We furthermore aspire to identify the specific sites of *S*-nitrosylation.

## **4.2 Materials and Equipment**

### **4.2.1 Materials**

Argon Grade 5 300 SZ: Praxair Distribution, Division of Praxair Canada Inc., Mississauga, ON

Dithiothreitol: MP Biomedicals, Solon, OH

Glutathione, reduced (GSH): Sigma-Aldrich Canada, Oakville, ON

Gold (III) chloride (HAuCl<sub>4</sub>): Sigma-Aldrich Canada, Oakville, ON

Mouse anti-HSP70 antibody: Abcam Inc., Cambridge, MA

Mouse anti-PDI antibody RL90: Abcam Inc., Cambridge, MA

PNGase F: Sigma-Aldrich Canada, Oakville, ON

Rabbit anti-mouse antibody-HRP: Abcam Inc., Cambridge, MA

Sodium hydrosulfide (NaSH): Sigma-Aldrich Canada, Oakville, ON

Sodium nitrite ( $\text{NaNO}_2$ ): Sigma-Aldrich Canada, Oakville, ON

Sodium phosphate dibasic: ACP Chemicals, Montreal, PQ

Sodium phosphate monobasic: ACP Chemicals, Montreal, PQ

Sylgard 184 silicone elastomer kit (PDMS monomer and curing agent): Dow Corning, Toronto, ON

Trisodium citrate: Sigma-Aldrich Canada, Oakville, ON

Trypsin, sequencing grade: Promega, distributed by Fisher Scientific Ltd., Nepean, ON

#### **4.2.2 Equipment**

2 ml glass vials with black polypropylene screw top and septa: Supelco, Bellafonta, PA

27.5G syringe needles: Becton-Dickenson, Franklin Lakes, NJ

Bio-Rad PowerPac basic power supply: Bio-Rad Laboratories (Canada) Ltd, Mississauga, ON

GyroMini nutating mixer: Labnet International Inc., Woodbridge, NJ

Hamilton<sup>®</sup> syringe, 1800 series gastight, model 1801RN: Sigma-Aldrich Canada, Oakville, ON

Hettich EBA12 desktop centrifuge: Fisher Scientific, Mississauga, ON

Immobilon<sup>™</sup> PVDF transfer membranes: Millipore, Etobicoke, ON

MALDI-TOF DE-Pro mass spectrometer: Applied Biosystems, Foster City, CA

Micro-C18 ZipTips: Millipore, Etobicoke, ON

Philips CM-10 Transmission electron microscope (TEM): Electron Microscope Sciences, Hatfield, PA

Polystyrene 24-well plate: Sarstedt, Montreal, PQ

Polystyrene 96-well plate: Sarstedt, Montreal, PQ

Sievers 280i Nitric Oxide Analyzer: General Electric Canada, Mississauga, ON

Type 37900 culture incubator: Preiser Scientific, Louisville, KY



Vacutainer® ACD Solution A blood collection tubes and PrecisionGlide Vacutainer® brand blood collection needles: BD Canada, Mississauga, ON

### **4.3 Methods**

#### **4.3.1 Synthesis of gold nanoparticles**

Gold nanoparticles were synthesized as described in Chapter 3.3.1.

#### **4.3.2 Synthesis of PDMS-bound gold nanoparticles**

The synthesis of PDMS-bound gold nanoparticles (PDMS-AuNP) was adapted from Zhang *et al* (83). PDMS monomer and curing agent were mixed in a ratio,  $\eta$ , of 0.04 and incubated in a culture incubator at 70°C for 1.5 hours for the curing process. A mixture of 10 mM HAuCl<sub>4</sub> and 5 mM trisodium citrate was incubated on top of the PDMS overnight and washed four times with distilled water immediately before use.

#### **4.3.3 Isolation of plasma from whole blood**

Whole blood was collected from healthy donors into 8.5 ml ACD collection tubes and the cells were allowed to settle overnight. The platelet-rich plasma (PRP) was removed after settling and either used or centrifuged at 900 g for 15 minutes to remove the platelets and use the plasma.

#### **4.3.4 Isolation of proteins from serum**

##### **4.3.4.1 Using aqueous AuNP**


























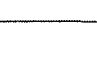
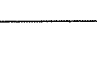




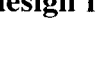
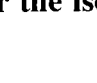

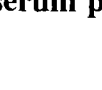

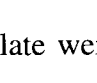

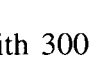
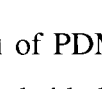
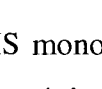
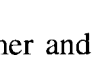
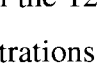
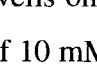
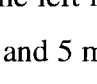
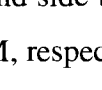
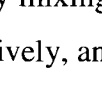
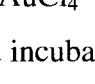
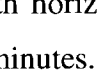
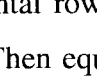
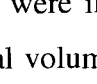
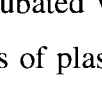
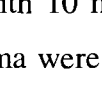
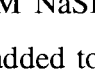
500  $\mu$ l of AuNP were saturated with 10 mM NaSH for 10 minutes after which the excess was washed off by centrifugation at 14000 rpm for 15 minutes. This and a separate, untreated 500- $\mu$ l AuNP sample were each mixed with 1000  $\mu$ l of plasma and incubated on the nutating mixer for 15 minutes. After the incubation with plasma, the samples were again centrifuged at 14000 rpm for 15 minutes and the supernatants containing unbound proteins were aspirated. The pellets were washed 4 times with 10

mM phosphate buffer, pH 7.4, by resuspension and centrifugation. Upon completion of the last centrifugation, the pellets were resuspended in 20  $\mu$ l of buffer each, mixed with 5  $\mu$ l of 5X loading dye, and subjected to sodium dodecyl sulfate polyacrylamide gel electrophoresis (SDS-PAGE) and mass spectrometry analysis.

#### **4.3.4.2 Using PDMS-AuNP**

All samples used were prepared in triplicate in a 24-well plate. The setup of the experiment is shown in Scheme 2. The 12 wells on the left-hand side of the plate contained PDMS-AuNP; the 12 on the right-hand side contained only PDMS. Half of the wells of the 24-well plate were pre-treated with 10 mM NaSH for 10 minutes, indicated in Scheme 2 with “+” or “-”, which was afterwards washed off with 4 rinses with phosphate buffer. Then every well of the plate was incubated on the shaker with 400  $\mu$ l of plasma for 15 minutes, and again washed off with 4 phosphate buffer washes. Finally, 400  $\mu$ l of 10 mM DTT was incubated for 5 minutes consecutively in each well of a triplicate series, thus pooling the protein elutions without increasing the final volume. This was done for half of the triplicates; the other half had the same procedure done with the phosphate buffer, as shown in Scheme 2 with “+” or “-” referring to the use or absence of DTT, respectively.

Following this procedure, the proteins were then concentrated by acetone precipitation. Each of the 8 samples were mixed with 3 volumes of ice-cold acetone and incubated at -20°C overnight. The samples were centrifuged the next day at 14000 rpm for 5 minutes. The supernatants, i.e. acetone and buffer, were pipetted out until ~100  $\mu$ l remained. Then the samples were spun in the speed-vac until the volume decreased to ~20  $\mu$ l, which took about 15 minutes. They were each mixed with 5  $\mu$ l of 5X loading dye and subjected to SDS-PAGE followed by mass spectrometry analysis.

		PDMS-AuNP			PDMS		
NaSH:	-						
DTT:	+						
	+						
	+						
	-						
	-						
	-						
	+						
	-						

**Scheme 2      Experimental design for the isolation of serum proteins using PDMS-AuNP**

All 24 wells of the plate were filled with 300  $\mu$ l of PDMS monomer and curing agent. AuNP were formed in the 12 wells on the left hand side by mixing  $\text{AuCl}_4^-$  and trisodium citrate to final concentrations of 10 mM and 5 mM, respectively, and incubated overnight. The second and fourth horizontal rows were incubated with 10 mM NaSH, which was washed off after 10 minutes. Then equal volumes of plasma were added to all 24 wells. After incubation and 4 washes, 10 mM DTT (first and second rows) or buffer (third and fourth rows) was added to the wells and the protein samples were collected in the indicated triplicates. These 8 samples were then concentrated by acetone precipitation and subjected to SDS-PAGE and mass spectrometry analysis.

### **4.3.5 Identification of the isolated proteins**

#### **4.3.5.1 SDS-PAGE and staining**

Typical 10% SDS-PAGE protocol was used for all the samples from the above two sections (113). Afterwards, the gels were stained for 1 hour in Coomassie stain and destained overnight in 40% methanol and 10% acetic acid.

#### **4.3.5.2 Analysis of gels**

The Coomassie-stained gels were scanned and analyzed by the computer program ImageJ. Each lane containing the proteins that had been bound to AuNP was selected and a histogram was prepared by the program. The histograms plotted the locations and densities of each protein band, allowing comparison between samples +/- NaSH pre-treatment as well as comparison between aqueous and PDMS-bound AuNP.

#### **4.3.5.3 Mass Spectrometry**

The 10 strongest bands from each gel were chosen and prepared for mass spectrometry analysis as described (114). Bands were excised from the gel, destained with acetonitrile and ammonium bicarbonate, and dried in the speed-vac. They were deglycosylated by incubation with PNGase F overnight, followed by washing and trypsin digestion for 8 hours. The peptides were extracted using a mixture of formic acid and acetonitrile, then concentrated in the speed-vac. Desalting was performed using micro-C18 ZipTips and then the samples were spotted onto a MALDI plate in a 1:1 ratio with matrix ( $\alpha$ -cyano-4-hydroxycinnamate in 50% acetonitrile and 1% formic acid).

Matrix-assisted laser desorption ionization – time of flight (MALDI-TOF) spectrometry was used for protein identification. For each sample, the protein fingerprint from the tryptic peptides was acquired in linear mode. Two of the strongest peaks from the fingerprint were chosen for further analysis, which was done using post-source decay

(PSD) in reflector mode. Peaks from the 11 subsets of each tandem mass spectrometry were stitched together in the program Data Explorer. The fingerprint peaks were inputted into the Protein Prospector database to identify candidate proteins, which were verified by the peptide sequences from the PSD. NCBI Structure searches were performed for each identified protein. The crystal structures and full protein sequences were obtained and then viewed in the program Cn3D.

#### **4.3.5.4 Western blot**

Western blotting was done on samples of platelet-rich plasma (PRP) and platelet-free plasma to probe for PDI and heat shock protein 70 (HSP70). Samples were run on two gels in SDS-PAGE and transferred to PVDF membranes for 1 hour at 110 V. The membranes were blocked overnight in 5% skim milk in tris-buffered saline (TBS) and washed in TBS 3 times for 5 minutes each. Mouse anti-PDI antibody (RL90) was diluted 1/1000 in TBS with 2% skim milk and incubated with one membrane on the shaker for 2 hours. A 1/5000 dilution of mouse anti-HSP70 antibody was incubated with the other membrane. Following the incubations and four 5-minute washes in TBS, rabbit anti-mouse secondary antibody, conjugated to horseradish peroxidase (HRP), was diluted 1/2000 and incubated on both of the membranes for 1 hour on the shaker. This was again washed in TBS. Finally, the membranes were exposed to luminol and the chemiluminescent reaction performed by HRP was imaged. Immediately afterward, each membrane was scanned to acquire an image of the protein ladder. Once identified, PDI and HSP70 were also searched in the NCBI Structure database and modified in Cn3D.

#### **4.3.6 Synthesis of GSNO**

S-nitrosoglutathione was prepared as previously described (115). Reduced glutathione (GSH) was prepared in distilled water and mixed in a 1:1 (mol:mol) ratio with

chilled sodium nitrite in 0.5 M HCl. The mixture was incubated at 4°C for 30 minutes and then the GSNO was crystallized with cold acetone. The powder was stored at -80°C. When needed, the appropriate mass of GSNO was weighed and dissolved in 10 mM phosphate buffer, pH 7.4.

#### **4.3.7 S-denitrosylation of GSNO by AuNP**

##### **4.3.7.1 Aqueous AuNP**

2-ml screw-top glass vials, as used in Chapter 2, were filled with 200  $\mu$ l of either AuNP, or phosphate buffer of pH 7.4; 8 vials of each type. These were all degassed in argon for 7 minutes each. 500- $\mu$ l GSNO solutions were prepared in vials in the following concentrations: 0, 1, 5, 10, 50, 100, 200, or 500  $\mu$ M. All of these vials were degassed as well. Then 50  $\mu$ l of each GSNO solution was injected using a gastight syringe into its corresponding vial of AuNP or buffer and these samples were incubated for 10 minutes at room temperature. Following the incubation, 50  $\mu$ l of air above each solution was injected into the NOA which contained 10 mM phosphate buffer, pH 7.4; the NO in the air was detected by the machine and displayed as peaks. As in Chapter 2, peak areas were compared to nitrite standard curves, which were generated afterwards, to obtain the concentration of NO detected.

##### **4.3.7.2 PDMS-AuNP and PDMS**

The same experimental design was performed as above with the following exceptions. The concentrations of GSNO used were 0, 1, 10, 50, 100, 200, 350, or 500  $\mu$ M. 200  $\mu$ l of these degassed solutions were added to degassed vials containing PDMS-AuNP or PDMS using a syringe. After the 10-minute incubation, 1 ml of air above the solution was injected into the NOA. Data processing followed the same procedure as for AuNP or buffer.

#### **4.3.8 Flow device design**

A flow device was designed in the SketchUp program for Mac OSX. In the model, two tubes act as inlets and then merge into a mixing chamber inside the square device foundation. Two outlet tubes also emerged from the mixing chamber: one to release the merged liquids, and one to connect to a nitric oxide detector. After the design was prepared, a prototype flow device was assembled. A teflon square was made approximately 2.5 cm x 2.5 cm. A similarly-sized glass microscope coverslip was sealed to the bottom using PDMS, and teflon tubing was used for the inlet and outlet tubes. PDMS was used to fill the teflon square and a hole in the middle served as the mixing chamber.

#### **4.3.9 S-denitrosylation of GSNO using the flow device**

Serial dilutions of GSNO were added to 12 wells of a 96-well plate, 100  $\mu$ l per well. The concentrations used were 0, 1.34, 2.68, 5.37, 10.7, 21.4, 42.9, 85.9, 172, 343, 687, and 1375  $\mu$ M. 100  $\mu$ l of AuNP were also added to the 12 adjacent wells. One inlet tube was placed in the GSNO solution of the lowest concentration while the other was placed in the first well of AuNP solution. A pump was used to induce flow through the tubing into the mixing chamber and through the outlet. The mixture was collected from the outbound tube using a syringe and injected directly into the NOA. This was repeated immediately for all dilutions of GSNO and their corresponding wells of AuNP.

## **4.4 Results**

### **4.4.1 Synthesis of PDMS-AuNP**

Gold nanoparticles were successfully synthesized on the surface of PDMS using Adam Faccenda's (Mutus lab) modified protocol which involves 5 mM trisodium citrate and a higher concentration of  $\text{AuCl}_4^-$  than the originally published method (83). The result is a deep red to purple colour, indicating that this PDMS-AuNP has a high density of gold nanoparticles formed; this was verified by TEM. The higher density of nanoparticles provides an increased surface area onto which thiols and proteins can bind.

### **4.4.2 Identification of AuNP-bound plasma proteins**

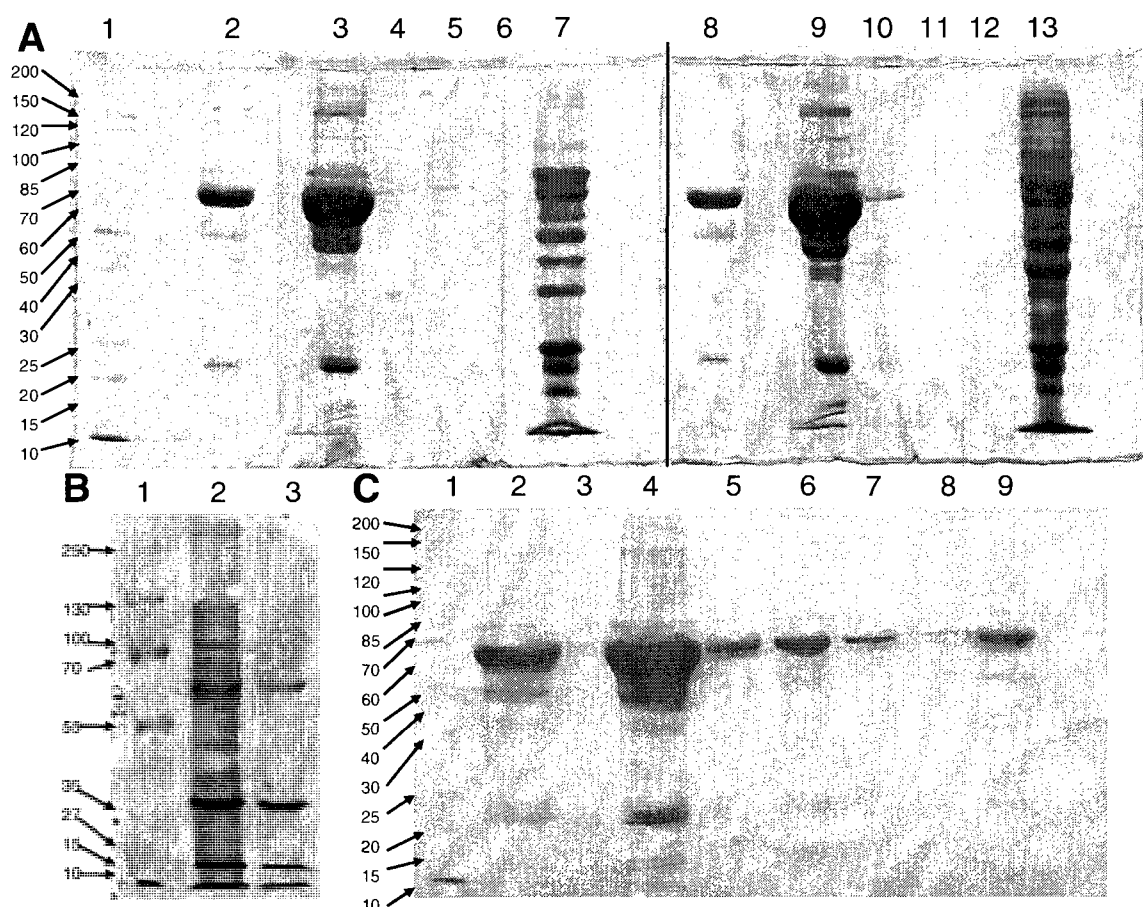
Part I of the project was to examine and identify components of the thiol proteome. Both aqueous AuNP and PDMS-AuNP were used to this end. First, one 500- $\mu\text{l}$  sample of AuNP was saturated with NaSH, and one was left coated with citrate; 1 ml of plasma was added to each 500- $\mu\text{l}$  AuNP sample, which was then washed four times and run on a gel. Figure 4.1A depicts the gels that included the supernatants from the washes to verify their effectiveness at removing unbound protein. The gel on the left contains the sample that did not have NaSH bound before mixture with plasma, and the gel on the right contains the sample that had been saturated with NaSH. The supernatants from the first centrifugation were diluted 1/100 and 20  $\mu\text{l}$  of each were added to lanes 2 or 8. 20  $\mu\text{l}$  from each subsequent wash step were added to lanes 3-6 and 9-12. The AuNP samples containing their bound proteins were loaded in lanes 7 and 13. **B** is an image of the gel whose proteins were excised for mass spectrometry; it shows the AuNP-bound proteins after the final wash.

A separate experiment was done to isolate plasma proteins using PDMS-AuNP. Wells of PDMS-AuNP were either saturated with NaSH, with the excess washed off, or



untreated. Plasma was incubated on the surface followed by washing. Then the proteins that had bound to the surface were eluted with excess DTT. Control groups were eluted with buffer rather than DTT, and all groups were repeated with PDMS alone, making 8 triplicates in total to fill the 24-well plate. Figure 4.1C depicts a typical gel after this process. While the PDMS-AuNP samples that were eluted with DTT had many bands, there is evidence of some non-specific binding since certain proteins appear in samples from PDMS in the absence of AuNP. The strongest bands were prepared for mass spectrometry analysis.

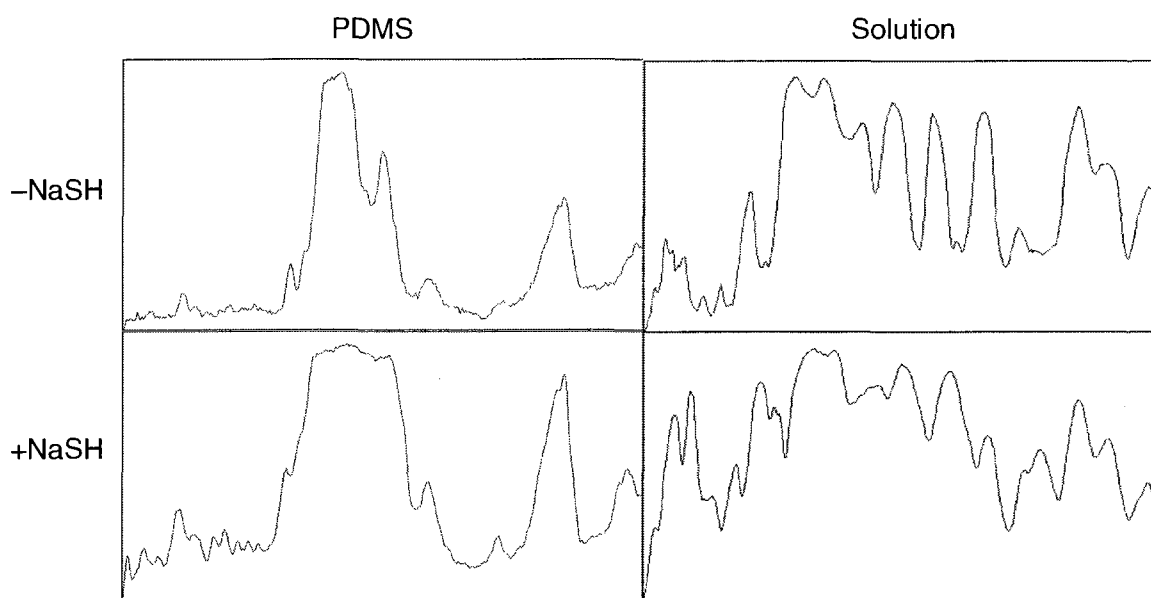
The gels from Figure 4.1A and C were compared to one another using the program ImageJ before mass spectrometry was performed. The program analyzed the lanes containing the proteins that had been isolated by aqueous AuNP, and the lane containing proteins eluted by DTT after binding to PDMS-AuNP. The order and intensity of the bands were plotted on histograms shown in Figure 4.2. The AuNP were saturated with NaSH to ensure that proteins would bind by thiol exchange rather than by amines or other functional groups. It can be seen from the gels and the histograms that the proteins were all found at the same molecular weights whether they bound directly to the AuNP or exchanged with NaSH. Therefore, saturating the AuNP with NaSH was not necessary. Another observation is that there were several proteins that may be common to the thiol proteomes of aqueous and PDMS-bound AuNP. The most notable examples are the proteins found at ~65 kDa, ~50 kDa, and ~23 kDa. The main difference between the two types of protein isolation is that these three proteins are much stronger in the PDMS-AuNP samples, making it more difficult to identify other common proteins. However, since these same proteins bind to PDMS alone as well, their concentrations in the samples may be at least partially due to non-specific binding.



**Figure 4.1 AuNP-bound proteins**

500- $\mu$ l samples of AuNP were incubated with plasma, either with or without pre-treatment with NaSH. The samples were washed four times each and 20  $\mu$ l of each supernatant were loaded into gels, along with the final samples of protein bound to the AuNP. Additionally, samples of proteins bound to PDMS-AuNP with or without NaSH pre-treatment were eluted with DTT and run in a gel along with control samples. The gels in **A** show that 4 washes were sufficient to remove unbound proteins. The samples derived from untreated AuNP were run in the gel shown on the left, and the samples from NaSH-saturated AuNP were in the gel shown on the right. **B** depicts the gel whose protein bands were excised and prepared for mass spectrometry. The gel in **C** is from the PDMS-AuNP experiment. Lane assignments are as follows. In **A**: Lane 1, protein standards; lanes 2 and 8, first centrifugation diluted 1/100; lanes 3 and 9, supernatant from the first

wash; lanes 4 and 10, supernatant from the second wash; lanes 5 and 11, supernatant from the third wash; lanes 6 and 12, supernatant from the fourth wash; and lanes 7 and 13, proteins isolated by AuNP. In **B**: Lane 1, protein standards; lane 2, proteins isolated from plasma by AuNP; lane 3, isolated proteins diluted  $\frac{1}{2}$ . In **C**: Lane 1, protein standards; lane 2, proteins bound to PDMS-AuNP with DTT elution; lane 3, PDMS with DTT elution; lane 4, proteins bound to NaSH-saturated PDMS-AuNP and eluted by DTT; lane 5, NaSH-saturated PDMS and DTT elution; lane 6, PDMS-AuNP with buffer elution; lane 7, PDMS with buffer elution; lane 8, NaSH-saturated PDMS-AuNP and buffer elution; lane 9, NaSH-saturated PDMS and buffer elution. The masses of the protein standards are shown in kDa to the left of the gels. The banding patterns of isolated proteins are similar whether or not they were exchanged with NaSH, and when the AuNP were aqueous or PDMS-bound. However, the concentrations of certain proteins vary in different samples.

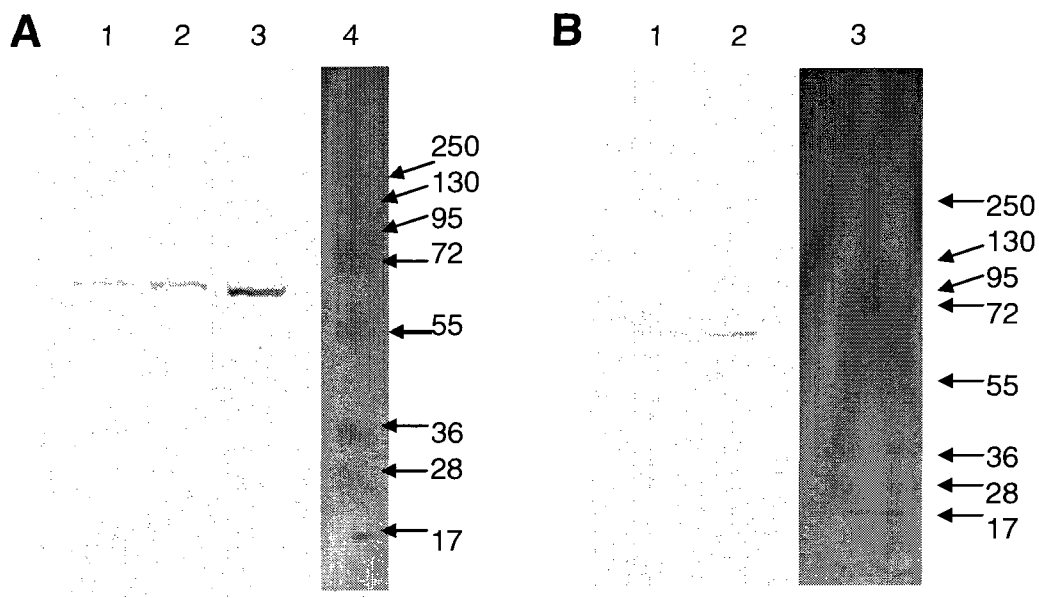


**Figure 4.2 Histograms of the protein banding of pre-mass spectrometry gels**

ImageJ was used to plot histograms of the proteins in lanes 7 and 13 of Figure 4.1A above and lanes 2 and 4 of Figure 4.1C. Despite differences in the relative abundances of each protein, the four histograms reveal similar patterns of proteins in the presence or absence of NaSH saturation, and when the AuNP were aqueous or PDMS-bound. This supports the hypothesis that AuNP will bind to the same proteins based on the proportions and localizations of their cysteine residues.

After qualitative comparison of the protein contents of the gels, MALDI-TOF mass spectrometry was used to identify some of those proteins. Linear mode was used to acquire the fingerprint of each protein, and PSD mode allowed the identification of the proteins via their sequence. The mass spectrometry raw data can be found in Appendix A. Proteins identified by this method were histidine-rich glycoprotein precursor (60 kDa); actin (40 kDa); filamin A alpha actin-binding protein 280 (280 kDa); myosin heavy polypeptide 9, non-muscle (226 kDa); and tyrosine-3-monooxygenase/tryptophan-5-monooxygenase activation protein, zeta polypeptide (28 kDa).

In addition, Western blotting was performed to probe for PDI and HSP70 as they were suspected to have bound to the AuNP. Two gels were run containing protein standards, washed AuNP-bound PRP proteins, washed AuNP-bound plasma proteins, and in one gel, purified PDI as a positive control. After the gels finished running the proteins were transferred to PVDF membranes and Western blotted: one using antibodies against PDI and one using antibodies against HSP70. Figure 4.3 shows one representative blot for each protein, with **A** as the PDI blot and **B** as the HSP70 blot. Since both PDI and HSP70 had bands in PRP and plasma, it can be concluded that they were both pulled down by the AuNP and thus may be part of the thiol proteome along with those identified by mass spectrometry.



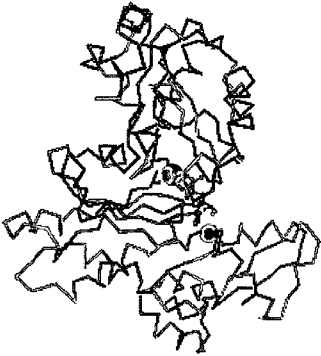
**Figure 4.3 Identification of PDI and HSP70 by Western blot**

Gels were run containing samples of PRP and plasma and Western blotting was performed to probe for PDI and HSP70. **A** shows a blot for PDI. Lane 1, plasma; lane 2, PRP; lane 3, PDI control; and lane 4, protein standards. **B** shows the blot for HSP70. Lane 1, plasma; lane 2, PRP; and lane 3, protein standards. The molecular weights of the protein standards are shown in kDa to the rights of the blots. Bands were observed in both the PRP and plasma for both proteins, making these two putative members of the thiol proteome. Other proteins were identified by mass spectrometry.

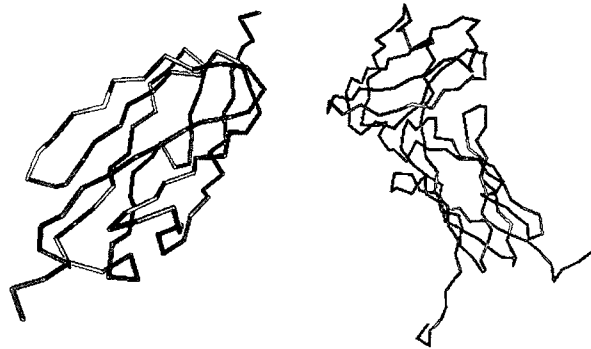
#### **4.4.3 Properties of identified proteins**

Since the identified proteins most likely bound to the AuNP through their thiols, their cysteine content and structures were searched. PDI, HSP70 ATPase domain, actin, certain domains of filamin A, and myosin heavy chain were found using NCBI Structure and viewed in Cn3D. A glycoprotein similar to histidine-rich glycoprotein precursor was also found. The cysteines of each protein were highlighted in red; it was found that there are several thiols or disulfide bonds at the exterior of each protein. Figure 4.4 shows a compilation of these proteins with the surface cysteines highlighted in red. These are the main candidates for the binding sites of these proteins to the AuNP. All of the proteins were also determined to be present in plasma and/or platelets, supporting the accuracy of the present mass spectrometry identification. Table 4.1 summarizes the location and main role of each identified protein.

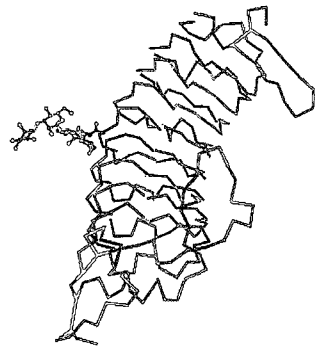
Actin



Filamin A Actin-binding protein  
– domains 23 and 18-19



Glycoprotein



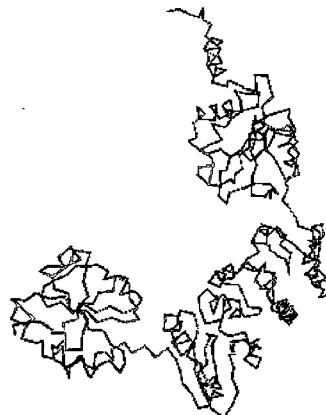
HSP70 ATPase  
domain



Myosin Heavy  
Chain 9



PDI





#### **Figure 4.4     Structures of identified possible thiol proteome members**

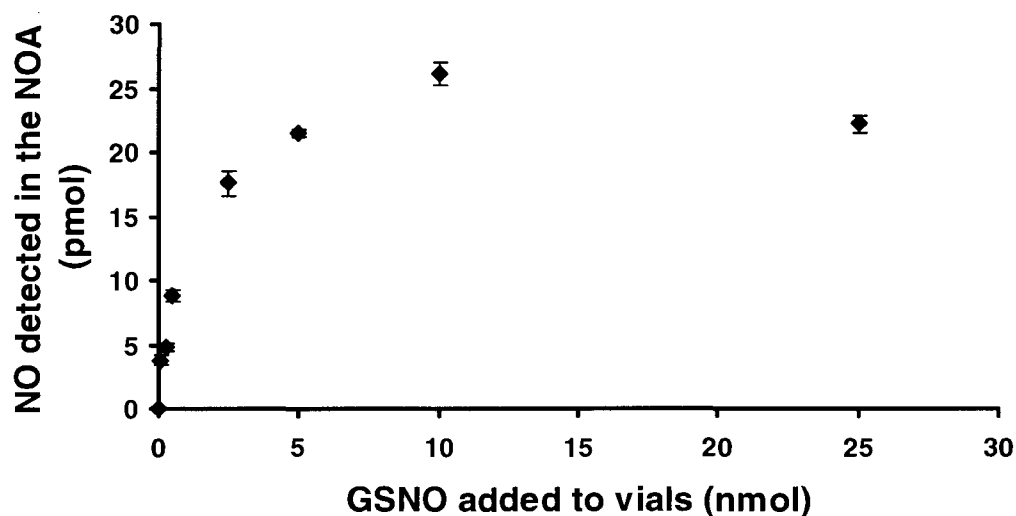
Seven proteins were identified as putative components of the thiol proteome by mass spectrometry and Western blot. The structures of seven of these were found in NCBI Structure searches and viewed with the program Cn3D. Cysteine residues were highlighted with red to indicate their locations in the proteins. It can be seen that each protein contains cysteine residues on their surface: these are the possible binding sites to the AuNP.

**Table 4.1      Locations and functions of the identified proteins**

<b>Protein</b>	<b>Localization</b>	<b>Main function</b>
Actin (116)	All cells	Cell motility
Filamin A – actin-binding protein 280 (117)	All cells	Promotes orthogonal branching of actin filaments; links actin filaments to membrane glycoproteins
Histidine-rich glycoprotein precursor (118)	Plasma and platelets	Role in blood coagulation and fibrinolysis
HSP70 (119)	All cells and cell surface	Protein folding
Myosin heavy polypeptide 9 non-muscle (116)	Leukocytes and platelets	Role in cytokinesis, cell shape, secretion, capping
PDI (120)	ER, cell surface and platelet surface	Protein folding; platelet aggregation
Tyrosine 3-monooxygenase/tryptophan 5-monooxygenase activation protein (121)	Serotonin-producing cells; secreted by macrophages into plasma	Binds phosphoserines to mediate signal transduction; cytoskeletal structure; possible inflammation regulator

#### 4.4.4 AuNP can *S*-denitrosylate GSNO

Part II of the project entailed the characterization of AuNP-mediated *S*-denitrosylation of thiols, leading to the production of a flow device for high-throughput analysis. In the first experiment, 50  $\mu$ l of degassed GSNO were injected into vials containing 200  $\mu$ l of degassed aqueous AuNP or 10 mM phosphate buffer, pH 7.4, in the following amounts: 0, 0.05, 0.25, 0.5, 2.5, 5, 10, or 25 nmol. One GSNO sample was injected per vial, totaling 16 vials. These were incubated for 10 minutes after which 50  $\mu$ l of the air above each solution were injected into the NOA in duplicate. The peak areas were translated into pmol of NO detected with the use of a nitrite standard curve. The amounts of GSNO mixed with AuNP plotted against the amounts of NO detected by the NOA is shown in Figure 4.5; no peaks were detected when GSNO was added to buffer. As more GSNO was added to the vials of AuNP, more NO was released until the AuNP surface was saturated at about 10 nmol GSNO. Data presented are the average of 2 repeat injections and the error bars represent the standard deviation for each average.

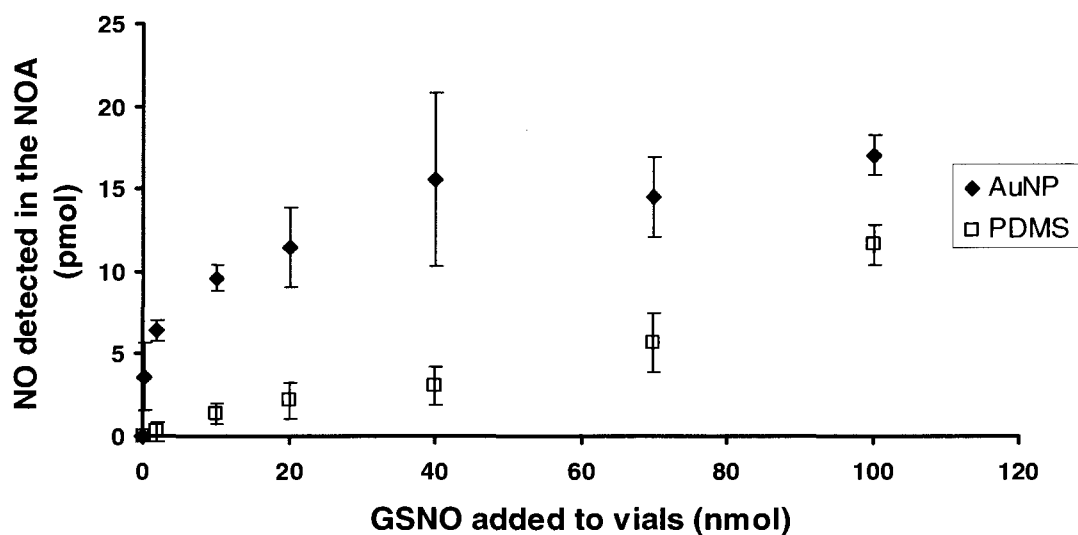


**Figure 4.5** *S*-denitrosylation of GSNO by AuNP

0, 0.05, 0.25, 0.5, 2.5, 5, 10, or 25 nmol of GSNO were added to vials of AuNP or buffer and incubated for 10 minutes. Then 50  $\mu$ l of air above the solution was injected in duplicate into the NOA. The resultant peaks were compared to a nitrite standard curve to calculate the concentration of NO for each sample, and these concentrations were plotted against the amounts of GSNO originally added to the vials. The graph shows that saturation occurred at 10 nmol GSNO for 200  $\mu$ l of AuNP; no peaks were detected for GSNO added to buffer alone. Each data point is the average for 2 injections, with the standard deviations denoted by the error bars.

#### 4.4.5 PDMS-AuNP can *S*-denitrosylate GSNO

A similar experiment as described above was performed in vials containing PDMS-AuNP or PDMS instead of aqueous AuNP or buffer. The amounts of GSNO used were 0, 0.2, 2, 10, 20, 40, 70, or 100 nmol; and 200  $\mu$ l were added to each sample vial rather than 50  $\mu$ l. In addition, 1 ml of air was injected into the NOA instead of 50  $\mu$ l. Figure 4.6 shows a plot of the amount of GSNO added to PDMS or PDMS-AuNP versus the amount of NO detected by the NOA. As with aqueous AuNP, the NO release increases with GSNO concentration until the surface is saturated at about 40 nmol GSNO for the PDMS-AuNP. In contrast, in the absence of AuNP, PDMS alone caused little *S*-denitrosylation and there is no apparent saturation point for the GSNO concentrations used. Data points are the average of 4 independent experiments, and error bars represent their standard deviations.

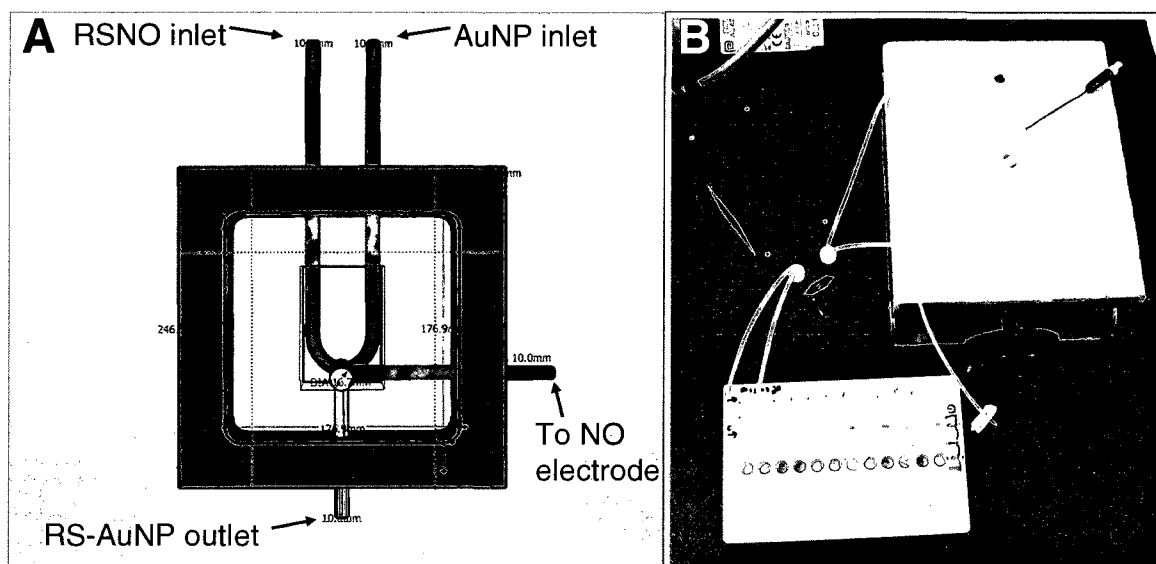


**Figure 4.6 S-denitrosylation of GSNO by PDMS and PDMS-AuNP**

Various concentrations of GSNO were added to vials of PDMS or PDMS-AuNP. After a 10-minute incubation, 1 ml of the air above each solution was injected into the NOA. The PDMS-AuNP surface was saturated by GSNO at about 40 nmol, while PDMS alone bound less GSH, releasing less NO, and did not saturate. Data are the averages with standard deviations of amounts of NO released, detected by the NOA (n=4 for each point).

#### 4.4.6 S-denitrosylation of GSNO using the flow device

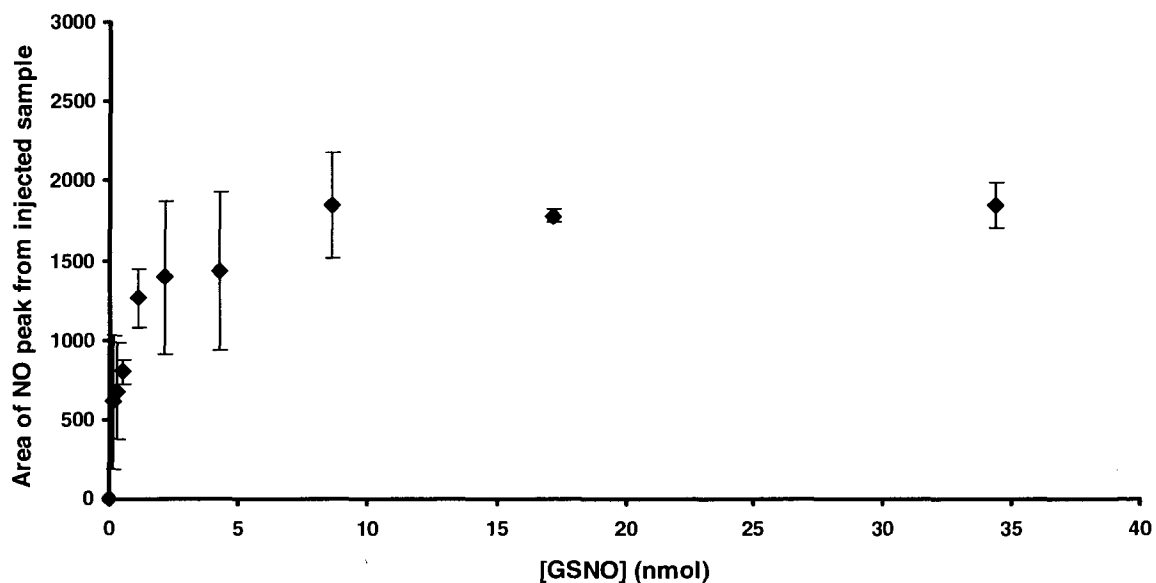
The original flow device was designed electronically with the aid of SketchUp for Mac OSX, and then assembled from teflon materials and PDMS. Figure 4.7A shows a sketch of the design, containing the inlet tubes, mixing chamber, liquid outlet and the outlet to connect to an NO detector. Figure 4.7B is a photograph taken of the prototype model and apparatus. 100- $\mu$ l samples of 12 amounts of GSNO in buffer – 0 0.134, 0.268, 0.537, 1.07, 2.14, 4.29, 8.59, 17.2, 34.3, 68.7 and 137.5 nmol – were pumped sequentially from a 96-well plate through an inlet tube alongside 100  $\mu$ l of AuNP. They were injected into the NOA after mixing with AuNP inside the flow device. The resultant graph is shown in Figure 4.8. In this experiment the AuNP saturation appeared to occur at ~10 nmol. Since there was no significant change in peak area beyond that point the two highest GSNO concentrations were omitted from the graph. Data points are the average peak areas of three independent experiments, and error bars represent the standard deviation of each average.



**Figure 4.7 The flow device**

A flow device was designed on SketchUp for Mac OSX and a prototype was built. **A** is the computational model with two tubes as inlets, one for RSNO and one for AuNP; an outlet for RS-AuNP; and an outlet for NO to be hooked up to an NO detector. The centre of the flow device contains the mixing chamber where the RSNO would bind to the AuNP. **B** shows the implementation of the design. A 96-well plate was filled with 12 GSNO samples of varying concentrations and AuNP in adjacent wells. This was connected through a pump to the teflon flow chamber. An outlet tube on the right can connect to an NO electrode and a tube on the left released the GS-AuNP mixture, which can be injected into an NOA.





**Figure 4.8 S-denitrosylation of GSNO using a flow device**

100  $\mu$ l of GSNO in buffer was added to 12 wells of a 96-well plate in the final amounts of 0, 0.134, 0.268, 0.537, 1.07, 2.14, 4.29, 8.59, 17.18, 34.3, 68.75 and 137.5 nmol. The contents of the first well were pumped alongside 100  $\mu$ l of AuNP where they merged in the mixing chamber of the flow device, and the combination was injected into the NOA. The other dilutions of GSNO were pumped sequentially in the same manner. The peak area, and thus the amount of NO detected, increased with the concentration of GSNO. Beyond 10 nmol there was little change in area, indicating saturation of the AuNP by GSH at that point; consequently, the two highest concentrations of GSNO were omitted from the graph. The data shown are the averages of three independent experiments and the error bars represent the standard deviations of each average.

## 4.5 Discussion

Chapter 3 described a novel AuNP-based reagent for the detection of LMWT. Here, the use of AuNP was extended further as an agent to detect thiols in plasma. The aim of Part I was to use AuNP to isolate these thiol proteins from the rest of the plasma, enabling their later identification. Part II used AuNP as an integral component of a flow system in which GSNO was *S*-denitrosylated by thiol binding to the AuNP. The ultimate goal is to extend its use to proteins to identify the *S*-nitrosoproteome and the sites of *S*-nitrosylation therein.

In Part I, aqueous AuNP was initially used to pull down proteins from the plasma and later PDMS-AuNP was used as well. Since thiols form near-covalent bonds with AuNP, the hypothesis was that these proteins were isolated on the basis of surface thiols, as those would have the best access to the AuNP. After several gels were run the similar banding patterns made it evident that the same proteins were being isolated each time. To ensure that the common factor between them was surface thiols, additional samples were prepared in which the AuNP had been saturated with NaSH. Thiols can exchange at the surface of the nanoparticles but cannot be displaced by other functional groups whose interactions with AuNP are much weaker. Figures 4.1 and 4.2 show that there was little difference between the proteins isolated by untreated or NaSH-saturated AuNP, giving credence to the hypothesis. Additionally, it can be seen that gels in which PDMS-AuNP isolated the proteins exhibited similar banding to aqueous AuNP-isolated proteins. It is important to note that the relative abundances of each protein differed between the two methods. This point will be elaborated upon later in the Discussion.

Once it was established that certain proteins were repeatedly isolated from plasma using AuNP, mass spectrometry was used to attempt to identify them. The first samples

were isolated using aqueous AuNP and prepared without a deglycosylation step. When they were analyzed on the mass spectrometer there was difficulty in mass fingerprint acquisition and PSD analysis. Of the 12 proteins analyzed, only the histidine-rich glycoprotein precursor and actin were identified. Since proteins destined for secretion are glycosylated in the Golgi of the cell (122), we thereafter incorporated a deglycosylation step in sample preparation. A deglycosylating enzyme, peptide N-glycosidase F (PNGase F), was used on 10 protein samples before trypsin digestion. Filamin A actin-binding protein 280, myosin heavy polypeptide 9 non-muscle, and tyrosine 3-monooxygenase/tryptophan 5-monooxygenase activation protein were identified following the modified protocol. Additionally, actin was identified for the second time.

While the deglycosylation ameliorated the identification of these proteins, it also brought a new barrier. The mass fingerprints for several samples contained many of the same peaks; these monopolized the detector so that most of the sample-unique peaks were not strong enough for PSD analysis. The protein sequence of PNGase F was searched in the NCBI Protein database and the “peptide cutter” tool of ExPASy was used to determine theoretical tryptic peptides. It was found that the masses of these peptides corresponded to many of the recurrent peaks of the mass spectrometry samples. Therefore, it was determined that PNGase F contamination precluded identification of more proteins than those listed above. The third mass spectrometry attempt used proteins isolated by PDMS-AuNP rather than aqueous AuNP. Although the washing protocol was followed stringently after the deglycosylation step, PNGase F-specific peaks were present in all 10 of the samples. The peaks unique to each sample were insufficient to identify the proteins.

These results obtained are purely preliminary due to the difficulties in the identification process. Protocol optimization must be achieved prior to subsequent work on this project. One potential method of avoiding PNGase F contamination could be to deglycosylate all of the proteins before running the gel. That way the enzyme would have its own band in the gel at ~36 kDa and not be present in the excised protein samples. Alternatively, chemical rather than enzymatic deglycosylation methods could be explored.

Seven proteins were nevertheless identified by mass spectrometry and by Western blotting. The protein structures were viewed in Cn3D whenever possible. The cysteine residues were highlighted in red and the proteins were shown in Figure 4.4. All of the proteins except for HSP70 had more than one cysteine at the surface, and in several cases, such as PDI, the cysteines were vicinal. These residues are the most likely candidates for binding to AuNP. The cysteines of HSP70 ATPase domain are partially buried; however, the flexibility of proteins may allow one or more cysteine to become exposed and bind to the AuNP. Additionally, HSP70 may have instead bound to AuNP by its substrate-binding domain or C-terminal domain. Therefore, these structures strengthen the hypothesis that surface thiols cause the selective binding of certain proteins to AuNP.

Table 4.1 is a compilation of the localizations and functions of each identified protein. While 3 of the proteins can be found in the plasma, the others are located inside the platelets. This suggests that some platelets remained in the plasma after centrifugation. Subsequent plasma isolation procedures should therefore use higher speeds and longer centrifugation times to ensure that all the platelets have been removed.

Once proteins are identified, the next objective will be to verify the binding sites of the proteins. This may be accomplished as follows. The proteins would be isolated

from the plasma by incubation with aqueous or PDMS-bound AuNP. PNGase F would deglycosylate the proteins and be washed off. Then the samples would be digested with trypsin, followed by washing. At that point the only peptides remaining in the sample would be those that bound directly to the AuNP. They could be eluted using an excess of DTT or another small thiol, separated with high-performance liquid chromatography and spotted onto the MALDI plate. Once the masses of the peptides and PSD fragments were detected, database searching would reveal the sequence and the specific cysteines that bound to the AuNP. In summary, there is more to be done to identify the thiol proteome in addition to the steps that have been made.

Part II was the progress toward building a flow device to identify the *S*-nitrosoproteome. AuNP had already been shown to be capable of *S*-denitrosylation by binding to the thiols, thereby releasing NO (123). Here, we used this knowledge to test our experimental design before using it to determine whether or not PDMS-AuNP *S*-denitrosylates thiols as well. All of the samples of GSNO and AuNP were kept in screw-top vials with septa and blown with argon before use. This was because GSNO may have partially *S*-denitrosylated in the buffer, either spontaneously or after exposure to light. Argon treatment eliminated the NO from the solutions and the air inside the vials. Therefore, any NO detected by the NOA was purely from the *S*-denitrosylation by the AuNP. Additionally, only the headspaces above the solutions were injected to eliminate the possibility that GSNO would spontaneously *S*-denitrosylate inside the NOA through the bubbling solution or through reaction with ozone.

As seen in Figure 4.5, no peaks were observed in the control containing only buffer without GSNO, indicating that the purging with argon removed all NO from the air in the vial. It was also demonstrated that all NO detected was the result of *S*-

denitrosylation by AuNP, since no peaks were observed when the GSNO solutions were added to buffer instead. The clear saturation curve indicated that the limit of the surface area of 200  $\mu$ l of AuNP was 10 nmol of GSNO.

The next step was to test the ability of PDMS-AuNP to *S*-denitrosylate GSNO. PDMS-AuNP would be useful in a flow device because it is immobilized, allowing a sample to pass over it without dilution. The experimental design used was similar to that of aqueous AuNP. 200  $\mu$ l of PDMS-AuNP or PDMS control were prepared in vials and degassed; degassed GSNO samples were injected into those vials; and the NO released was injected into the NOA from the headspace. Here, an additional concentration of 350  $\mu$ M was used and more nmol of GSNO were added to the PDMS-AuNP or PDMS vials. The result with PDMS-AuNP was a similar saturation curve as with aqueous AuNP, shown in Figure 4.6. In this case, the saturation limit was about 40 nmol from 4 independent trials. These data show that PDMS-AuNP has potential as an *S*-denitrosylation agent in a flow device.

One problem observed in this experiment was that PDMS alone *S*-denitrosylated GSNO in the absence of AuNP. Furthermore, in the thiol proteome portion of the project, the controls showed that nonspecific protein binding occurred as well. In both sub-projects, therefore, the use of PDMS has had drawbacks. A solution would be to find another substance that can immobilize the AuNP while remaining inert to the proteins and other molecules added. One possibility is organometallic chemical vapor deposition (OMCVD), which synthesizes nanoparticles on a glass surface (124). Thus alternatives to PDMS, or improvements to the methods currently used with PDMS and PDMS-AuNP, should be explored before a flow device is planned that incorporates immobilized AuNP.

With that in mind, we designed a flow device that utilizes aqueous AuNP. In the trial model the solution was pumped into a flow chamber along with a sample containing GSNO. When they mixed, the resultant solution was injected into the NOA. Figure 4.8 shows that as increasing concentrations of GSNO were pumped, the amount of NO detected followed the same saturation curve as seen in the prior Figures. As this was simply a more streamlined approach to the same experiment that yielded Figure 4.5 above, the similar results were expected. However, half as much AuNP was present in the solution with the flow device, meaning half the surface area was available to *S*-denitrosylate the GSNO compared to the original experiment, yet they had the same saturation point of 10 nmol GSNO. This is likely to be because the GSNO solutions were not degassed prior to mixing with AuNP, and the solutions themselves were injected into the NOA rather than the gas headspace. This means there probably was NO in the solution other than that released by AuNP and this would have been detected, skewing the results. Therefore, the design of the flow system may require modification.

Ultimately, the desired system would be fully automated so that the researcher would only need to apply the sample, such as plasma, to acquire the results. Total RSNO of the sample would be quantified. Additionally, the flow device would be used in conjunction with high-performance liquid chromatography (HPLC) and mass spectrometry to identify the *S*-nitrosoproteome. Finally, the sites of *S*-nitrosylation would be identified by the method of thiol binding detection described above. The use of an NO electrode would ameliorate detection since the NO released from a protein or small molecule could immediately travel to the detector, eliminating the need to inject the samples manually. Thus, Parts I and II both have future work to be accomplished but the groundwork has been established with promise for important results to come.

## 5.1 Conclusions

Nitric oxide and thiols are intimately linked in physiology. As molecules that both protect and transport NO, thiols have great influence on NO signaling. Conversely, when NO is bound to a protein or small molecule it may act as an inhibitor, hindering reductase or catalytic activity. Both are found in high concentrations in the bloodstream, making blood an important tissue for NO and thiol chemistry. For these reasons it is difficult to study one without considering the other.

The first project studied the role of nitric oxide synthase under hypoxia. In experiments using cells, inhibitors and purified enzymes, it was concluded that eNOS is the one NOS isozyme capable of reducing  $\text{NO}_2^-$  to NO when limited oxygen supply precludes its proper biosynthesis. Since oxygen is dependent on blood flow, endothelial cells are among the first cells to detect the decrease in supply and it is logical that they would be equipped to compensate for it. NO produced from extracellular nitrite can cause dilation of blood vessels to transport oxygen and generally restore conditions to normal when possible. Even in hypoxic conditions, NO would depend on the thiols in the blood to operate after its synthesis from nitrite.

Next the gold nanoparticle-based reagent was synthesized. By virtue of their optical properties and a disulfide bond in the middle of the crosslinking GSSG, the AuNP were used here to detect low molecular weight thiols. It was found that only molecules less than 310  $\text{D}_a$  were able to cleave the disulfide bond; the rate of this reaction depended on both the size and the concentration of the thiol. This gives it potential to quantify the total LMWT in plasma or other samples, which could be extended to a comparison of plasma small thiols between conditions. For example, since RSNO cannot reduce disulfide bonds, their concentrations could be calculated indirectly by the loss of free



thiols from a pool measured before and after an NO donor is added. Therefore, this rapid reagent to detect thiols has usefulness for studying both thiol and NO chemistry.

The third project applied gold nanoparticles to both protein thiols and RSNO. The AuNP isolated certain proteins from plasma repeatedly. Seven were identified by mass spectrometry and Western blot. Based on the structures of the identified proteins, and by a comparison of the gels when NaSH was exchanged or not present, the proteins were likely bound to the AuNP by their surface thiols. This began the work toward characterizing the thiol proteome of plasma which may be extended in the future to other groups of proteins.

Both aqueous and PDMS-bound AuNP were also used to begin the process of *S*-nitrosoproteome identification. AuNP were shown to *S*-denitrosylate GSNO to establish that AuNP could be the basis for one or more type of future flow device that would rapidly and automatically quantify RSNO in a sample. It will be modified to identify the *S*-denitrosylated proteins, thereby revealing the *S*-nitrosoproteome. Finally, the sites of *S*-nitrosylation of identified proteins will be identified as well. The prototype model is manual and requires optimization of its operation. However, it is able to *S*-denitrosylate GSNO and shows the potential of the flow system.

The importance of both small and protein thiols has been stressed throughout these three projects, as well as the connection between NO and thiols. The correct oxidation state of thiols must be maintained to keep individuals healthy, and gold nanoparticles have been exploited in several applications that may aid in identification of this state. Therefore, the present advancements in NO and thiol research have interest in medical, academic, and industrial settings.

## REFERENCES

1. Ignarro, L. J. (ed) (2000) *Nitric Oxide: Biology and Pathobiology*, Academic Press, San Diego, CA
2. Ignarro, L. J., Buga, G. M., Wood, K. S., Byrns, R. E., and Chaudhuri, G. (1987) *Proc Natl Acad Sci U S A* **84**, 9265-9269
3. Palmer, R. M., Ferrige, A. G., and Moncada, S. (1987) *Nature* **327**, 524-526
4. Bassenge, E. (1991) *Z Kardiol* **80 Suppl 5**, 17-21
5. Roberts, D. D., Isenberg, J. S., Ridnour, L. A., and Wink, D. A. (2007) *Clin Cancer Res* **13**, 795-798
6. Marletta, M. A., Yoon, P. S., Iyengar, R., Leaf, C. D., and Wishnok, J. S. (1988) *Biochemistry* **27**, 8706-8711
7. Brecht, D. S., and Snyder, S. H. (1990) *Proc Natl Acad Sci U S A* **87**, 682-685
8. White, K. A., and Marletta, M. A. (1992) *Biochemistry* **31**, 6627-6631
9. Fischmann, T. O., Hruza, A., Niu, X. D., Fossetta, J. D., Lunn, C. A., Dolphin, E., Prongay, A. J., Reichert, P., Lundell, D. J., Narula, S. K., and Weber, P. C. (1999) *Nat Struct Biol* **6**, 233-242
10. Masters, B. S., McMillan, K., Sheta, E. A., Nishimura, J. S., Roman, L. J., and Martasek, P. (1996) *FASEB J* **10**, 552-558
11. Lamas, S., Marsden, P. A., Li, G. K., Tempst, P., and Michel, T. (1992) *Proc Natl Acad Sci U S A* **89**, 6348-6352
12. Garcia-Cardena, G., Martasek, P., Masters, B. S., Skidd, P. M., Couet, J., Li, S., Lisanti, M. P., and Sessa, W. C. (1997) *J Biol Chem* **272**, 25437-25440
13. Stuehr, D. J. (1999) *Biochim Biophys Acta* **1411**, 217-230
14. Stuehr, D. J., Kwon, N. S., Nathan, C. F., Griffith, O. W., Feldman, P. L., and Wiseman, J. (1991) *J Biol Chem* **266**, 6259-6263
15. Sakuma, I., Stuehr, D. J., Gross, S. S., Nathan, C., and Levi, R. (1988) *Proc Natl Acad Sci U S A* **85**, 8664-8667
16. Shaw, A. W. a. V., A. J. (1977) *J Chem Soc Faraday Trans* **8**, 1239-1244
17. Malinski, T., Taha, Z., Grunfeld, S., Patton, S., Kapturczak, M., and Tombouliau, P. (1993) *Biochem Biophys Res Commun* **193**, 1076-1082
18. Lancaster, J. R., Jr. (1997) *Nitric Oxide* **1**, 18-30
19. Lancaster, J. R., Jr. (1996) *Methods Enzymol* **268**, 31-50
20. Viinikka, L. (1996) *Scand J Clin Lab Invest* **56**, 577-581
21. McKellar, A. R. W., Watson, J. K. G., and Howard, B. J. (1995) *Mol. Phys.* **86**, 273-286
22. Olbregts, J. (1985) *International Journal of Chemical Kinetics* **17**, 835-848
23. Huie, R. E. (1994) *Toxicology* **89**, 193-216
24. Sliskovic, I., Raturi, A., and Mutus, B. (2005) *J Biol Chem* **280**, 8733-8741
25. Pogrebnaya, V. L., Usov, A. P., Baranov, A. V., Nesterenko, A. I., and Bez'yazchnyi, P. I. . (1975) *J. Appl. Chem. USSR* **48**, 1004-1007
26. Blough, N. V. a. Z., O. C. (1985) *Inorg Chem* **24**, 3502-3504
27. Lyman, S. V. a. H., J. K. (1995) *J Am Chem Soc* **117**, 8867-8868
28. Miles, A. M., Bohle, D. S., Glassbrenner, P. A., Hansert, B., Wink, D. A., and Grisham, M. B. (1996) *J Biol Chem* **271**, 40-47

29. Bryan, N. S., Fernandez, B. O., Bauer, S. M., Garcia-Saura, M. F., Milsom, A. B., Rassaf, T., Maloney, R. E., Bharti, A., Rodriguez, J., and Feelisch, M. (2005) *Nat Chem Biol* **1**, 290-297
30. Lundberg, J. O., and Weitzberg, E. (2005) *Arterioscler Thromb Vasc Biol* **25**, 915-922
31. Mikula, I., Durocher, S., Martasek, P., Mutus, B., and Slama-Schwok, A. (2009) *Biochem J* **418**, 673-682
32. Halliwell, B. (1995) *Am J Clin Nutr* **61**, 670S-677S
33. Darley-USmar, V. M., Hogg, N., O'Leary, V. J., Wilson, M. T., and Moncada, S. (1992) *Free Radic Res Commun* **17**, 9-20
34. O'Donnell, V. B., Chumley, P. H., Hogg, N., Bloodsworth, A., Darley-USmar, V. M., and Freeman, B. A. (1997) *Biochemistry* **36**, 15216-15223
35. Wink, D. A., Hanbauer, I., Krishna, M. C., DeGraff, W., Gamson, J., and Mitchell, J. B. (1993) *Proc Natl Acad Sci U S A* **90**, 9813-9817
36. Hadzic, T., Li, L., Cheng, N., Walsh, S. A., Spitz, D. R., and Knudson, C. M. (2005) *J Immunol* **175**, 7965-7972
37. Hawkins, H. C., de Nardi, M., and Freedman, R. B. (1991) *Biochem J* **275** ( Pt 2), 341-348
38. Foster, M. W., McMahon, T. J., and Stamler, J. S. (2003) *Trends Mol Med* **9**, 160-168
39. Gow, A. J., Buerk, D. G., and Ischiropoulos, H. (1997) *J Biol Chem* **272**, 2841-2845
40. Greco, T. M., Hodara, R., Parastatidis, I., Heijnen, H. F., Dennehy, M. K., Liebler, D. C., and Ischiropoulos, H. (2006) *Proc Natl Acad Sci U S A* **103**, 7420-7425
41. Stubauer, G., Giuffre, A., and Sarti, P. (1999) *J Biol Chem* **274**, 28128-28133
42. Williams, D. L. H. (1988) *Nitrosation*, Cambridge Univ. Press, Cambridge, UK
43. van der Vliet, A., Hoen, P. A., Wong, P. S., Bast, A., and Cross, C. E. (1998) *J Biol Chem* **273**, 30255-30262
44. Singh, R. J., Hogg, N., Joseph, J., and Kalyanaraman, B. (1996) *J Biol Chem* **271**, 18596-18603
45. Eich, R. F., Li, T., Lemon, D. D., Doherty, D. H., Curry, S. R., Aitken, J. F., Mathews, A. J., Johnson, K. A., Smith, R. D., Phillips, G. N., Jr., and Olson, J. S. (1996) *Biochemistry* **35**, 6976-6983
46. Wade, R. S., and Castro, C. E. (1990) *Chem Res Toxicol* **3**, 289-291
47. Zhao, Y., Hoganson, C., Babcock, G. T., and Marletta, M. A. (1998) *Biochemistry* **37**, 12458-12464
48. Zhao, Y., Schelvis, J. P., Babcock, G. T., and Marletta, M. A. (1998) *Biochemistry* **37**, 4502-4509
49. Tsai, E. J., and Kass, D. A. (2009) *Pharmacol Ther* **122**, 216-238
50. Wiley, J. W. (2007) *Neurogastroenterol Motil* **19**, 541-544
51. Terada, K., Manchikalapudi, P., Noiva, R., Jauregui, H. O., Stockert, R. J., and Schilsky, M. L. (1995) *J Biol Chem* **270**, 20410-20416
52. Jourdain, D., Hallen, K., Feelisch, M., and Grisham, M. B. (2000) *Free Radic Biol Med* **28**, 409-417
53. Nedospasov, A., Rafikov, R., Beda, N., and Nudler, E. (2000) *Proc Natl Acad Sci U S A* **97**, 13543-13548

54. Hobbs, A. J., Gladwin, M. T., Patel, R. P., Williams, D. L., and Butler, A. R. (2002) *Trends Pharmacol Sci* **23**, 406-411
55. Hellermann, G. R., and Solomonson, L. P. (1997) *J Biol Chem* **272**, 12030-12034
56. Fulton, D., Babbitt, R., Zoellner, S., Fontana, J., Acevedo, L., McCabe, T. J., Iwakiri, Y., and Sessa, W. C. (2004) *J Biol Chem* **279**, 30349-30357
57. Wakayama, Y., Inoue, M., Kojima, H., Murahashi, M., Shibuya, S., and Oniki, H. (2001) *Microsc Res Tech* **55**, 154-163
58. Morris, S. M., Jr. (2005) *Vasc Med* **10 Suppl 1**, S83-87
59. Rogers, N. E., and Ignarro, L. J. (1992) *Biochem Biophys Res Commun* **189**, 242-249
60. Nakayama, D. K., Geller, D. A., Lowenstein, C. J., Chern, H. D., Davies, P., Pitt, B. R., Simmons, R. L., and Billiar, T. R. (1992) *Am J Respir Cell Mol Biol* **7**, 471-476
61. Nussler, A. K., Di Silvio, M., Billiar, T. R., Hoffman, R. A., Geller, D. A., Selby, R., Madariaga, J., and Simmons, R. L. (1992) *J Exp Med* **176**, 261-264
62. Griscavage, J. M., Rogers, N. E., Sherman, M. P., and Ignarro, L. J. (1993) *J Immunol* **151**, 6329-6337
63. Wang, W. W., Jenkinson, C. P., Griscavage, J. M., Kern, R. M., Arabolos, N. S., Byrns, R. E., Cederbaum, S. D., and Ignarro, L. J. (1995) *Biochem Biophys Res Commun* **210**, 1009-1016
64. Kojima, H., Nakatsubo, N., Kikuchi, K., Kawahara, S., Kirino, Y., Nagoshi, H., Hirata, Y., and Nagano, T. (1998) *Anal Chem* **70**, 2446-2453
65. Sievers. Nitric Oxide Analyzer Liquid Applications, online manual.
66. Jaffrey, S. R., Erdjument-Bromage, H., Ferris, C. D., Tempst, P., and Snyder, S. H. (2001) *Nat Cell Biol* **3**, 193-197
67. Zhang, X., Kim, W. S., Hatcher, N., Potgieter, K., Moroz, L. L., Gillette, R., and Sweedler, J. V. (2002) *J Biol Chem* **277**, 48472-48478
68. Huang, B., and Chen, C. (2006) *Free Radic Biol Med* **41**, 562-567
69. Daniel, M. C., and Astruc, D. (2004) *Chem Rev* **104**, 293-346
70. Hayat, M. A. (ed) (1989) *Colloidal gold: Principles, methods and applications*, Vol. 1, Academic, New York, NY
71. Faraday, M. (1857) *Philos. Trans. R. Soc. London* **147**, 145
72. Capek, I. (2004) *Adv Colloid Interface Sci* **110**, 49-74
73. Turkevich, J., Stevenson, P. C., Hillier, J. (1951) *Discuss. Faraday Soc.* **11**, 55-75
74. Frens, J. (1973) *Nature: Phys. Sci.* **241**, 20-22
75. Grabar, K. C., Freeman, R. G., Hommer, M. B., and Natan, M. J. (1995) *Analytical Chemistry* **67**, 735-743
76. N. R. Jana, L. Gearheart, and C. J. Murphy. (2001) *Advanced Materials* **13**, 1389-1393
77. Sau, T. K., and Murphy, C. J. (2004) *J Am Chem Soc* **126**, 8648-8649
78. Brust, M., Walker, M., Bethell, D., Schiffrin, D. J., and Whyman, R. J. (1994) *J. Chem. Soc., Chem. Commun.*, 801-802
79. Wallraff, G. M., and Hinsberg, W. D. (1999) *Chem Rev* **99**, 1801-1822
80. Eustis, S., Hsu, H. Y., and El-Sayed, M. A. (2005) *J Phys Chem B* **109**, 4811-4815
81. Kuncova-Kallio, J., and Kallio, P. J. (2006) *Conf Proc IEEE Eng Med Biol Soc* **1**, 2486-2489

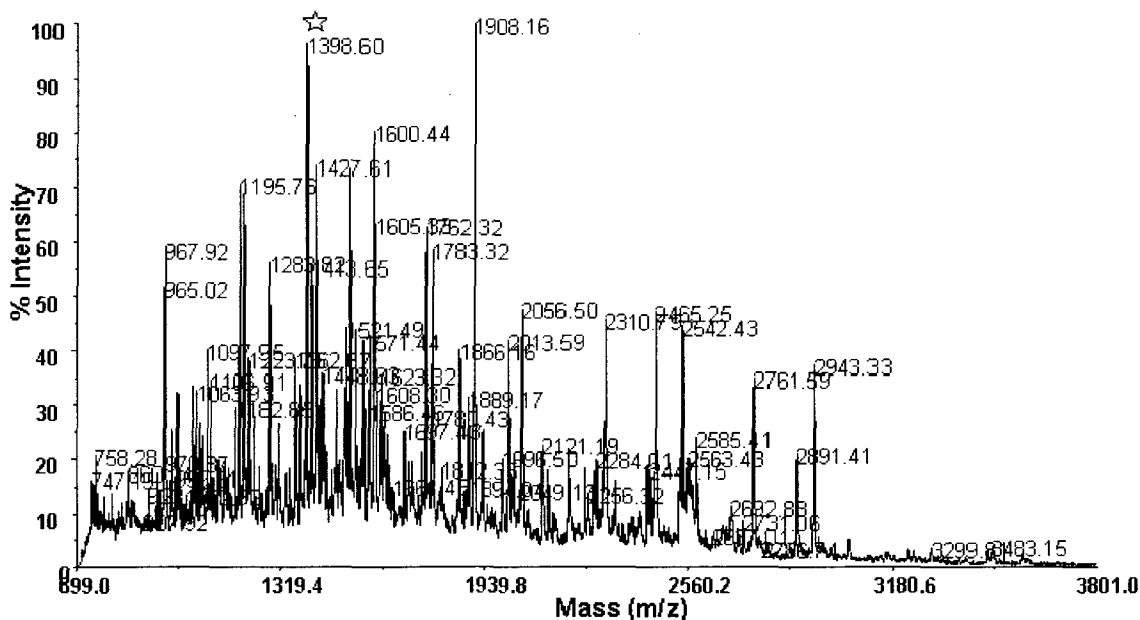
82. Simpson, T. R. E., Tabatabaian, Z., Jeynes, C., Parbhoo, B., Keddie, J. L. (2003) *Journal of Polymer Science: Part A: Polymer Chemistry* **42**, 1421-1431
83. Zhang, Q., Xu, J. J., Liu, Y., and Chen, H. Y. (2008) *Lab Chip* **8**, 352-357
84. Eustis, S., and el-Sayed, M. A. (2006) *Chem Soc Rev* **35**, 209-217
85. Kelly, K. L., Coronado, E., Zhao, L. L., Schatz, G. C. (2003) *J. Phys. Chem. B* **107**, 668-677
86. Maier, S. A., Kik, P. G., and Atwater, H. A. . (2002) *Appl. Phys. Lett.* **81**, 1714-1716
87. Jadzinsky, P. D., Calero, G., Ackerson, C. J., Bushnell, D. A., and Kornberg, R. D. (2007) *Science* **318**, 430-433
88. Wessels, J. M., Nothofer, H. G., Ford, W. E., von Wrochem, F., Scholz, F., Vossmeier, T., Schroedter, A., Weller, H., and Yasuda, A. (2004) *J Am Chem Soc* **126**, 3349-3356
89. Schmitt, J., Machtle, P., Eck, D., Mohwald, H., and Helm, C. A. (1999) *Langmuir* **15**
90. Lakowicz, J. R., Geddes, C. D., Gryczynski, I., Malicka, J., Gryczynski, Z., Aslan, K., Lukomska, J., Matveeva, E., Zhang, J., Badugu, R., and Huang, J. (2004) *J Fluoresc* **14**, 425-441
91. Medina, C., Santos-Martinez, M. J., Radomski, A., Corrigan, O. I., and Radomski, M. W. (2007) *Br J Pharmacol* **150**, 552-558
92. Winter, P. M., Morawski, A. M., Caruthers, S. D., Fuhrhop, R. W., Zhang, H., Williams, T. A., Allen, J. S., Lacy, E. K., Robertson, J. D., Lanza, G. M., and Wickline, S. A. (2003) *Circulation* **108**, 2270-2274
93. Kneipp, J., Kneipp, H., and Kneipp, K. (2008) *Chem Soc Rev* **37**, 1052-1060
94. Kneipp, K., Kneipp, H., Itzkan, I., Dasari, R. R., and Feld, M. S. (1999) *Chem Rev* **99**, 2957-2976
95. Hao, E., Schatz, G. C., and Hupp, J. T. (2004) *J Fluoresc* **14**, 331-341
96. Elghanian, R., Storhoff, J. J., Mucic, R. C., Letsinger, R. L., and Mirkin, C. A. (1997) *Science* **277**, 1078-1081
97. Storhoff, J. J., Lucas, A. D., Garimella, V., Bao, Y. P., and Muller, U. R. (2004) *Nat Biotechnol* **22**, 883-887
98. Gautier, C., van Faassen, E., Mikula, I., Martasek, P., and Slama-Schwok, A. (2006) *Biochem Biophys Res Commun* **341**, 816-821
99. Vanin, A. F., Bevers, L. M., Slama-Schwok, A., and van Faassen, E. E. (2007) *Cell Mol Life Sci* **64**, 96-103
100. Bland-Ward, P. A., Pitcher, A., Wallace, P., Gaffen, Z., Babbedge, R. C. and Moore, P. K. (1994) *Br J Pharmacol* **112**, 312
101. Crane, M. S., Ollosson, R., Moore, K. P., Rossi, A. G., and Megson, I. L. (2002) *J Biol Chem* **277**, 46858-46863
102. Ivanov, A. R., Nazimov, I. V., and Baratova, L. A. (2000) *J Chromatogr A* **870**, 433-442
103. Ivanov, A. R., Nazimov, I. V., and Baratova, L. (2000) *J Chromatogr A* **895**, 157-166
104. Ivanov, A. R., Nazimov, I. V., and Baratova, L. A. (2000) *J Chromatogr A* **895**, 167-171
105. Liang, S. C., Wang, H., Zhang, Z. M., and Zhang, H. S. (2005) *Anal Bioanal Chem* **381**, 1095-1100

106. Ondarza, R. N., Iturbe, A., Hernandez, E., and Hurtado, G. (2003) *Biotechnol Appl Biochem* **37**, 195-204
107. Raturi, A., Vacratsis, P. O., Seslija, D., Lee, L., and Mutus, B. (2005) *Biochem J* **391**, 351-357
108. Raturi, A., and Mutus, B. (2007) *Free Radic Biol Med* **43**, 62-70
109. Pastore, A., Piemonte, F., Locatelli, M., Lo Russo, A., Gaeta, L. M., Tozzi, G., and Federici, G. (2001) *Clin Chem* **47**, 1467-1469
110. Lundstrom, J., and Holmgren, A. (1990) *J Biol Chem* **265**, 9114-9120
111. Bindoli, A., Fukuto, J. M., and Forman, H. J. (2008) *Antioxid Redox Signal* **10**, 1549-1564
112. Laurindo, F. R., Fernandes, D. C., Amanso, A. M., Lopes, L. R., and Santos, C. X. (2008) *Antioxid Redox Signal* **10**, 1101-1113
113. Raymond, S., and Weintraub, L. (1959) *Science* **130**, 711
114. Sharda, P. R., Bonham, C. A., Mucaki, E. J., Butt, Z., and Vacratsis, P. O. (2009) *Biochem J* **418**, 391-401
115. Root, P., Sliskovic, I., and Mutus, B. (2004) *Biochem J* **382**, 575-580
116. Muranyi, A., Erdodi, F., Ito, M., Gergely, P., and Hartshorne, D. J. (1998) *Biochem J* **330** ( Pt 1), 225-231
117. Xu, W., Xie, Z., Chung, D. W., and Davie, E. W. (1998) *Blood* **92**, 1268-1276
118. Ohta, T., Ikemoto, Y., Saeki, K., Koide, T., and Wakabayashi, S. (2009) *Cell Immunol* **259**, 5-12
119. Li, Z., and Srivastava, P. (2004) *Curr Protoc Immunol* **Appendix 1**, Appendix 1T
120. Turano, C., Coppari, S., Altieri, F., and Ferraro, A. (2002) *J Cell Physiol* **193**, 154-163
121. Kobayashi, R., Deavers, M., Patenia, R., Rice-Stitt, T., Halbe, J., Gallardo, S., and Freedman, R. S. (2009) *Cancer Immunol Immunother* **58**, 247-258
122. Ungar, D. (2009) *Semin Cell Dev Biol*
123. Jia, H. Y., Liu, Y., Zhang, X. J., Han, L., Du, L. B., Tian, Q., and Xu, Y. C. (2009) *J Am Chem Soc* **131**, 40-41
124. Aliganga, A. K. A., Lieberwirth, I., Glasser, G., Duwez, A. S., Sun, Y. Z. and Mittler, S. (2007) *Org. Electron.* **8**

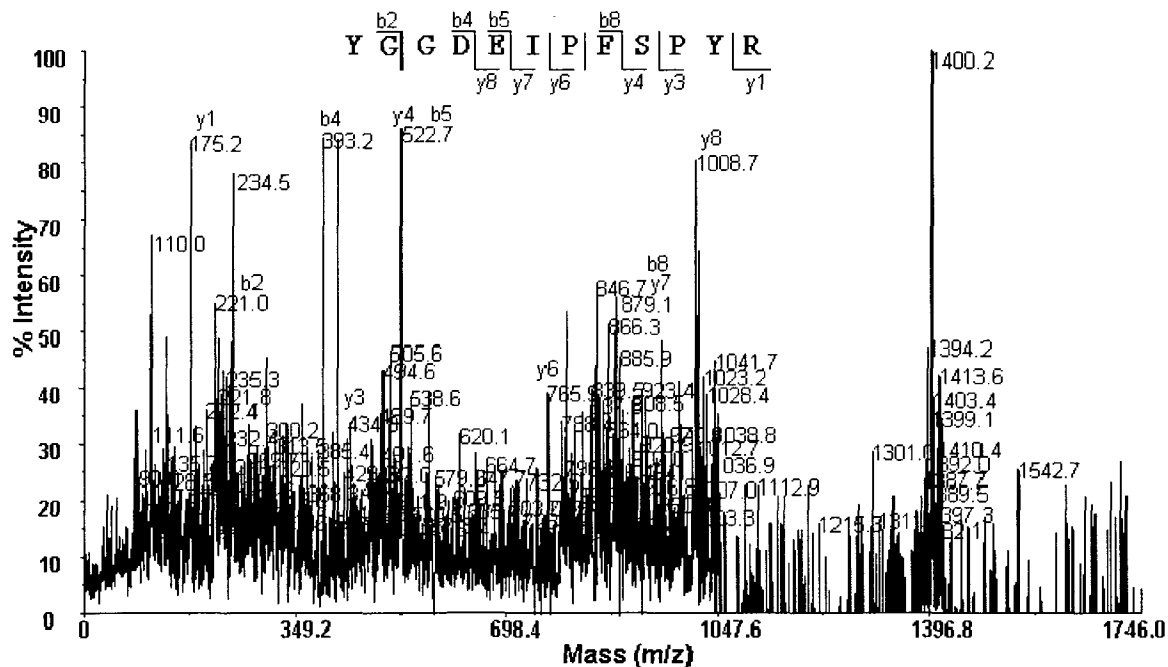
## APPENDIX A

Below is the mass spectrometry raw data used to identify the proteins actin, filamin A actin-binding protein 280, complement C1qB, histidine-rich glycoprotein precursor, myosin heavy polypeptide 9 non-muscle, and tyrosine 3-monooxygenase/tryptophan 5-monooxygenase activation protein. The fingerprints for each protein are shown, as well as their PSD data that aided in the identification. The fingerprint peaks that were used for PSD are indicated with stars. In addition, the last figure shows two examples of fingerprints in which PNGase F tryptic peptides are suspected to have contaminated the samples, precluding identification. The fingerprint masses suspected or known to correspond to PNGase F fingerprint masses are boxed.

# Filamin A actin-binding protein 280

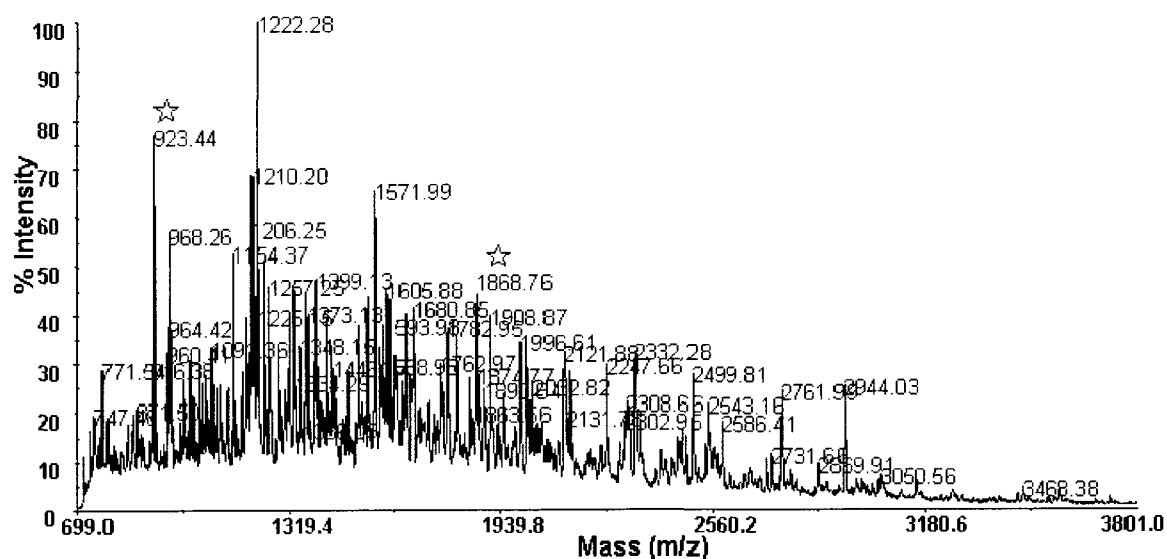


## Filamin A actin-binding protein 280 PSD

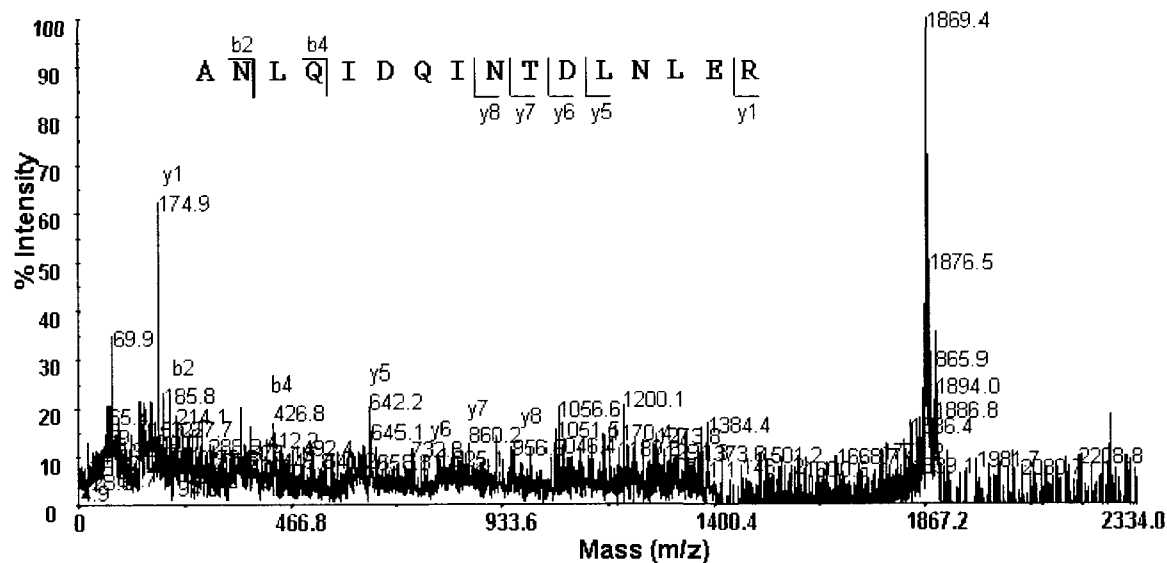




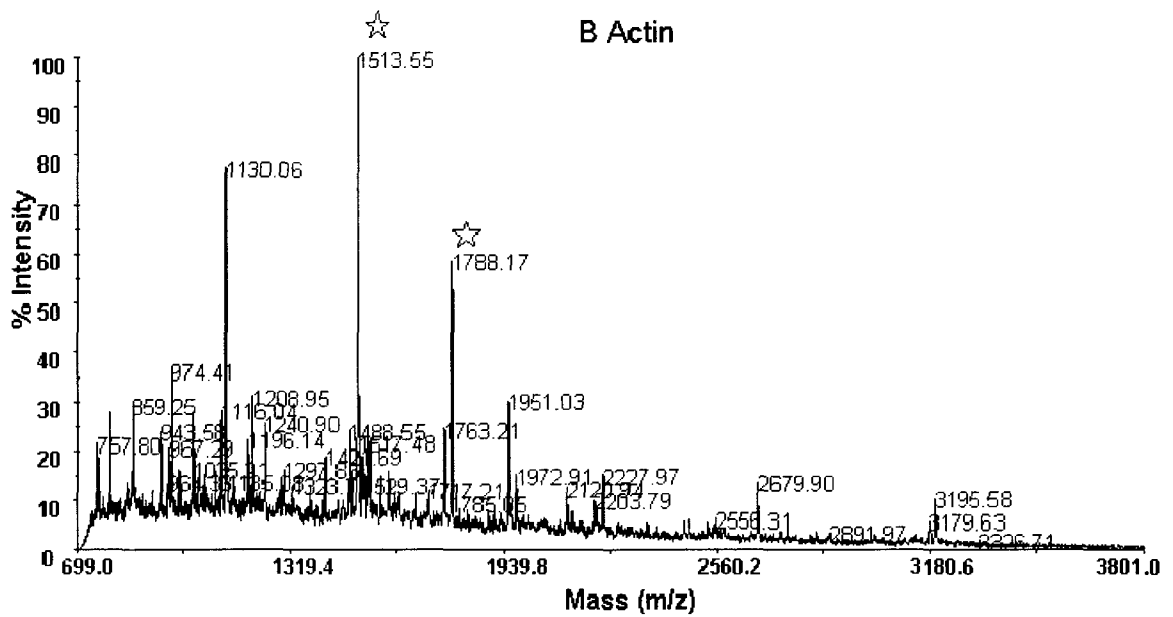
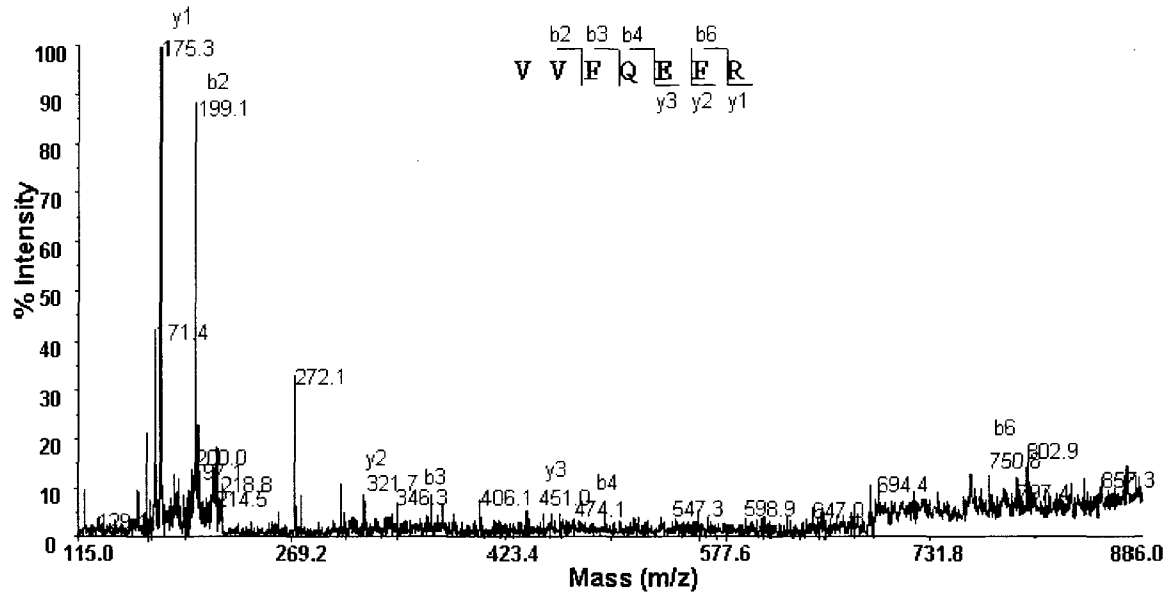
# Myosin heavy polypeptide 9 non-muscle

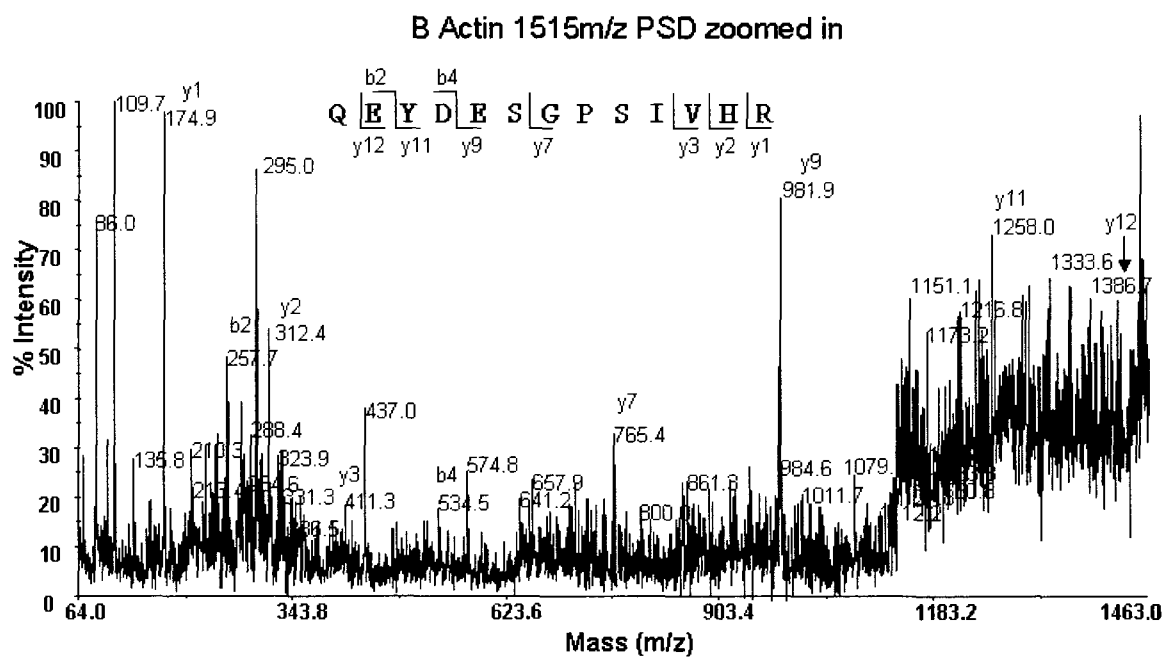
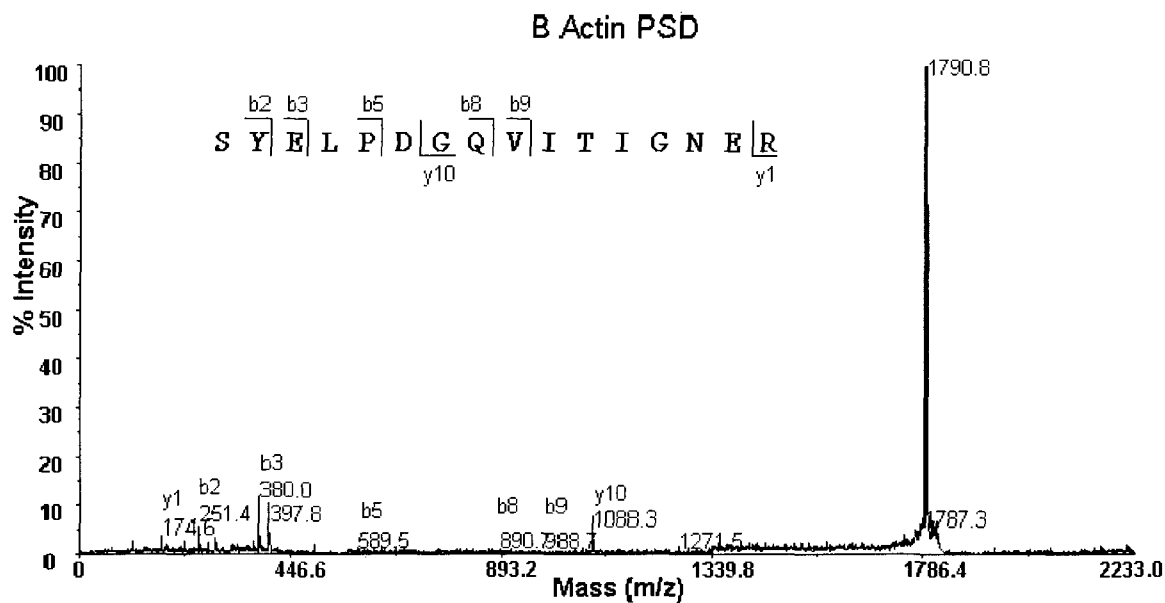


## Myosin heavy polypeptide 9 non-muscle PSD

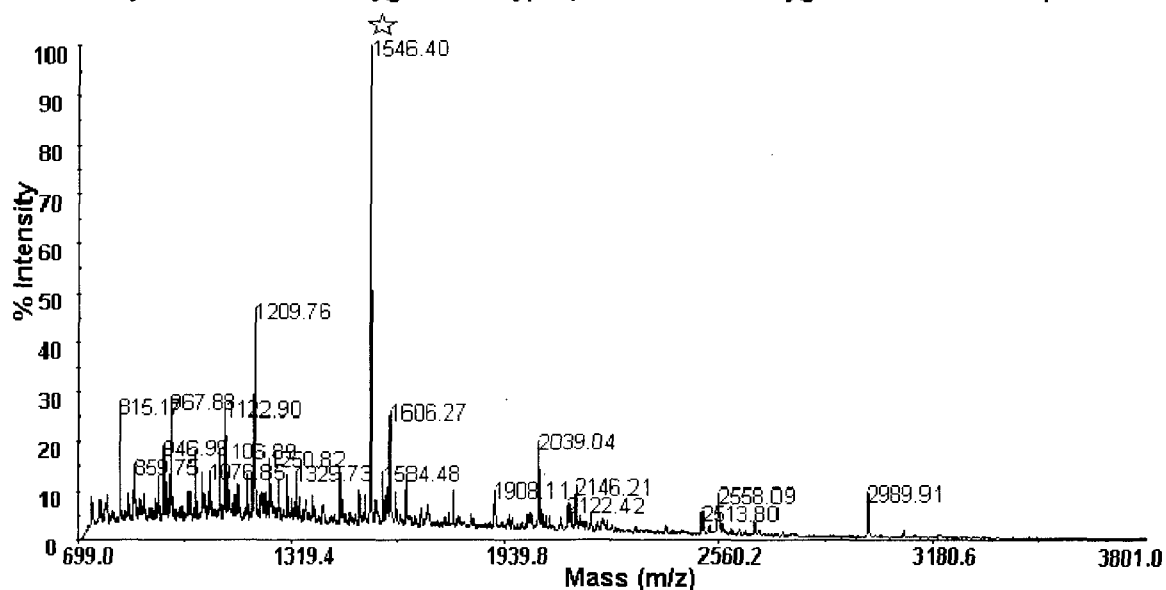


Myosin heavy polypeptide 9 non-muscle  
923m/z PSD zoomed in

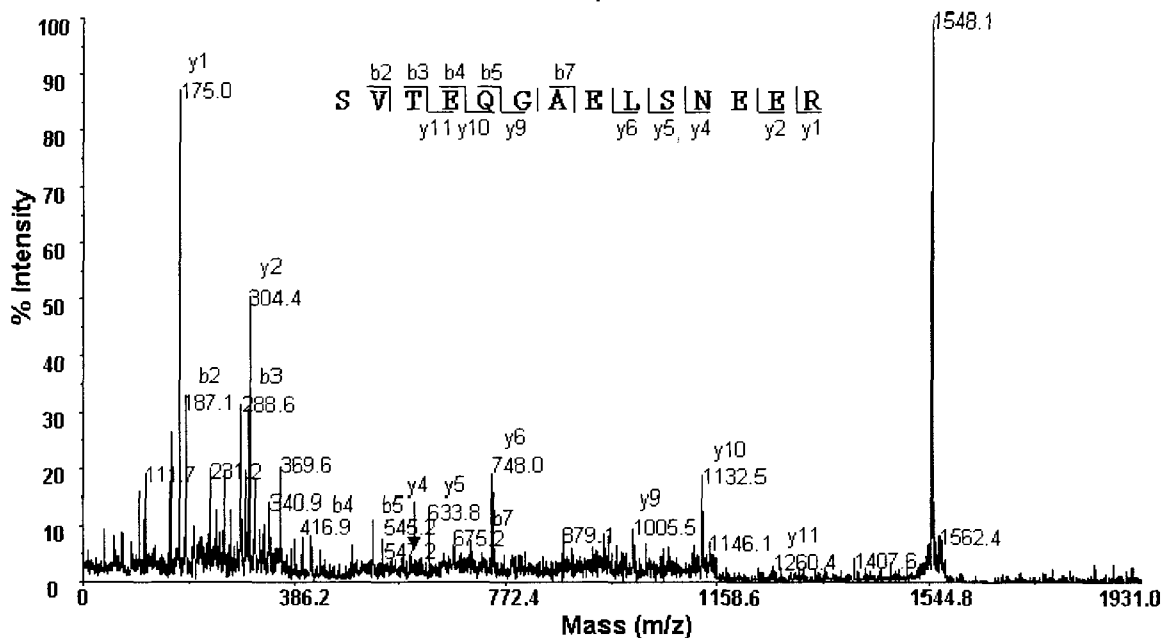


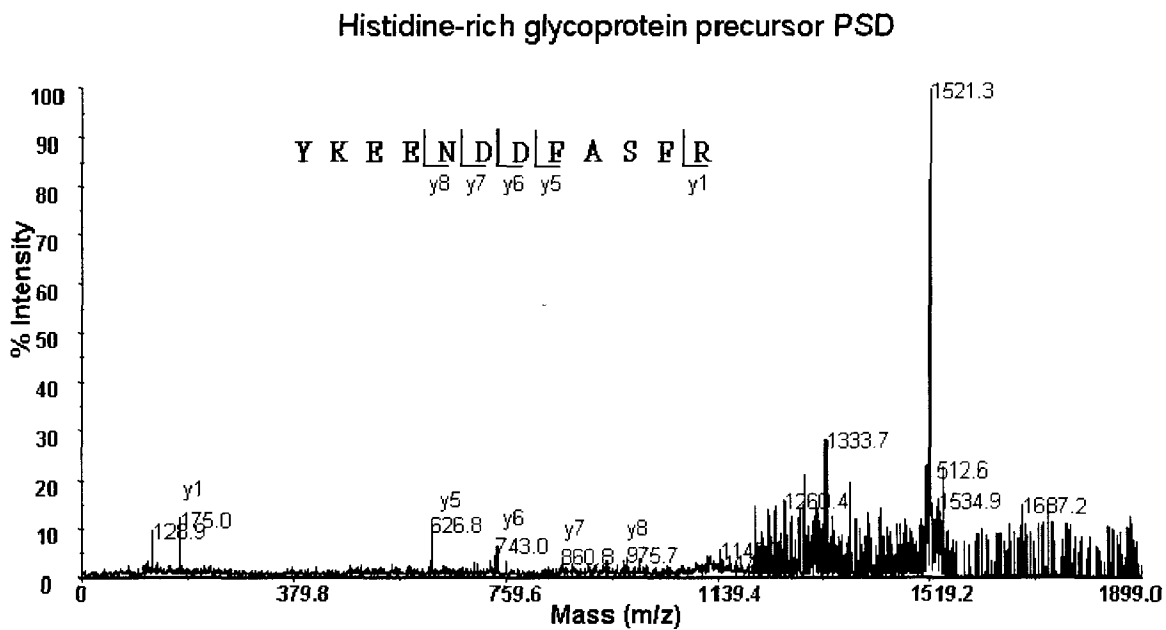
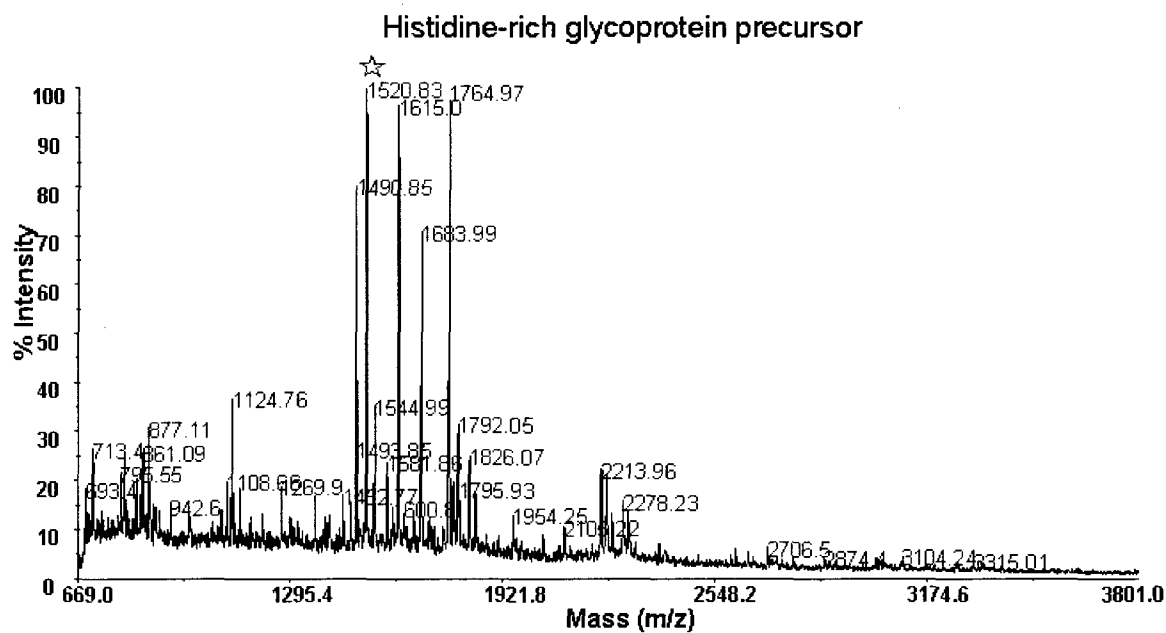


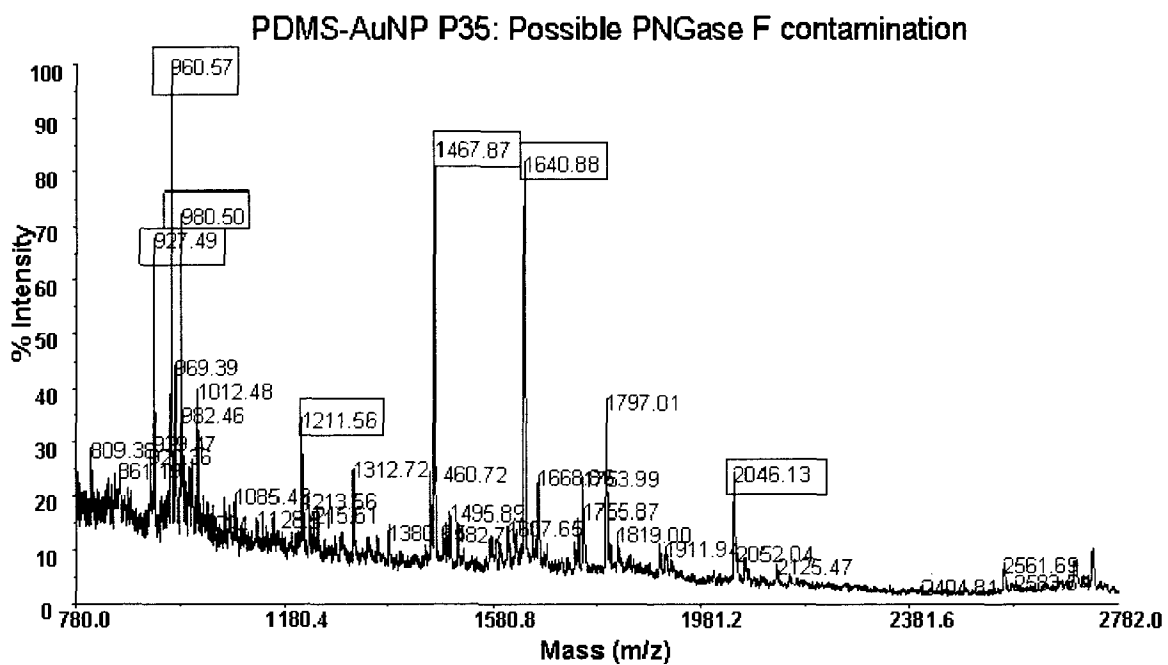
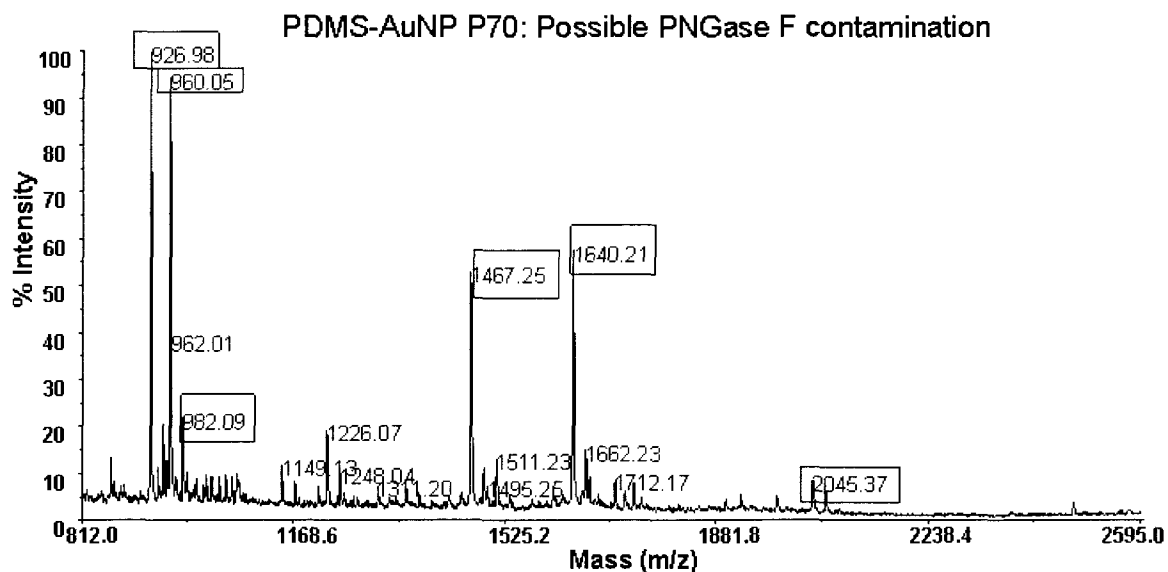
# Tyrosine 3-monooxygenase/tryptophan 5-monooxygenase activation protein



## Tyrosine 3-monooxygenase/tryptophan 5-monooxygenase activation protein PSD







## VITA AUCTORIS

Name: Suzanne Bonnie Durocher

Place of Birth: London, Ontario

Year of Birth: 1985

### Education

2007-2009 University of Windsor, Windsor, Ontario  
M.Sc. Biochemistry

2003-2007 University of Windsor, Windsor, Ontario  
Honours B.Sc. Biology and Biotechnology

1999 – 2003 Honourable Vincent Massey Secondary School  
Windsor, Ontario

### Awards

2008 – 2009 Ontario Graduate Scholarship

2007 – 2008 University of Windsor Tuition Scholarship

### Publications

Durocher, S., Rezaee, A., Hamm, C., Rangan, C., Mittler, S., Mutus, B. (2009). Disulfide-linked, gold nanoparticle-based reagent for detecting small molecular weight thiols. *J Am Chem Soc* **131**(7): 2475-7.

Mikula, I., Durocher, S., Martasek, P., Mutus, B., Slama-Schwok, A. (2009). Isoform-specific differences in the nitrite reductase activity of nitric oxide synthases under hypoxia. *Biochem J* **418**(3): 673-82.